

UNIVERSITÀ DEGLI STUDI DI TRENTO

**QUANTUM DEGENERATE
POTASSIUM-RUBIDIUM MIXTURES**

**DOCTORAL THESIS PRESENTED BY
GIACOMO ROATI**

Supervisor:

Prof. Massimo Inguscio

Referees:

Prof. Rodolfo Bonifacio

Dr. Mario Scotoni

To Viviana, with love

*Tunc Caesar: "Eatur", inquit, "quo deorum
ostenta et inimicorum iniquitas uocat.
Alea iacta est".*

Svetonio, De vita Caesarum XXXII

Acknowledgements

Tutti i risultati sperimentali presentati in questa tesi sono il frutto di tre anni di intenso lavoro ma soprattutto di numerosi momenti di estrema gioia e felicità!

Ringrazio innanzi tutto il Prof. Massimo Inguscio ed il Prof. Sandro Stringari per avermi dato la possibilità di vivere un'esperienza tanto intensa quanto entusiasmante presso il LENS di Firenze e l'Università di Trento: un grazie di cuore.

Grazie al Prof. Bonifacio ed al Dr. Scotoni per avere letto il manoscritto, al Dr. Ricci che è stato sempre disponibile, nonostante la mia lontananza da Trento.

Non dimentico la Sg.ra Rossi Doria, una super segretaria, tanto gentile e tanto pronta ad aiutarmi in ogni mia necessità: grazie, grazie, grazie!

Ringrazio con affetto grande soprattutto il Dr. Giovanni Modugno, con il quale ho passato quattro anni indimenticabili e grazie al quale ho potuto scrivere tutto ciò che è scritto in questa tesi. Non dimenticherò mai le notti passate con lui ad Arcetri...a lavorare... e la sensazione di felicità divina e di irrefrenabile contentezza nell'osservare per la prima volta il condensato di ^{41}K ed il gas di Fermi di ^{40}K mentre sorgeva giorno. Non sono e non saranno solo ricordi, ma molto di più. Grazie per avermi insegnato tanto e avere sopportato i miei momenti di esuberanza...e di tristezza. Sei un mio amico sincero oltre che uno scienziato vero che conosce e ama la fisica.

Grazie a tutti i ragazzi del LENS ed in particolare al Dr. Gabriele Ferrari, con il quale ho avuto la possibilità di lavorare e dal quale ho imparato molto. L'unica mia perplessità riguarda i suoi gusti musicali che, devo dire, mi lasciano abbastanza sbigottito... Comunque, mi sono divertito moltissimo ad allineare il sistema sulle note di Romina ed Albano e della Carra'...

Grazie al Dr. Michele Modugno per i consigli e le elucidazioni "teoriche" e per avere collaborato alla versione finale di questa tesi e grazie al Dr. Andrea Simoni, l'uomo delle collisioni fredde.

Grazie a tutto il gruppo della BEC: alla gentile e dolce Dr.sa Chiara Fort, al

Prof. Francesco Cataliotti, non così dolce (...), ma super disponibile, con il quale ho realizzato il primo condensato di rubidio della mia vita, ed al Dr. Francesco Minardi (quante risate).

Ma un pensiero va soprattutto al Dr. Pasquale Maddaloni, con il quale ho vissuto i momenti di libertà qui a Firenze (quante pizze, eh Pasquale ???), a Francesco Riboli (Ohhrrriboli) e a Nicola Poli che sono stati miei compagni di lavoro, oltre che amici pronti allo scherzo, sempre.

Un ringraziamento poi va al Prof. Robert Brecha, al Prof. Wlodek Jastrzebski, al Prof. Peter Hannaford ed, infine, al Prof. Vanderlei Bagnato che durante la loro permanenza qui al LENS si sono sempre dimostrati disponibili a partecipare attivamente al lavoro sperimentale.

Un affettuoso abbraccio alla mia famiglia tutta che mi ha sempre aiutato con tanto affetto e amore, comprendendo le mie scelte: un grande bacio a tutti !!!

Un bacio alla mia ragazza Viviana: la sua dolcezza ed il suo amore senza confine mi hanno supportato e spinto durante questo dottorato. Questa tesi è dedicata a te Viviana: sei la persona più importante della mia vita: grazie amore!

Firenze, 24 Febbraio 2003

Contents

Table of contents	i
1 Trapped Quantum Gases	5
1.1 Principles of scattering theory	6
1.1.1 Low-energy limit and unitary limit of the scattering length	8
1.2 Cooling atoms by elastic collisions	10
1.2.1 Evaporative cooling	10
1.2.2 Sympathetic cooling	11
1.3 Properties of trapped atoms	13
1.3.1 Properties of trapped fermions	14
1.3.2 Properties of a Bose-Einstein condensate	19
1.4 Mean-field interaction in the mixtures	22
1.4.1 Bose-Bose quantum mixture	23
1.4.2 Fermi-Bose quantum mixture	24
1.4.3 BCS-like transition in a dilute mixture of fermions	25
2 How to produce the mixtures	27
2.1 Potassium and rubidium atoms	27
2.2 Laser sources and experimental set up	32
2.2.1 General idea	32
2.2.2 Rubidium laser set-up	34
2.2.3 Potassium laser set-up	35
2.3 Experimental procedure	36
2.3.1 Magnetic trapping of the mixture	38
2.3.2 Optical pumping procedure	42
2.3.3 Imaging the atoms	43

3	Sympathetic cooling of potassium and K-Rb interactions	47
3.1	Evaporative cooling of rubidium atoms in the mixture	47
3.1.1	Cooling the potassium atoms to quantum degeneracy	48
3.2	Measuring K-Rb ultracold interactions	51
3.2.1	Thermalization by elastic interspecies collisions	53
3.2.2	Dipolar oscillations	57
3.3	Potassium-rubidium interactions	58
4	Bose-Bose degenerate mixture	61
4.1	Producing the degenerate mixture	61
4.2	Stability of the degenerate mixture	64
4.3	Dynamics of binary potassium-rubidium BECs: collision-induced scissors mode	68
4.3.1	Expansion of a rotating BEC	73
5	Fermi-Bose degenerate mixture	77
5.1	Motivations and experimental procedure	77
5.2	Measuring the interaction: parametric heating and dipolar oscillations	80
5.2.1	From hydrodynamic to collisionless regime	82
5.3	^{40}K - ^{87}Rb degenerate mixture	84
5.3.1	Dipolar oscillations in the quantum degenerate regime	86
5.4	Mean-field interaction in the degenerate mixture	89
5.4.1	Evidence of the mean-field interaction: study of the expansion of the clouds	91
5.5	Collapse of the Fermi gas	96
5.5.1	Determination of the scattering length by the collapse	102
5.5.2	Beyond the mean-field description of the mixture	104
5.6	Towards BCS-like transition in the ^{40}K - ^{87}Rb degenerate mixture . . .	107

Introduction

After the achievement of Bose-Einstein condensation (BEC) in dilute gases of alkali atoms [1–3], many experimental efforts were dedicated to the study of the fundamental properties of the condensate. The most attractive feature of such a system is that it can be completely described theoretically [4] due to the weakly interacting nature, and thus it represents a testing ground for studying more general physical phenomena, such as superfluidity and coherence. Indeed, since Bose-Einstein condensation is the macroscopic occupation of the lowest available quantum state, the system is described by a single wavefunction. Bose-Einstein condensate is thus phase-coherent as an optical laser field and it shows all the features related to superfluidity, as experimentally observed [5; 6]. Bose-Einstein condensation in dilute gases shows up at very low temperatures. These sub-microKelvin temperatures are reached by combining two cooling procedures, laser cooling and evaporative cooling, which have allowed so far the observation of BEC in samples of Rb [1; 7], Na [2], Li [3], H [8], He [9], Cs [10].

In recent years, considerable interest has been devoted to extend these experimental techniques to the production of other degenerate systems composed by fermionic atoms and by more exotic species like molecules. In particular, the quest of Cooper-pairing transition in a dilute gas of fermions and the realization of molecular BEC pose the challenge of new and exciting developments in this area of physics.

The work of this thesis takes place inside this new context of research. We have produced degenerate mixtures composed by isotopes of potassium and by rubidium atoms. The novelty of this system relies on the possibility of investigating the properties of samples consisting either of two Bose-Einstein condensates or of a Fermi gas interacting with a Bose condensate. Potassium atoms are cooled to quantum degeneracy by means of sympathetic cooling with rubidium atoms. In this way it has been possible to achieve for the first time a BEC of ^{41}K atoms, so far

prevented by the inefficacy of the standard cooling techniques in cooling potassium [11]. The study of the boson-boson ^{41}K - ^{87}Rb mixture has allowed the realization of a binary Bose-Einstein condensate of two different species [12]. This system composed by two strongly interacting superfluids appears very suitable for the production of ultracold dipolar molecules [13], whose main and more interesting feature relies on the long-range character of the dipole-dipole interaction. These interactions are indeed partly attractive and partly repulsive and they can be much stronger than the usual Van der Waals forces. In case of dipolar bosons new quantum phase-transitions have been predicted and it has been also suggested that bosonic dipoles can represent a promising system for implementing quantum computing [14].

Sympathetic cooling of the fermionic ^{40}K with ^{87}Rb atoms has instead permitted us to produce a Fermi gas of potassium interacting with the BEC of rubidium, overcoming the fundamental limitations in cooling identical fermions due to the suppression of collisions at ultralow temperatures [15]. The possibility of having a degenerate gas where the interactions between the particles are absent is important, for example, for increasing the precision and the stability of atomic clocks [16], actually limited by the frequency shifts induced by collisions between particles. While the interactions between the atoms in the Fermi gas are not relevant, the ones between the degenerate fermions and the Bose-Einstein condensate has been suggested to strongly influence the stability of the mixture [17]. In our system, we were actually able to observe the collapse of the Fermi gas of ^{40}K , driven by the presence of the Bose gas of rubidium [18]. This observation shows that the interactions between fermions can be effectively manipulated with the use of a BEC and this is particularly important for the quest of superfluidity in a dilute gas of fermions. Indeed, it has been proposed [19] that such boson-fermion interaction is likely to induce an effective attraction between fermions. This attractive interaction is similar to the phonon-induced correlation between pairs of electrons in superconductors and it is predicted to largely favour the pairing between fermions. The optimal conditions for observing BCS-like transition occurs at the onset of collapse where the critical temperature for achieving fermion superfluidity is comparable with the Fermi temperature of the system.

The outline of this thesis is the following.

In the first chapter we briefly introduce the physics of ultracold interactions, pointing out the substantial differences between fermionic and bosonic systems. We also give the theoretical background on degenerate trapped fermions and bosons, and we describe the experimental techniques to achieve the degenerate regime in such systems. The second chapter is dedicated to the description of the experimental apparatus we have used for producing the potassium-rubidium mixtures and also to the physical properties of potassium and rubidium atoms.

In the third chapter we report on the achievement of Bose-Einstein condensation of ^{41}K by means of sympathetic cooling with rubidium atoms. In particular, the efficiency of sympathetic cooling is assured by the large interspecies interaction between potassium and rubidium. We also discuss the experimental results of accurate collisional measurements performed on the ^{41}K - ^{87}Rb mixture from which we have been able to deduce the interaction properties of all the potassium-rubidium isotopic pairs.

In the fourth chapter we describe the experimental realization of the binary BEC composed by a Bose-Einstein condensate of ^{41}K interacting with a Bose-Einstein condensate of ^{87}Rb , and we also give the theoretical tools which describe such mixture. The stability against collapse of such degenerate mixture depends on the large and repulsive character of the ^{41}K - ^{87}Rb interaction. We present also the results of our investigations on the dynamics of these two superfluids in the magnetic trap, showing how it has been possible to induce scissors-like oscillations by forcing collisions between the two BECs.

The last chapter is dedicated to the ^{40}K - ^{87}Rb degenerate mixture. We produce a system composed by a Bose-Einstein condensate of ^{87}Rb immersed in a Fermi sea of ^{40}K . Also in this case, the efficiency of sympathetic cooling is assured by a large interaction between potassium and rubidium atoms, which is predicted to be attractive. We also present the main theoretical issues which describe the mixture. We report on the observation of the collapse of the Fermi gas, induced by the large and attractive interaction with the Bose gas of rubidium, discussing the implications of such an observation for the achievement of superfluidity state in a gas of potassium atoms.

CHAPTER 1

Trapped Quantum Gases

All the particles in nature belong to two families: the bosons and the fermions. The spin of the bosons is a multiple integer of \hbar , while the one of the fermions is a half-integer of \hbar . This characteristic determines the different quantum behaviour of the two classes.

The quantum nature of bosons and fermions becomes evident as soon as the spread of the wavepacket associated at each particle becomes comparable with the mean distance between two of them. At this point the system is said to be degenerate. As a direct consequence of the different statistics, bosons can occupy macroscopically the ground state of the system, while fermions arrange themselves individually in each quantum state.

In this chapter we show how the different statistics largely affects also the collisional behaviour of fermions and bosons. In particular, in the regime of ultracold temperature and weak interactions identical fermions do not collide while the collisional properties of a gas of bosons are determined by only one parameter, the scattering length a .

We also discuss the main characteristics of trapped Fermi and Bose gases and the experimental procedures by which it is possible to produce and investigate such systems.

1.1 Principles of scattering theory

Consider two particles of mass M interacting via a potential $V(\mathbf{r}_1 - \mathbf{r}_2)$ [20]. The Hamiltonian which describes this system is given by:

$$H = \frac{P_1^2}{2M} + \frac{P_2^2}{2M} + V(\mathbf{r}_1 - \mathbf{r}_2) \quad (1.1)$$

It is worth to consider the same problem in the center of mass frame, introducing the following variables:

$$\mathbf{R}_G = (\mathbf{r}_1 + \mathbf{r}_2)/2 \quad (1.2)$$

$$\mathbf{P}_G = \mathbf{p}_1 + \mathbf{p}_2 \quad (1.3)$$

and

$$\mathbf{r} = \mathbf{r}_1 - \mathbf{r}_2 \quad (1.4)$$

$$\mathbf{p} = (\mathbf{p}_1 - \mathbf{p}_2)/2 \quad (1.5)$$

Substituting these new variables inside the Hamiltonian, one gets:

$$H = \frac{P_G^2}{4M} + \frac{p^2}{M} + V(\mathbf{r}) \quad (1.6)$$

As we see from (1.6), the center of mass moves as a free particle of mass $2M$, while all the collisional physics is contained inside the second term of (1.6), that corresponds to the scattering of a particle of mass $m_r = M/2$ by the potential $V(\mathbf{r})$. Then the study of this scattering process reduces to find the eigenstates of the Hamiltonian of the relative motion:

$$\left(\frac{p^2}{2m_r} + V(\mathbf{r}) \right) \psi_{\mathbf{k}}(\mathbf{r}) = E_k \psi_{\mathbf{k}}(\mathbf{r}) \quad (1.7)$$

where $E_k = \hbar^2 k^2 / 2m_r$ and we suppose $V(\mathbf{r}) \rightarrow 0$ when $|\mathbf{r}| \rightarrow \infty$. We look for the asymptotic solutions of (1.7) that have the following form:

$$\psi_{\mathbf{k}}(\mathbf{r}) \sim e^{i\mathbf{k}\mathbf{r}} + f(k, \mathbf{n}, \mathbf{n}') e^{ikr}/r \quad (1.8)$$

where $\mathbf{n} = \mathbf{k}/k$ and $\mathbf{n}' = \mathbf{r}/r$. This kind of solutions has an intuitive meaning: the first part of (1.8) represents an incident plane wave propagating with wave-vector \mathbf{k} , while the second one is the diffuse wave. The amplitude of the diffuse wave, $f(k, \mathbf{n}, \mathbf{n}')$ is called "scattering amplitude" and it is related in a very simply way to the scattering cross-section for this potential:

$$\sigma(k, \mathbf{n}) = \int |f(k, \mathbf{n}, \mathbf{n}')|^2 d^2 n' \quad (1.9)$$

To solve the 3D Shrödinger equation and to find the scattering amplitude, is usually a very difficult task and only in few cases it is possible to get the exact solution. To considerably simplify our problem, it is possible to consider the special case of a spherical symmetric potential $V(\mathbf{r}) = V(r)$. Indeed, as we will show soon, our 3D problem is then reduced to a 1D problem for which it is easy to write the exact solution. To take advantage of the new symmetry of the problem, it is useful to expand the incident and the scattered wave functions on a basis set of the relative angular momentum operators L^2 and L_z , where we defined z as the direction of the incoming wave.

$$\psi_{\mathbf{k}}(\mathbf{r}) = \sum_{l=0}^{\infty} \sum_{m=-l}^{m=l} Y_l^m(\theta, \phi) \frac{u_{k,l,m}(r)}{r} \quad (1.10)$$

where ϕ is the azimuthal angle and $Y_l^m(\theta, \phi)$ are the spherical harmonic functions. The scattering state $\psi_{\mathbf{k}}(\mathbf{r})$ is asymptotically the sum of the incoming wave and the diffuse wave $f(k, \theta)e^{ikr}/r$:

$$\psi_{\mathbf{k}}(\mathbf{r}) \sim \frac{1}{2ikr} \sum_{l=0}^{\infty} (2l+1)(\cos\theta)((-1)^{l+1}e^{-ikr} + e^{2i\delta_l}e^{ikr}) \quad (1.11)$$

where the phase shifts are real, and they have to be determined in order to solve our initial scattering problem. In order to do this, we have to solve the 1D Schrödinger equation for the radial function $u_{k,l,m}(r)$:

$$u''_{k,l,m}(r) + \left(k^2 - \frac{l(l+1)}{r^2} - \frac{2m_r V(r)}{\hbar^2}\right)u_{k,l,m}(r) = 0 \quad (1.12)$$

We consider as asymptotic expression for $u_{k,l,m}(r)$ the following:

$$u_{k,l,m}(r) \propto (-1)^{l+1}e^{-ikr} + e^{2i\delta_l}e^{ikr} \quad (1.13)$$

Then the scattering amplitude becomes:

$$f(k, \theta) = \frac{1}{2ik} \sum_l (2l+1)(e^{2i\delta_l} - 1)P_l(\cos\theta) \quad (1.14)$$

where $l = 0, 1, 2, \dots$ for the s, p, d, .. partial waves contribution. The scattering cross-section $\sigma(k)$ reads as:

$$\sigma(k) = \sum_{l=0}^{\infty} \sigma_l(k) \quad (1.15)$$

with

$$\sigma_l(k) = \frac{4\pi}{k^2} (2l+1) \sin^2 \delta_l(k) \quad (1.16)$$

The expressions we have written so far have implicitly assumed that the particles were distinguishable, since we could separate the contribution of positive and negative momenta $+k$ and $-k$. To consider the case of identical particles, we have to (anti)symmetrize the two particles wavefunction of identical (fermions) bosons respectively. It is possible to show that this corresponds to change the angle θ in $\pi - \theta$, so that (1.11) becomes:

$$\psi_{\mathbf{k}}(\mathbf{r}) \sim e^{i\mathbf{k}\cdot\mathbf{r}} + \epsilon e^{-i\mathbf{k}\cdot\mathbf{r}} + e^{ikr}/r (f(k, \theta) + \epsilon f(k, \pi - \theta)) \quad (1.17)$$

where $\epsilon = -1, 1$ for fermions and bosons respectively. The differential cross-section becomes then:

$$\frac{d\sigma_l(k)}{d\Omega} = \frac{1}{2k^2} \left| \sum_{l_{even}, l_{odd}} (2l+1)(e^{i2\delta_l} - 1)P_l(\cos\theta) \right|^2 \quad (1.18)$$

and

$$\sigma(k) = \frac{8\pi}{k^2} \sum_{l_{even}, l_{odd}} (2l+1) \sin^2 \delta_l \quad (1.19)$$

As we can read from (1.19), in the case of identical bosons and fermions, the partial cross-section is twice as large as the one for classical particles. Furthermore, due to the parity of the Legendre Polynomials $(-1)^l$, only few partial wave give contribution to the scattering cross-section. In the case of identical bosons, only the partial waves with l even contribute, while for identical fermions are non zero only the odd ones. Consequently the scattering cross-sections can be written as:

$$\sigma(k) = \frac{8\pi}{k^2} \sum_{l_{even}} (2l+1) \sin^2 \delta_l \quad (1.20)$$

$$\sigma(k) = \frac{8\pi}{k^2} \sum_{l_{odd}} (2l+1) \sin^2 \delta_l \quad (1.21)$$

for bosons and fermions respectively.

1.1.1 Low-energy limit and unitary limit of the scattering length

So far we do not have considered any effect of the temperature on the scattering process. In fact, the collisional properties are strongly affected by the temperature. In particular, the quantum features of the scattering become evident at very low temperatures, typically $T \ll 1$ mK, which are however accessible in the standard cold atoms experiments [5; 6]. To gain a more quantitative insight to this dependence, consider the equation (1.12). The effective potential is composed by two terms: one, $V(r)$ is simply the atom-atom interaction and it is the cause of the phase shifts that we have seen before. The second one, $\hbar^2 l(l+1)/2m_r^2$ describes instead the centrifugal barrier due to the relative angular momentum between the

two particles and it is zero only in the case of the $l = 0$ partial wave. Suppose now that $l \neq 0$: if the relative particle has an energy E lower than the height of this effective potential, it will not feel any potential $V(r)$ and it will be then reflected by the centrifugal barrier. Subsequently, we expect that only the contribution of the $l = 0$ partial wave will survive at very low temperatures. It is possible to show [20], that for $k \rightarrow 0$:

$$\delta_l(k) \propto k^{2l+1} \quad (1.22)$$

so that the scattering cross-section becomes:

$$\sigma_{l \neq 0} = \frac{8\pi}{k^2} (2l+1) \sin^2 \delta_l \propto k^{4l} \rightarrow 0 \quad (1.23)$$

In the case of $l = 0$, we find that:

$$\lim_{k \rightarrow 0} \sigma_{l=0}(k) = 8\pi a^2 \quad (1.24)$$

for bosons, where the scattering length a is defined by:

$$a = -\lim_{k \rightarrow 0} \frac{\tan \delta_0(k)}{k} \quad (1.25)$$

From equation (1.23), we see that the contribution of all the partial waves with $l \neq 0$ goes to zero as T^{2l} as observed experimentally in the case of the fermionic ^{40}K [21] and this behaviour is particularly crucial in the case of identical fermions. It is possible to derive [22] the energy dependence of the total scattering length in the effective range theory:

$$\sigma(k) = \frac{8\pi a^2}{(1 - 1/2k^2 a r_e)^2 + k^2 a^2} \quad (1.26)$$

where r_e is the effective range of the potential. For large ka , the elastic cross-section saturates to the so called "unitary limit" for s-wave collisions $\sigma = 8\pi/k^2$. This energy dependence of the cross-section has been demonstrated in the experiment of J. Dalibard on cold Cs atoms [23]. Only few words to comment on the physical meaning of the unitary limit. The unitary limit is reached when the magnitude of the scattering length becomes larger than the deBroglie wavelength associated to the atoms: in this case, the scattering cross-section is independent from the scattering length but proportional to the square of the deBroglie wavelength and it reaches its maximum value.

Comments

The most important results we have obtained from the previous discussion is that at, very low temperatures, identical fermions do not collide, while the scattering cross-section for identical bosons is described by a single parameter, the scattering length a by $\sigma = 8\pi a^2$.

Indeed, in the case of fermionic atoms, only the odd l partial waves contribute to the scattering cross-section, but these ones are highly suppressed in this temperature regime, since the contribution of all the partial waves with $l \neq 0$ goes to zero as T^{2l} . This peculiar behaviour strongly affects the possibility of cooling fermions down to quantum degeneracy. Indeed because of this suppression in the collisional processes, it is not possible to perform the standard technique of evaporative cooling by which it has been reached the degeneracy in dilute atomic systems [5]. However, this strong limitation in cooling fermions can be circumvented using essentially two different strategies. The first is to use a system composed by distinguishable fermions as in the experiment running at Jila [24] and at Duke University [25; 26]. In both cases, mixtures of two spin states of ^{40}K and ^6Li atoms respectively were brought to quantum degeneracy by exploiting allowed s-wave collisions between particles trapped in two states.

Another way of proceeding is to mix together the fermionic atoms with bosons, belonging to the same atomic specie [28], [29], or to a completely different one [15; 30]. By cooling selectively the bosonic component it is possible to cool down the fermionic one by means of elastic interspecies collisions (*sympathetic cooling*). The general advantage of this cooling method is that it allows the production of degenerate mixtures composed either by two interacting Bose-Einstein condensates [12; 27] or by a Fermi gas interacting with a BEC [15; 28–30].

1.2 Cooling atoms by elastic collisions

In the previous sections we have derived the relevant results of the scattering theory in the case of dilute atomic systems, for which the range of the interatomic force is small compared to the mean distance between particles and the scattering involves only pairs of atoms (binary collisions). We have shown that at sufficiently low temperatures (in the range of μK), the scattering cross-section for identical bosons is simply $\sigma = 8\pi a^2$ while identical fermions do not collide.

In the first part of this section, we describe the mechanism of *evaporative cooling* which directly exploits elastic collisions between atoms and which is the only cooling method which allows to reach the degeneration regime in dilute gases. In the last part, we instead discuss the other cooling technique, *sympathetic cooling*, by which it is possible to obtain degenerate mixtures of atoms of different species, and also the achievement of the degenerate regime for identical fermions.

1.2.1 Evaporative cooling

Evaporative cooling is a quite familiar phenomenon. Indeed, everybody exploits it, for example, for cooling a cup of tea. The main idea is that, for decreasing the temperature of a system, the easier thing to do is to continuously remove the particles with higher energy. In this way, after the subsequent thermalization

mediated by elastic collisions between the remnant atoms, the temperature of the system will decrease.

The first developing of evaporative cooling in the context of cooling atomic gases was proposed and then realized at MIT as a method for cooling atomic hydrogen [31; 32], and later was used for cooling below microKelvin every alkali atoms [5; 6].

Evaporative cooling of dilute gases is usually performed in magnetic or in optical traps. In the former case, the atoms previously all pumped in one specified *low – field seeking internal state* are trapped in a minimum of the magnetic field. The coupling energy between the particles and the external potential is $U = g_F m_F \mu_B |B|$, where m_F is the Zeeman level, g_F is the Lande' factor and μ_B is the Bohr magneton. Since not every atomic internal state is trapped by the potential (the so called *high – field seeking internal state*), the removal of the atoms is performed by driving RF or μ -wave transitions from the trapped to the untrapped states. The selectivity in the energy is achieved since the resonances of these transitions depend from $|B|$ due to the Zeeman effect. Different classes of atoms can thus be cut out from the trap by the knife depending on their spatial position inside the trap and hence on their temperature.

One of the most important parameter which characterizes the efficiency of the evaporation is $\eta = E_c/k_B T$, the ratio between the cutting energy E_c and the temperature of the system. The evaporation works well if η ranges from 4 to 10: indeed if we cut too hard inside the thermal distribution of the sample we induce losses, since we do not allow an efficient thermalization between atoms. Evaporation decreases the temperature of the system, but also decreases the ability of the system to thermalize. Indeed, by writing the relation between the elastic collisional rate and the temperature as $\Gamma = n\sigma v_T$ where $\sigma \propto a^2$ and $v_T \propto \sqrt{T}$ we see that a reduction in the temperature corresponds to a reduction in the collisional rate. This is the reason why the evaporation must be forced by keeping the η parameter constant. Anyway, since the elastic collisional rate depends also from the atoms number, the rate at which temperature is reduced must be accomplished by a similar and if possible smaller decrease in the number of atoms.

Since inside the trap we do not have only elastic collisions between atoms, but also inelastic collisions which cause losses and heating of the sample, evaporative cooling mechanism is efficient only if the number of elastic collisions exceeds the number of inelastic processes $\Gamma_{el}/\Gamma_{in} > 200$ [33]. In this regime, called runaway evaporation, Γ_{el} increases during the time, while increasing the efficiency of the evaporative cooling.

1.2.2 Sympathetic cooling

We have seen that evaporative cooling works efficiently if the elastic collisional rate is large enough to allow fast thermalization and to exceed the inelastic processes that limit the lifetime of the sample. However, if this elastic rate is not sufficiently high, because the scattering length is too small or the initial density of the sample

is too low (as for ^{41}K [34]), this cooling mechanism is not efficient. The same limitation occurs for identical trapped fermions, for which the elastic scattering cross-section is suppressed.

In both cases, another cooling technique can be exploited, the sympathetic cooling. The idea of sympathetic cooling is to take advantage of elastic collisions between the atomic sample that we want to cool and another gas, easily coolable, which acts like a thermal bath.

This method, initially proposed for the cooling of ions [35], at the beginning has allowed the achievement of quantum degeneracy in a sample of rubidium atoms in two different internal states [27] or in case of the two isotopes of lithium [28], [29]. Recently, [11; 12; 15; 30], by means of sympathetic cooling it was also possible to achieve the quantum degenerate regime in mixtures composed by atoms of two different atomic species, opening in this way new directions in the field of ultracold and degenerate matter, for example in the context of producing ultracold heteronuclear molecules [36].

Sympathetic cooling exploits elastic collisions between distinguishable atoms and the important parameter to consider is the interspecies scattering cross-section is $\sigma = 4\pi a_{ij}^2$, where a_{ij} is the interspecies scattering length. The larger is the magnitude of the scattering length and the better and more efficiently works sympathetic cooling.

The mixtures composed by ^{41}K - ^{87}Rb and ^{40}K - ^{87}Rb atoms present an interspecies interaction quite large in both cases and sympathetic cooling is very efficient.

Also the sign of the interspecies scattering length plays a relevant role in the efficacy of this cooling mechanism. Indeed, in the case of ultracold thermal gases, the mean-field interaction between the specie i and j , proportional to a_{ij} is negligible respect to the kinetic energy of the particles. When the system approaches to the degenerate regime this is no more true. In fact the sign of a_{ij} determines if the two degenerate clouds continue to overlap, $a_{ij} < 0$, or they spatially separate, $a_{ij} > 0$. In the former case the thermal contact is preserved and sympathetic cooling is still efficient, while if phase-separation occurs the minimum temperature achievable is lower [37].

In the experiments, sympathetic cooling is realized by loading simultaneously inside the magnetic trap two different atomic species (by now, for simplicity we consider only the case of two separate atomic species, like in the experiments running at LENS, JILA and MIT). Since one of the two species must be directly cooled, i.e. continuously lost, its atom number must be sufficiently higher than the one of the other sample. Sympathetic cooling works efficiently until the thermal capacity of the thermal bath is higher than the one of the specie that must be cooled. For understanding this, we indicate with i the thermal bath and with j the other specie, and with C_i and C_j the corresponding thermal capacities. Sympathetic cooling is efficient only if $C_i > C_j$ and this condition must be kept in all the stages of the evaporation. In the case of thermal gases, since $C_\alpha/k_B = 3N_\alpha$, where $\alpha = i, j$, this condition becomes simply $N_i > N_j$.

In the case of Bose and Fermi gas, the expressions for the thermal capacities

are given by [4; 38]:

$$C_B = 12 \frac{\zeta(4)}{\zeta(3)} N_B k_B \left(\frac{T}{T_C}\right)^3 \quad (1.27)$$

$$C_F = \pi^2 N_F k_B \frac{T}{T_F}$$

that are valid for $T \leq T_C$ and $T \leq T_F$ respectively and where ζ is the Reiman zeta function. To comment (1.27), it useful to describe the two different situations met in our experiments: the Bose-Bose system and the Fermi-Bose system. In our Bose-Bose system, the ^{41}K - ^{87}Rb mixture, due to the different mass ($m_{Rb} \sim 2m_K$) Bose-Einstein condensation is reached before for potassium atoms and then for rubidium sample. The typical transition temperatures are $T=120$ nK, and $T=80$ nK for potassium and rubidium respectively and for $N_K = N_{Rb} = 10^4$ atoms in the condensates. In the temperature interval 80-120 nK we have then a potassium BEC interacting with a thermal gas of rubidium. If we evaluate the thermal capacities at $T = T_C(K) = 120$ nK, we find that $C_B(K)/C_c(Rb) \sim 3$ at $T = T_C(K) > T_C(Rb)$: this means that at this stage of evaporation the number of Rb atoms must be almost three times the one of K for still having an efficient sympathetic cooling.

The same must occur in the case of the Fermi-Bose system, the one composed by ^{40}K and ^{87}Rb atoms. Indeed, since in our system, the Fermi temperature is higher than the one for Bose-Einstein condensation, we have that at $T = T_F$ the thermal capacity of the Fermi system is $C_F/k_B = \pi^2 N_F$, while the one for the thermal bosons is still the classical $C_B/k_B = 3N_B$. This means that for decreasing furthermore the potassium temperature we must have $N_B > \pi^2/3 N_F \sim 3N_F$. When both the species are degenerate, for $T \leq T_C$, only the thermal fraction of the Rb sample contributes to the thermal capacity of Rb. If the number of thermal atoms is not sufficiently high to balance the heat capacity of the Fermi gas, sympathetic cooling does not work anymore and the cooling of the fermion stops.

1.3 Properties of trapped atoms

In the first part of this chapter, we have derived the main results of the scattering theory in the case of ultracold atoms and we have seen how the collisional properties are deeply modified by the quantum nature of the particles. We have also described the standard experimental techniques, namely evaporative cooling and sympathetic cooling, by which it is possible to produce such degenerate systems. In this last part of the chapter, we will discuss in more detail the features of these quantum gases, describing the main physical properties that distinguish them from classical gases.

1.3.1 Properties of trapped fermions

Consider N identical fermions of mass m , trapped in a cylindrical harmonic potential [38],

$$V(\rho) = \frac{1}{2}m\omega_r^2\rho^2 \quad (1.28)$$

where ρ is defined as $\rho^2 = (x^2 + y^2 + \lambda z^2)$, and $\lambda = \omega_a/\omega_r$ is the ratio between the two trap frequencies ω_r and ω_a along the radial and the axial directions respectively. Since the Pauli exclusion principle forbids the multiple occupation of a single energetic level, the fermions go to occupy one by one all the energy levels of the system. The energy of the highest level is called the Fermi energy E_F , and it corresponds to the Fermi temperature $T_F = E_F/k_B$, where k_B is the Boltzmann's constant. The ratio between the temperature T and T_F , T/T_F , defines the degree of degeneration of the system. Indeed, if $T/T_F \gg 1$, the probability that a single quantum state is occupied is low and the system is said to be classical, while if $T/T_F \leq 1$ the system enters in the degenerate regime. The Fermi-Dirac distribution function is given by:

$$f_F(\epsilon) = \frac{1}{e^{\beta(\epsilon-\mu)} + 1} \quad (1.29)$$

where $\beta = 1/k_B T$ and μ is the chemical potential. In the following, we consider, for simplicity, the case of $T = 0$, when the system is completely degenerate. In this particular situation, the chemical potential is just the Fermi energy, $\mu = E_F$ and the Fermi distribution is one for $\epsilon \leq E_F$ and zero otherwise. In the momentum space, this corresponds to define a sphere of radius $k_F \equiv (2mE_F/\hbar^2)^{1/2}$: at $T = 0$, all the particles of the system must have momentum $k \leq k_F$ and all momentum states with $k \leq k_F$ are occupied. If $\hbar\omega_r, \hbar\omega_a \ll k_B T$, it is possible to neglect the discrete structure of the harmonic oscillator levels, and to write the density of states as follows:

$$g(\epsilon) = \frac{\epsilon^2}{2(\hbar\varpi)^3} \quad (1.30)$$

where ϖ is the geometrical average of the oscillation frequencies of the trap, $\varpi = (\omega_r^2\omega_a)^{1/3} = \omega_r(\lambda)^{1/3}$. The total number of atoms of the system is directly related to the Fermi energy by:

$$N = \int d\epsilon \frac{g(\epsilon)}{e^{\beta(\epsilon-\mu)} + 1} \quad (1.31)$$

from which follows the explicit expression for the Fermi energy:

$$E_F = \hbar\varpi[6N]^{1/3} \quad (1.32)$$

The first important information it is possible to get from (1.32) is the radial size of the Fermi gas, given by:

$$R_F \equiv [2E_F/M\omega_r^2]^{1/2} \quad (1.33)$$

Comparing the Fermi radius R_F with the radial width of the harmonic oscillator ground state of the trap $a_{r0} = (\hbar/m\omega_r)^{1/2}$,

$$R_F = a_{r0}(48\lambda N)^{1/6} \quad (1.34)$$

we observe that if the number of fermions $N \gg 1$, the size of the trapped Fermi cloud is much greater than a_{r0} : this is a consequence of the Pauli exclusion principle. Indeed the Pauli exclusion principle induces an effective "repulsion" between fermions in the trap (Fermi pressure), leading to a size bigger than the quantum length a_{r0} . This characteristic differentiates the Fermi gas both from Bose gas and from a "classical" gas. Indeed, the size of a noninteracting gas of bosons is exactly a_{r0} , because at $T = 0$ they all occupy the lowest state, while the width of a classical gas at $T = 0$ continuously shrinks by decreasing the temperature.

Spatial and momentum distribution of trapped fermions

In the experiments, most of the information about the sample are obtained looking to the absorption signal of the cloud, after the sudden release from the trap [1]. In particular, it is possible to measure the density and the temperature of the atoms and directly reconstruct the spatial and the momentum distributions inside the trapping potential. The features of these distributions are strictly related to the different statistics and then are different in the case of degenerate Fermi or Bose gas. In the following, we will first compare the results obtained for a Fermi gas at $T = 0$ with the ones for a classical gas at the same temperature. The comparison with the Bose gas will be shown later on the chapter.

We start briefly recalling the properties of a classical gas composed by distinguishable particles, trapped in the same cylindrical potential (1.28). The distribution function that describes such a system is the Boltzmann distribution [39],

$$f_c(\epsilon) = Ae^{-\beta\epsilon} \quad (1.35)$$

where A is a normalization constant to be determined, and $\beta = 1/k_B T$. Since the Hamiltonian that describes the system is

$$H = \frac{(\hbar\vec{k})^2}{2m} + V(\rho) \quad (1.36)$$

it is possible to evaluate the normalization constant A , simply solving

$$N = \int d^3\vec{k}d^3\vec{r}f(H(\vec{k}, \vec{r}), T) \quad (1.37)$$

and obtaining $A = N\lambda/(2\pi\sigma_r\sigma_k)^3$, where $\sigma_r = (k_B T/m\omega_r^2)^{1/2}$ and $\sigma_k = \sqrt{2\pi}/\lambda_{db}$, with $\lambda_{db} = \sqrt{\hbar^2/2\pi mk_B T}$ the deBroglie wavelength. Then after substituting the value of A inside 1.35 we can finally write the expression for the spatial and the momentum distribution of a classical gas as:

$$f_c(\vec{r}, \vec{k}, T) = \frac{N\lambda}{(2\pi\sigma_r\sigma_k)^3} \exp\left[-\beta\frac{\hbar^2\vec{k}^2}{2m}\right] \exp\left[-\beta\frac{m\omega_r^2}{2}\right] \quad (1.38)$$

As we see from 1.38, the momentum distribution of a classical gas is isotropic and Gaussian (Maxwell velocity distribution) and the width is σ_k . On the contrary, the spatial distribution of the atoms inside the harmonic trap, reflects the anisotropy of the trap, with aspect ratio λ . The radial size of the distribution is just $\sigma_r = (k_B T/m\omega_r^2)^{1/2}$, and as said before, for $T \rightarrow 0$, it goes to zero.

In order to determine the spatial and the momentum distribution of a Fermi gas trapped in the potential (1.28) we can define, at $T = 0$, a "local" Fermi wavenumber $k_F(\vec{r})$ by [38]:

$$\frac{\hbar^2 k_F^2}{2m} + V(\rho) = E_F \quad (1.39)$$

The spatial density $n(\vec{r})$ is given by the volume of the Fermi sea in momentum space k times the density of state $1/(2\pi)^3$, i.e.

$$n(\vec{r}, T = 0) = \frac{k_F^3(\vec{r})}{6\pi^2} \quad (1.40)$$

with the assumption that $n(\vec{r}) \neq 0$ only if $\rho < R_F$. If we substitute (1.39) inside (1.40), we obtain:

$$n(\vec{r}, T = 0) = \frac{m^3 \omega_r^3 R_F^3}{6\pi^2 \hbar^3} \left[1 - \frac{\rho^2}{R_F^2}\right]^{3/2} \quad (1.41)$$

Remembering that $R_F = \sqrt{\hbar/m\omega_r}(48\lambda N)^{1/6}$, follows that

$$n(\vec{r}, T = 0) = \frac{8\lambda N}{\pi^2 R_F^3} \left[1 - \frac{\rho^2}{R_F^2}\right]^{3/2} \quad (1.42)$$

The cloud is an ellipsoid with diameters $2R_F$ and $2R_F/\lambda$ in the x-y plane and in the z directions respectively, and the aspect ratio is the same as that of a classical gas in the same potential. The momentum distribution for a Fermi gas is similarly obtained like (1.42) and it is:

$$n(\vec{k}, T = 0) = \frac{N}{k_F^3} \frac{8}{\pi^2} \left[1 - \frac{|\vec{k}|^2}{k_F^2}\right]^{3/2} \quad (1.43)$$

where the maximum wavenumber populated is $k_F = (48N\lambda/R_F^3)^{1/3}$. As the momentum distribution of the classical gas, the momentum distribution of a Fermi gas is isotropic despite the anisotropy of the trap due to dependence of (1.43) only from the magnitude of \vec{k} .

Comparison between the expansion of a classical and a Fermi gas.

As said above, in the experiments, all the quantities of interest, such as the number of atoms and the temperature are extracted from the absorption imaging of the expanded cloud after the release from the trap. Indeed, this signal is related to the momentum distribution of the atoms inside the trap. In the case of thermal gas, as we see from equation (1.38), we expect that the shape of the cloud is well fitted by a Gaussian because the velocity distribution of a thermal gas is a Gaussian. Furthermore, if we write the time-dependence of the classical mean square radii, we find:

$$\begin{aligned} \langle r_r^2 \rangle &= r_{0r}^2 (1 + \omega_r^2 t^2) \\ \langle r_a^2 \rangle &= r_{0a}^2 (1 + \omega_a^2 t^2) \end{aligned} \quad (1.44)$$

and if we consider the ratio ("*aspect ratio*") of the two,

$$\mathfrak{R} = \sqrt{\frac{\langle r_a^2 \rangle}{\langle r_r^2 \rangle}} = \frac{1}{\lambda} \sqrt{\frac{1 + \omega_a^2 t^2}{1 + \omega_r^2 t^2}} \quad (1.45)$$

we see that it goes to 1 if $t \rightarrow 0$, i.e. the shape of the cloud becomes spherical at large expansion time t , independently from the initial anisotropy of the trapping potential.

If now we switch to the noninteracting Fermi gas, the situation remains almost the same. From equation (1.43), we see that we expect to have a complete isotropic expansion of the cloud, even if the initial momentum distribution is not Gaussian. Indeed, solving the Boltzmann transport equation [40] for this case, and then extracting the temporal evolution of the radii of the Fermi gas, we get:

$$\langle r_r^2 \rangle = \frac{1}{3N} E_{rel} \frac{2}{m\omega_r^2} (1 + \omega_r^2 t^2) \quad (1.46)$$

$$\langle r_a^2 \rangle = \frac{1}{3N} E_{rel} \frac{2}{m\omega_a^2} (1 + \omega_a^2 t^2) \quad (1.47)$$

where E_{rel} is the release energy $E_{rel} = 3/4N E_F$. If we now calculate the aspect ratio,

$$\mathfrak{R} = \sqrt{\frac{r_a^2}{r_r^2}} = \frac{1}{\lambda} \sqrt{\frac{1 + \omega_a^2 t^2}{1 + \omega_r^2 t^2}} \quad (1.48)$$

we see that it has the same form and the same asymptotic behaviour of equation (1.45): it goes to unity at long expansion times.

Consequences of the statistics on the scattering properties of the Fermi gas

So far we have derived the expressions for the main quantities of a gas composed by identical fermions, without considering any effect due to possible interactions

between fermion themselves. As we have shown in the previous section, identical fermions are always noninteracting, because, at this ultralow temperature, elastic collisions processes are forbidden for fermions in the same quantum state. In real experiment, this feature prohibits the direct cooling of fermions by means of the "standard" evaporative cooling technique. Therefore other techniques are performed for achieving the Fermi degenerate regime, such as mixing together two different spin states of the same atom [24], or mixing fermions with bosons and cooling indirectly the fermions through thermal contact with the other coolable specie [11; 28–30].

This *noninteracting* behaviour makes similar the Fermi gas to an ideal gas. Furthermore, the Fermi statistics and the Pauli exclusion principle deeply modify the dynamic processes in which particles are scattered from a degenerate Fermi gas. Consider, for example, a scattering process that produces a fermion with final momentum $k < k_F$: for low T/T_F all the momentum state inside the Fermi sphere are highly occupied and then this scattering event is likely to be suppressed. This phenomenon is known as Pauli blocking [41; 42]. The degree of the suppression depends from the degree of degeneration of the system (it is maximum for zero temperature) and from the energy of the scattered particle. G. Ferrari in [41] has proposed to study the relaxation in the motion of a test particle inside the Fermi gas showing that from this kind of measurement it could be possible to get information on the degeneration of the system. Indeed, the collisional rate is strongly affected by the Pauli blocking, resulting in to a decrease of the rate Γ of the collision. In particular, he have pointed out that a reduction of the collisional rate proportional to T^3 respect to the rate calculated for a classical gas should be observed: by measuring this behaviour, one could in principle determine in a direct and completely independent way the ratio T/T_F . In our experiment, we could see this effect of the statistics on the collisional properties of the Fermi gas, by studying the damping of the dipole oscillation between the Fermi gas of potassium atoms and a Bose-Einstein condensate of rubidium atoms (see 5.3.1).

Even the scattering of photons is predicted to be strongly influenced by the Pauli blocking. Several works [43–45] showed that Pauli blocking should cause a reduction of the width of absorbed light from a degenerate Fermi gas and a modification of the angular distribution of the scattered photons. If the recoil momentum of the incoming photon is less than the Fermi momentum k_F , atoms cannot find a free final state and then the scattering and the absorption mechanism is inhibited. In fact, this change in the absorption and then the consequent narrowing of the linewidth is difficult to observe in the experiment, because the density of a Fermi gas after during the expansion is too low, while the imaging in situ with resonant light is diffraction limited.

1.3.2 Properties of a Bose-Einstein condensate

Bose-Einstein Condensation (BEC) is the macroscopic occupation of a single quantum state [46–48]. When a system composed by N identical bosons reaches some critical value for some parameters (temperature and density), it collapses to a new state of the matter, in which each particle loses completely its identity. In this case, the whole system can be described by only one "macroscopic" quantum wavefunction, namely the *order parameter*.

In the case of neutral atoms, trapped in anisotropic potential, BEC shows up not only in the momentum space (as occurs in the homogeneous case), but also in the real space. Differently to what happens in the case of identical degenerate fermions that were completely noninteracting, the interaction between atoms in the condensate is one of the main feature and plays a relevant role in all the observed properties of such a system (for a complete review, see for example [4; 49]). In the following of this section we will discuss the principal characteristics of Bose Einstein Condensation in dilute gases, in particular analyzing the quantities that are usually investigated in the experiments.

The wavefunction describing a system composed by N identical bosons is symmetric under the exchange of two particles: the main consequence of this is that an arbitrarily large number of bosons can occupy the same energy level of the trapping potential. The energy distribution function for boson is thus given by [39]:

$$f_B(\epsilon) = \frac{1}{e^{\beta(\epsilon-\mu)} - 1} \quad (1.49)$$

where μ is the chemical potential. We note that, as for the Fermi distribution function, at high temperatures the (1.49) is approximately:

$$f_B(\epsilon) \simeq f_c(\epsilon) = e^{-\beta(\epsilon-\mu)} \quad (1.50)$$

i.e. the Boltzmann distribution (1.35). It is worth to define the fugacity $\Lambda = \exp(\beta\mu)$, by which (1.49) can be written as:

$$f_B(\epsilon) = \frac{\Lambda}{e^{\beta\epsilon} - \Lambda} \quad (1.51)$$

It is evident that $0 < \Lambda < 1$: if we assume that $\epsilon = 0$ is the energy of the ground state, then (1.51) becomes:

$$f_B(\epsilon = 0) = \frac{\Lambda}{1 - \Lambda} \quad (1.52)$$

that is the occupation number $f_B(\epsilon = 0)$ of the lowest energy level of the system can be quite large if the fugacity Λ goes to 1. It is possible to show that the mean occupation number of all the other energy states with energy bigger than zero cannot exceed a certain value fixed the temperature T [49]. This means that

all the other atoms that are added to the system must be arranged in the ground state, whose population becomes then macroscopically large.

For better understanding the physics of Bose Einstein condensation, it is convenient to start from the case of noninteracting bosons trapped in a harmonic potential, and then to switch to the interacting case.

The starting point is the relation that sets the critical values for the parameters for achieving degenerate regime,

$$n\lambda_{DB}^3 = \zeta(3/2) = 2.6 \quad (1.53)$$

where n is the density of atoms, while λ_{DB} is the deBroglie wavelength given by $\lambda_{DB} = (h^2/2\pi mk_B T)^{1/2}$, that gives the *quantum size* of a classical object. The equation (1.53) shows that when the mean interparticle distance $d \propto (n)^{-1/3}$ is bigger than the DeBroglie wavelength λ_{DB} then we lose completely the possibility of distinguish the particles, because the wavepackets associated to each atom start to interfere. The system must be described by quantum mechanics laws and in particular, in the case of N identical bosons by a single wavefunction. It is possible to show ([4]) that in the case of a cylindrical potential ($\omega_a = \lambda\omega_r$),

$$N - N_0 = \frac{\zeta(3)}{\lambda} \left(\frac{k_B T}{\hbar\omega} \right)^3 \quad (1.54)$$

where N_0 is the condensate fraction and $\zeta(x)$ is the Riemann function. If we set $N_0 = 0$, then we can obtain the expression for the critical temperature T_C :

$$T_C = \frac{\hbar\omega_r}{k_B} \left(\frac{N\lambda}{\zeta(3)} \right)^{1/3} = 0.94 \hbar\omega_r (N\lambda)^{1/3} \quad (1.55)$$

Combining equation (1.54 and 1.55) we get the T-dependence of the condensate fraction:

$$\frac{N_0}{N} = \left(1 - \frac{T}{T_C} \right)^3 \quad (1.56)$$

The wavefunction describing a noninteracting BEC trapped in a harmonic is simply the ground state wavefunction of such a potential, thus is a Gaussian, with width given by the harmonic oscillator length, $a_{ho} = (\hbar/m\omega)^{1/2}$. The width is independent from the number of atoms, N , while the central density (related to the modulus square of the wavefunction) turns out to be proportional to N .

The situation changes completely if we "turn on" the interaction between the atoms in the condensate. We must say that the dilute nature of these systems (the mean interparticle distance is almost ten times the range of the interatomic force), allows to describe the interaction between atoms by a single parameter, the s-wave scattering length, a . This means that for taking into account the interaction is "sufficient" to insert a mean-field potential inside the many body Hamiltonian, given by

$$U = \frac{4\pi\hbar^2 a}{m} n(\vec{r}) = gn(\vec{r}) \quad (1.57)$$

where we have defined the coupling constant $g = 4\pi\hbar^2 a/m$. We note that the sign of the scattering length gives the nature of the interaction. Indeed in case of positive sign of a , the interaction between atoms is repulsive, while it is attractive if $a < 0$. In the following we will consider always the case of positive a , in which the system is stable against collapse whatever is the number of particles inside the condensate ([50]).

In this mean-field approximation, the ground state of the system it is obtained by solving the following equation, the Gross-Pitaevskii equation (GPE):

$$\frac{\partial}{\partial t} \Phi(\vec{r}, t) = \left(-\frac{\hbar^2 \nabla^2}{2m} + V_{ext}(\vec{r}) + g|\Phi(\vec{r}, t)|^2 \right) \Phi(\vec{r}, t) \quad (1.58)$$

with $n(\vec{r}) = |\Phi(\vec{r}, t)|^2$. In this approximation is possible to write the wavefunction as $\Phi(\vec{r}, t) = \phi(\vec{r}) \exp(-i\mu t/\hbar)$ and the (1.58) as:

$$\left(-\frac{\hbar^2 \nabla^2}{2m} + V_{ext}(\vec{r}) + g\phi^2(\vec{r}) \right) \phi(\vec{r}) = \mu\phi(\vec{r}) \quad (1.59)$$

where μ is the chemical potential and must be normalized to the total number of atoms. The solution of (1.59) is particularly simple if the mean-field energy is larger than the kinetic energy (*Thomas-Fermi regime*):

$$n(\vec{r}) = \phi^2(\vec{r}) = g^{-1}[\mu - V_{ext}(\vec{r})] \quad (1.60)$$

Since the trapping potential is quadratic, the shape of the density profile is an inverted parabola, as observed in the experiments. The Thomas-Fermi (TF) approximation is valid only if $Na/a_{ho} \gg 1$, thus for large number of atoms. From the normalization on the number of atoms, it is possible to obtain the expression for the chemical potential μ :

$$\mu = \frac{\hbar\varpi}{2} \left(\frac{15Na}{a_{ho}} \right)^{2/5} \quad (1.61)$$

It is also possible to write down the expression for the radius of the condensate in the TF regime,

$$R_i = \left(\frac{2\mu}{m\omega_i^2} \right)^{1/2} \simeq a_{ho} \left(\frac{Na}{a_{ho}} \right)^{1/5} \quad (1.62)$$

The effect of the interaction is then to increase the size of the condensate respect to the noninteracting case and to give a dependence of the radius from the number of atoms. Furthermore, the value of the density in the centre of the trap is $n(0) = \mu/g$ and if we compare it with the one found in the noninteracting regime, we get:

$$\frac{n(0)}{n_{ho}} \propto \left(\frac{Na}{a_{ho}} \right)^{-3/5} \quad (1.63)$$

i.e. $n(0)$ decreases if N increase: this is another effect due to the repulsive interaction between the atoms in the BEC.

Expansion of a Bose-Einstein condensate

The last results have shown that the role played by the interaction in a degenerate gas of bosons is particularly important. But one of the most evident effect of the mean-field interaction is the ballistic expansion of a trapped Bose Einstein condensate [4]. By solving the hydrodynamic equations for the BEC [52], it is possible to find the dependence of the condensate's radii from the expansion time:

$$\begin{aligned} R_r(t) &= R_r(0)\sqrt{1+\tau^2} \\ R_a(t) &= R_a(0)(1+\lambda^2[\tau \arctan \tau - \ln\sqrt{1+\tau^2}]) \end{aligned} \quad (1.64)$$

where $\tau = \omega_r t$. The velocity of the expansion is determined from the initial confinement of the cloud. The most confined directions expand faster. Consider the GPE: the interaction term is density depend ($U = gn$) and in particular, if we consider $\nabla U \approx g\nabla n$ we see that the "force" acting on the atoms when the trapping potential is switched off, is proportional to the gradient of the density thus larger in the more confined direction.

This means that if the initial shape of the condensate is a cigar-like, as in our system, it first becomes spherical after an expansion time $\tau \propto 1/\omega_r$ and finally it inverts completely the shape becoming pancake shaped. This change in the ellipticity is a clear signature of the BEC regime.

1.4 Mean-field interaction in the mixtures

As we have seen in the previous section, the mean-field interaction plays an important role in the stability of a BEC, and many of the features of the condensate are strictly related to this interaction between the atoms [6]. On the contrary, due to the suppression of any collisional processes, the characteristics of a Fermi gas are determined only by the quantum statistics rather than a real interaction between the atoms.

The situation is quite different when we go to consider a mixture composed by different atoms. Indeed, in this case both the Gross-Pitaevskii and the Thomas-Fermi equations, which describe the Bose and the Fermi gas must contain an additional term of interaction between the atoms composing the mixture. This additional term is proportional to the interspecies scattering length a_{ij} and depending from its magnitude and sign the mixture will be stable or will collapse [17; 104].

Since in our experiments we have studied both mixtures composed either by two different bosonic species ^{87}Rb - ^{41}K or a boson-fermion mixture ^{87}Rb - ^{40}K [12; 15], in the following of this section, we will illustrate the main features of these systems and we will write the mean-field equations which describe them.

1.4.1 Bose-Bose quantum mixture

The equation that describes a Bose Einstein condensate is the Gross-Pitaevskii equation:

$$\left[-\frac{\hbar^2}{2m}\nabla^2 + U(\mathbf{r}) + g|\psi|^2 \right] \psi = \mu\psi \quad (1.65)$$

where the coupling constant g is related with the scattering length a :

$$g = \frac{4\pi\hbar^2 a}{m} \quad (1.66)$$

In our experiment we were able to bring to the degenerate regimes simultaneously potassium and rubidium atoms, producing a double BEC. The ground state of such a system can be obtained by solving a system of two coupled Gross-Pitaevskii equations for the individual condensate wave functions ψ_i [104]:

$$\left[-\frac{\hbar^2}{2m_1}\nabla^2 + U_1(\mathbf{x}) + u_{11}|\psi_1|^2 + u_{12}|\psi_2|^2 \right] \psi_1 = \mu_1\psi_1 \quad (1.67)$$

$$\left[-\frac{\hbar^2}{2m_2}\nabla^2 + U_2(\mathbf{x}) + u_{21}|\psi_1|^2 + u_{22}|\psi_2|^2 \right] \psi_2 = \mu_2\psi_2 \quad (1.68)$$

where as above:

$$g_{11} = \frac{4\pi\hbar^2 a_{11}}{m_1} > 0 \quad (1.69)$$

$$g_{22} = \frac{4\pi\hbar^2 a_{22}}{m_2} > 0 \quad (1.70)$$

$$g_{12} = 2\pi\hbar^2 a_{12} \left(\frac{m_1 + m_2}{m_1 m_2} \right)$$

are the coupling constants. Respect to the case of a single condensate, as we can see from equations (1.67) and (1.68), we have an additional term inside the GPE that describes the interaction between atoms belonging to different condensates with a coupling constant proportional to the interspecies scattering length a_{12} . As the stability of a single BEC is assured by the negative sign of the scattering length ($a_{ii} > 0$), so in the case of a mixture of two BECs, the stability of the system is strictly related to the magnitude and the sign of a_{12} to respect to the individual scattering lengths a_{ii} . Indeed, defining the quantity,

$$\Delta = \frac{g_{12}}{\sqrt{g_{11}g_{22}}} \quad (1.71)$$

the stability of this double degenerate sample is assured only if $\Delta > -1$. In fact, if $\Delta < -1$, the mean-field attraction between atoms of the two separate condensates would overwhelm the corresponding repulsion between atoms of the same specie, leading to an instability and then to the collapse of the whole system.

1.4.2 Fermi-Bose quantum mixture

The ground state properties of a degenerate system composed by a Fermi gas interacting with a Bose-Einstein condensate, trapped in a harmonic potential, is obtained solving the coupled equations [17] :

$$n_F(\mathbf{r}) = \frac{\sqrt{2m_F^3}}{3\pi^2} \left[\mu_F - U_F(\mathbf{r}) - \frac{4\pi a_{BF}}{m_{BF}} n_B(\mathbf{r}) \right]^{3/2} \quad (1.72)$$

$$\left[-\frac{1}{2m_B} \nabla^2 + U_B(\mathbf{r}) + \frac{4\pi a_{BF}}{m_{BF}} n_F(\mathbf{r}) + \frac{4\pi a_B}{m_B} \phi^2(\mathbf{r}) \right] \phi(\mathbf{r}) = \mu_B \phi(\mathbf{r}) \quad (1.73)$$

where $\phi_B(\mathbf{r}) = \sqrt{n_B(\mathbf{r})}$, $M_{BF} = 2m_F m_B / (m_B + m_F)$ is twice the reduced mass of the pair, and the coupling between bosons is as usual given by the s-wave scattering length a_B , that in the following we consider positive. By solving simultaneously the coupled equations (1.72,1.73), we obtain the density profile of the two species. As in the case of the Bose-Bose quantum degenerate mixture, the additional term $4\pi a_{BF}/m_{BF}$ which describes the interspecies interaction, is the key parameter for determining the stability or the instability of this system.

In particular, it is possible to consider two different situations, if the interaction between bosons and fermions is repulsive or attractive. In the first case $a_{BF} > 0$. This is the situation met in the experiments with the mixtures ${}^6\text{Li}$ - ${}^7\text{Li}$ [28; 29] and ${}^6\text{Li}$ - ${}^{11}\text{Na}$ [30]. In these systems, the repulsion between Bose and Fermi gas is likely to cause spatial separation between the two clouds, strongly limiting the efficiency of the cooling and the lower temperature achievable for the fermionic component [53; 54].

The situation is completely different if the interaction between the two species is attractive, as we find in the ${}^{40}\text{K}$ - ${}^{87}\text{Rb}$ mixture [55], [15]. Indeed, we do not have any phase-separation of the two components that remain in thermal contact even in the degenerate regime. Furthermore, if the density of the two species exceed a critical value, the system is no more stable and it collapses [17], [18]. Indeed, despite the repulsive interaction between bosons and the non-interaction between fermions themselves, the bosons-fermions interaction generates an attractive mean field for bosons proportional to the density of fermions and one for fermions proportional to the density of bosons. In this way, both the densities increases in the overlap region and if the strength of this attraction is sufficiently big, the system is no more stabilized by the kinetic-energy contribution due to the bare repulsions between bosons and it collapses. Roth and Fedelmeier [17] have found the expression for the critical density in the case of a symmetric trap:

$$N_{cr}^{1/6}(a_B, a_{BF}, l) = \frac{0.863}{|a_{BF}/l|^{0.281}} + \frac{0.087(a_B/l)^{1.91}}{|a_{BF}/l|^{3.49}} \quad (1.74)$$

where $l = (m\omega)^{-1/2}$ is the harmonic oscillator length.

1.4.3 BCS-like transition in a dilute mixture of fermions

At low temperatures, electrons in superconductor metals undergo a phase transition to the superfluidity state, characterized by frictionless flow. The same transition is expected to take place in a dilute gas of fermions at temperatures typically much lower than the Fermi temperature of the system [56]. In particular, superfluidity in a Fermi dilute gas requires an attractive interaction between fermions with opposite momentum. Differently from the case of BEC in which all the particles in the ground state participate to the superfluidity, in this case only atoms at the Fermi surface can form Cooper pairs at finite temperature, although at $T = 0$ the system is completely superfluid. At these ultralow temperatures, the pairing is achievable only through s-wave interaction [58] and consequently only between two different fermionic species or fermions in two separate and equally populated hyperfine levels. This requirement is particularly important, since a different population implies different Fermi energy between the "systems": if the difference between the two Fermi energies overcomes the typical energy gap Δ [56], then the pairing is prevented.

If all the conditions are satisfied, it is possible to show [57] that the critical temperature for BCS-like transition is given by:

$$T_C = \frac{2^{7/3}}{e} T_F e^{\left[\frac{-\pi}{2k_F|a|}\right]} \quad (1.75)$$

where $k_F = \sqrt{2mT_F/\hbar^2}$ is the Fermi momentum and a is the negative scattering length. In the dilute regime $k_F|a| \ll 1$ and then BCS transition temperature is much lower than the corresponding Fermi temperature, making the achievement of the pairing experimentally a difficult task. However, several theoretical schemes have been proposed in order to increase the critical temperature for BCS, by considering Feshbach Resonances coupling [60], [61], [62], [63], [64], [65], highly confining potential [66], and in the case of mixtures composed by bosonic and fermionic atoms, the attractive interaction between fermions induced by the presence of a Bose gas [67], [68].

In this last case, L. Viverit [19] have shown that the critical temperature for the formation of Cooper pair have the following behaviour:

$$T_C \propto T_F e^{1/\lambda} \quad (1.76)$$

where T_F is the Fermi temperature, while the parameter λ is directly related to the scattering length boson-fermion and it reads:

$$\lambda = \frac{(m_F k_F)}{2\pi^2 \hbar^2} U_{FF} \left[1 - \frac{U_{BF}^2}{U_{BB} U_{FF}} \right] \quad (1.77)$$

where $U_{BF} \propto a_{BF}$, $U_{BB} \propto a_{BB}$ and $U_{FF} \propto a_{FF}$. In the case of $U_{BF}^2/U_{BB}U_{FF} \gg 1$, the critical temperature for the pairing can be only a fraction of the Fermi temperature. In particular, in the case of ^{40}K and ^{87}Rb , due to the large and attractive

interspecies scattering length, we have that T_C can be of the order of the Fermi temperature, $T_C \simeq 0.1 T_F$.

CHAPTER 2

How to produce the mixtures

In this chapter we present the experimental apparatus we have used for the production and the characterization of the degenerate potassium-rubidium mixtures. We start by illustrating the general properties of these atomic species, pointing out which is the state of the art in cooling these atoms, especially in the case of potassium. We then describe the experimental set-up, giving particular attention to the laser sources and to the magnetic trap.

2.1 Potassium and rubidium atoms.

Potassium is an alkali atom and in nature it is present in three different stable isotopes, ^{39}K , ^{41}K and ^{40}K with natural abundance of 93.26%, 6.73% and 0.012% respectively. Two isotopes, the ^{39}K and the ^{41}K are bosons (nuclear spin $I = 3/2$), while the ^{40}K is a fermion (nuclear spin $I = 4$). Therefore potassium offers the unique possibility of studying both fermionic and bosonic isotopes and eventually of investigating the properties of Bose-Bose and Fermi-Bose mixtures.

In particular, we have decided to work with ^{41}K and ^{40}K , because the other bosonic isotope, the ^{39}K , has a negative scattering length that prevents the formation of a stable Bose Einstein condensate. Indeed, the potassium scattering lengths, expressed in Bohr radius unit (a_0), are the following: $a_{^{41}\text{K}} = 60 a_0$, $a_{^{39}\text{K}} = -44 a_0$ [69; 70] and finally $a_{^{40}\text{K}} = 174 a_0$ [70].

Also rubidium is an alkali metal and it is present in two stable bosonic isotopes, ^{85}Rb (72.2%), and ^{87}Rb (27.8%). ^{85}Rb is characterized by a negative scattering length $a = -10 a_0$, that does not allow the formation of a stable BEC, even if, by means of Feshbach resonances, it was possible to achieve stable ^{85}Rb BEC [7; 72].

Conversely, the ^{87}Rb has a positive scattering length $a = 99 a_0$ [71] and it was the first atom brought to quantum degeneracy in 1995 [1]. Differently from potassium, ^{87}Rb is an easily and efficiently coolable atom and this is the reason why we have decided to use it for the sympathetic cooling of K atoms.

Before describing our experimental apparatus, it is worth to remember briefly the history of the cooling of potassium atoms, since it is strictly related with the one of our experimental group of cold atoms in Firenze. To this purpose, following are reported some sentences taken from the contribution of our group to the "Enrico Fermi International School" (Varenna 1998) [5], from which it is possible to understand the motivations of our decision of choosing potassium among all the other alkali atoms: *"Therefore potassium offers the opportunity of investigating the properties of different bosonic isotopes, for which the different values of the scattering length and the possibility of observing Feshbach resonances were predicted, and eventually will allow the comparison of a Bose condensate with a degenerate Fermi gas. [...] An alternative is sympathetic cooling of the fermions by interaction with a sample of ultracold bosons atoms. The latter has been the leading idea of our experiment: achieving BEC for ^{39}K or ^{41}K and using sympathetic cooling to cool ^{40}K ."*

Indeed, the initial works [34; 73] on potassium were in the direction of the achieve-

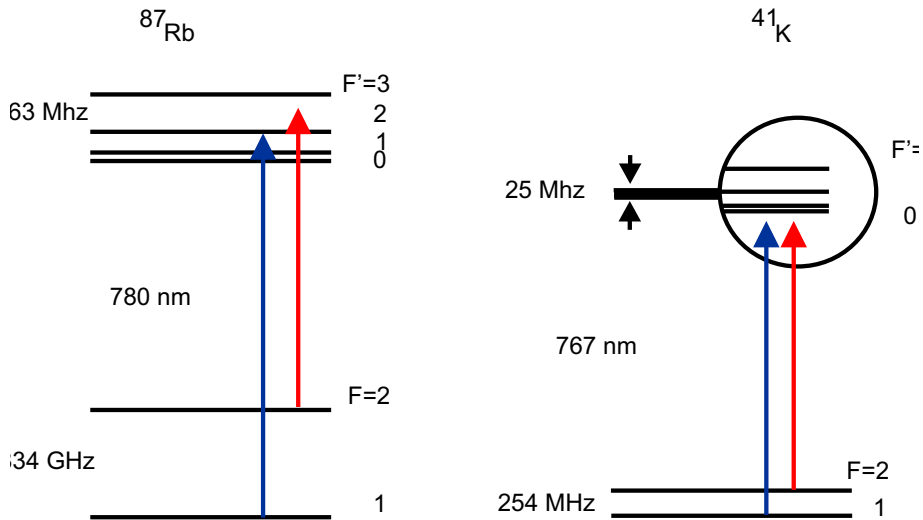


Figure 2.1: Level structure of ^{87}Rb and ^{41}K . In the case of potassium, the tiny spacing between the levels in the excited state, compared to the natural width of the line ($\Gamma = 2\pi \times 6.2 \text{ MHz}$) is the main cause of the inefficacy of the laser cooling.

ment of BEC for ^{39}K and ^{41}K . Very soon it was clear that reaching the degenerate regime for these two isotopes by means of the standard cooling techniques was not

an easy task and, on the contrary, it was not possible at all to reach Bose-Einstein condensation for bosonic K. The reasons of this difficulty is in the internal level structure of ^{41}K and ^{39}K . In Fig. (2.1) we show the levels structure of ^{41}K compared with the one of ^{87}Rb .

The internal states are labelled with F , where F is the total angular momentum of the atom $F = J + I$, with J total electronic angular momentum and I nuclear momentum. We also report the two optical wavelength used for laser cooling the atoms which corresponds to the D₂ line ($S_{1/2} \rightarrow P_{3/2}$ transition), with natural width $\Gamma_K = 2\pi \times 6.2$ MHz and $\Gamma_{Rb} = 2\pi \times 6.6$ MHz. As it is possible to see, the excited state of potassium shows a very tiny spacing between the levels, $\Delta\nu \sim 4\Gamma$. This feature is the main obstacle that must be overcome for cooling potassium. As reported in [34; 73] Sub-Doppler cooling does not work in the case of bosonic K. For this reason, the minimum temperature obtainable in the pre-cooling stage (essentially the magneto-optical trap MOT stage) is the Doppler temperature $T = 150$ μK . This limits also the maximum density of the sample before the transferring in the magnetic trap. Indeed the typical density obtained in the case of ^{41}K , at the end of the cooling stage, is $n = 2 \times 10^9$ at/cm³ [73]. It is worth to compare these values with the ones that we typically have in the case of rubidium atoms. Infact, we can load more efficiently Rb atoms in the magnetic trap, since the temperature after the compression is a few tens of μK (usually $T = 50$ μK), and the mean density is of the order of some parts in 10^{10} at/cm³.

On the other side, in case of potassium, the transfer in the magnetic potential results in a further worsening of the conditions for an efficient evaporative cooling: indeed an increase of the temperature to $T = 200$ μK is accompanied by a further decrease in the mean density of the sample $n \simeq 8 \times 10^8$ at/cm³. These parameters are not suitable for evaporative cooling, due to the lack in the elastic collisions caused by the low initial density of the gas.

These difficulties in reaching the degenerate regime by means of standard cooling techniques motivated our group to try a different cooling scheme: sympathetic cooling of bosonic potassium with rubidium atoms. As we will present in the next chapter, in this way we have overcome the intrinsic obstacles in cooling potassium and we have achieved Bose-Einstein condensation for ^{41}K atoms.

Also the history of ^{40}K is related with our group in Firenze. Indeed, the first magneto-optical trapping of ^{40}K was reported by F. Cataliotti et al. in 1998 [74]. In [74] they could observe a MOT of ^{40}K trapping almost 8000 atoms with a density of $\sim 10^8$ at/cm³, starting from a natural abundance sample. They have also had some preliminary evidence that the temperature of potassium, already in the MOT, was lower than the Doppler limit $T = 150$ μK , proving the efficacy of the standard laser cooling mechanisms that instead failed for the bosonic K. The future experimental strategies for trapping and cooling the fermionic potassium are presented clearly in the conclusions of that paper, in which the authors suggest two separate ways for achieving the degeneration regime for a sample of ^{40}K , the mixture of two internal states of potassium, and the sympathetic cooling with another atomic specie:

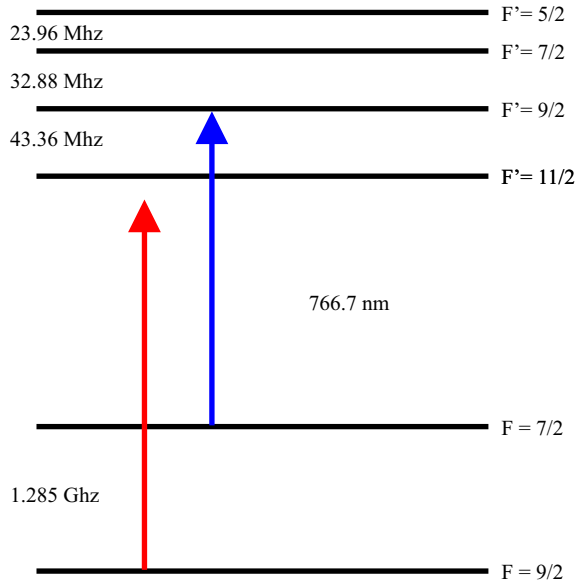


Figure 2.2: Level structure of ^{40}K . With respect to the structure of the boson ^{41}K the levels separation of the excited state is sufficient large and it is inverted. In this way, it is possible to have an efficient Sub-Doppler cooling.

” We are presently setting up an apparatus based on a double-MOT scheme. ^{40}K atoms will be collected in a first MOT and transferred in a second chamber where they can be accumulated.

... Further cooling can be achieved by simultaneously trapping ^{40}K and either ^{39}K and ^{41}K in a magnetic trap and using sympathetic cooling, or by producing coexisting ^{40}K subsystems in different hyperfine states. [...] Another possibility is sympathetic cooling ^{40}K with a different atomic species, such as rubidium, for which efficient evaporative cooling down to quantum degeneracy conditions is now a well-developed method.” This is exactly what was realized later in the experiment of D. Jin at JILA (^{40}K in two different hyperfine states) [24] and in our experiments in Firenze (sympathetic cooling with rubidium) [15].

The reasons why the fermionic potassium is more suitable for laser cooling essentially are found in the levels structure of the atom, shown in Fig. (2.2). Indeed, differently from ^{39}K and of ^{41}K , the hyperfine structure of the excited state is slightly larger and it is inverted. These properties allow the Sub-Doppler cooling mechanisms to work efficiently even in the MOT stage, as reported by our group in 1999 [75]. It follows that, as in the case of rubidium, we are actually able to load efficiently the cloud in the magnetic trap, typically $N \simeq 5 \times 10^5$ potassium atoms at $T \simeq 50 \div 70 \mu\text{K}$, corresponding to a density of the order of some parts

in 10^9 at/cm³.

However, as discussed in the previous chapter, identical fermions do not collide at this low temperature. In the case of ⁴⁰K, the group of D. Jin et al. could observe the suppression of the p -wave elastic cross-section [21] below 100 μ K, in a sample composed by potassium atoms all trapped in $|F = 9/2, m_F = 9/2\rangle$ state. The same group have overcome this limitation by trapping simultaneously a mixture of two spin states $|F = 9/2, m_F = 9/2\rangle$ and $|F = 9/2, m_F = 7/2\rangle$ and, by taking advantage of elastic collisions in s -wave between different atoms they could reach the degenerate regime for ⁴⁰K [24]. The higher degree of degeneration T/T_F they could achieve was $T = 0.25 T_F$, and it was limited by Pauli-blocking (see section 1.3.1) between the two degenerate components.

In our experiment we have decided to follow the second road proposed in [74], i.e. to achieve the degenerate regime for ⁴⁰K by sympathetic cooling with a different atomic specie, the ⁸⁷Rb. We can presently produce a Fermi gas of potassium interacting with a Bose condensate of ⁸⁷Rb [15]. Furthermore, due to the different cooling mechanism which does not exploit collisions between fermions themselves, we can measure temperatures for the fermionic component as lower as $T \simeq 0.2 T_F$.

2.2 Laser sources and experimental set up

2.2.1 General idea

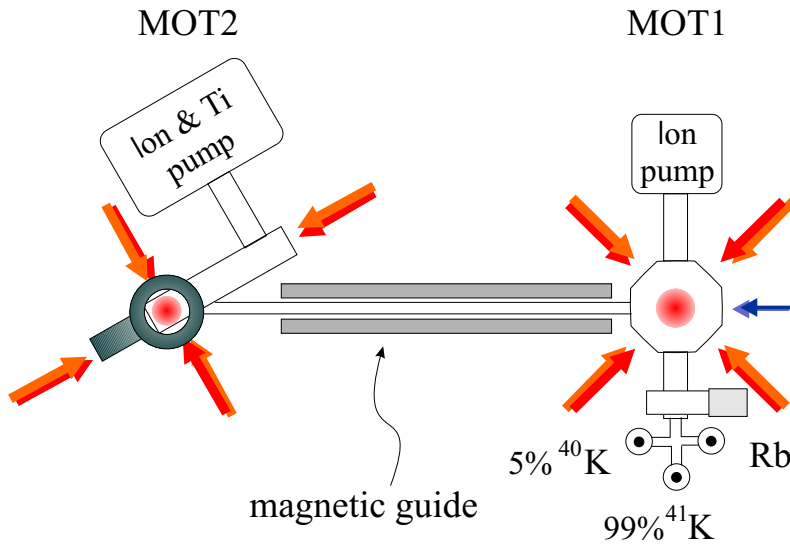


Figure 2.3: Experimental apparatus: atoms of both species are cooled and trapped in the first MOT and then transferred in the second MOT, where they are magnetically trapped. In the magnetic trap rubidium atoms are evaporatively cooled, while potassium sample is cooled to quantum degeneracy by means of elastic collisions with rubidium.

The aim of our experiment is to cool potassium by means of sympathetic cooling with rubidium atoms. To achieve this, we first cool and trap both atomic species in a standard double MOT system, schematically shown in Fig. (2.3) and then we transfer the cold samples in a magnetic trap where, by performing selective evaporative cooling on the rubidium component, we cool potassium atoms to the degenerate regime. The complexity of our apparatus is increased with respect to the standard single specie set-up by the fact that we have to trap and cool simultaneously two different atomic species. In particular, since the two optical transitions, necessary for the MOT stage are at 780 nm and at 766.7 nm for ^{87}Rb and ^{40}K respectively, we use three different laser sources for potassium and rubidium, as sketched in Fig. (2.4). In the case of rubidium, due to the large hyperfine splitting of the ground state ($\Delta\nu = 6.8$ GHz), we are forced to use two diode lasers at 780 nm, one operating on the repumper and the other on the cooling transition, while all the frequencies needed for manipulating potassium atoms are obtained by a single Ti:Sa laser.

The general laser scheme we use for producing the mixtures is presented in

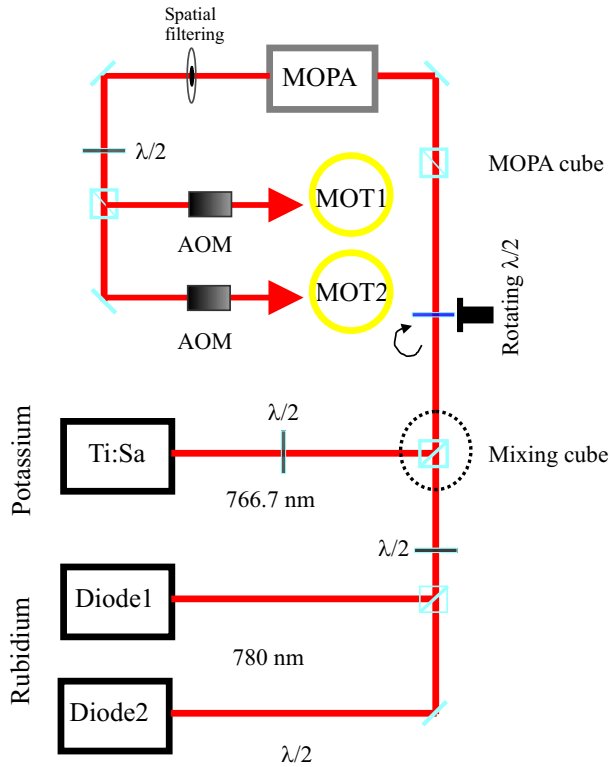


Figure 2.4: General scheme of the laser sources used for trapping simultaneously potassium and rubidium atoms.

Fig. (2.4). The general idea is to inject simultaneously the two frequencies of rubidium and the two of potassium in a semiconductor tapered amplifier (MOPA) that provides the necessary power for the two MOTs. In this way we have a complete spatial superposition between the potassium and rubidium beams before the two cells, facilitating the alignment of the two MOTs. We have the possibility of choosing the ratio between potassium and rubidium powers injected in the amplifier by electronically controlling a halfwave plate displaced in front of the MOPA, as shown in Fig. (2.4). The spatial mode of the beams after the MOPA is cleaned by a spatial filter, and we can control the fast switching of the two MOTs by means of two independent acousto-optic modulators (AOM).

In the following of this section, we are going to describe in more detail the two separate laser systems, starting from the one for rubidium atoms.

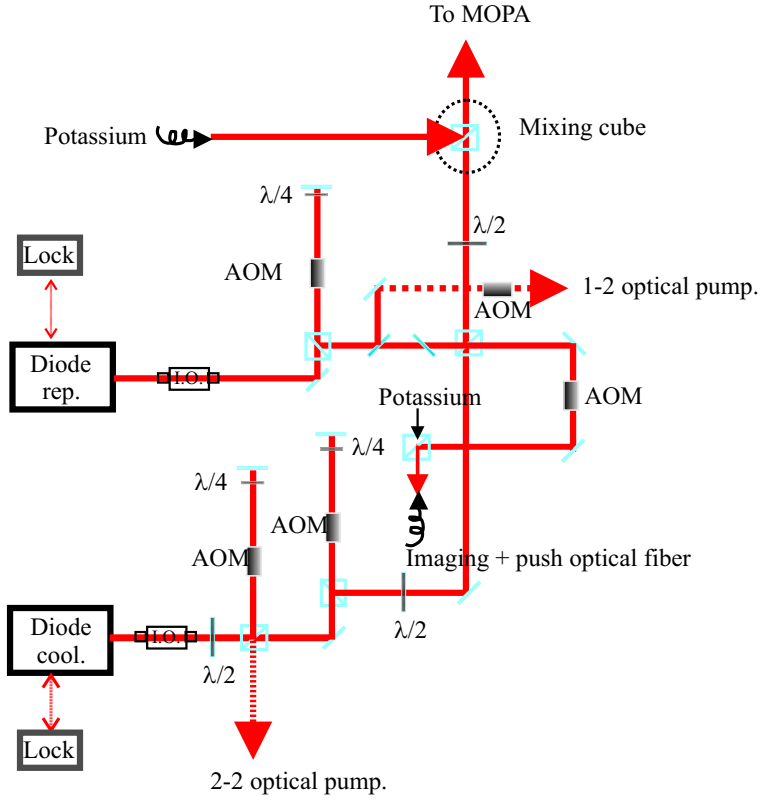


Figure 2.5: Laser set up for rubidium. The two frequencies at 780 nm needed for the MOTs stage are produced by means of two separate diode lasers.

2.2.2 Rubidium laser set-up

The detailed scheme of the rubidium laser system is shown in Fig. (2.5). As mentioned before, we used two different diode lasers for producing the two frequencies needed for the cooling of ^{87}Rb . Both diode lasers, home-made grating stabilized external cavity lasers, are locked to different atomic reference signals of ^{87}Rb by means of the standard *modulation transfer* technique [76]. The cooling light, exiting from the diode laser, is splitted in two part, whose power ratio is determined by a halfwave plate and by a polarizer beam-splitter. One part goes to generate the frequency resonant with the $F = 2 \rightarrow F' = 2$ transition needed for the optical pumping of rubidium, while the second one gives the frequency of the MOTs, red detuned respect to the $F = 2 \rightarrow F' = 3$ transition (the typical detuning is $\Delta \simeq -2\Gamma$, $\Gamma = 2\pi \times 6.6$ MHz). One part of this last beam is used alternatively for the production of the push beam (at -2Γ from $F = 2 \rightarrow F' = 3$ transition)

and for the imaging beam (resonant with the $F = 2 \rightarrow F' = 3$ transition), and it is injected in an optical fiber, in which it is mixed with potassium beams. The

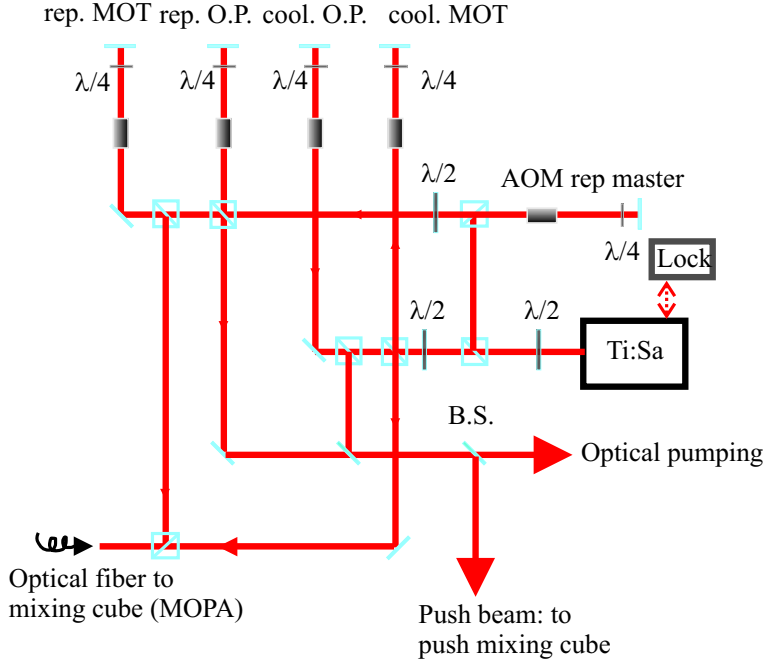


Figure 2.6: Laser scheme for producing the lights at 766.7 nm necessary for cooling potassium isotopes.

frequency of the repumper light, produced by a second diode laser, is resonant with the $F = 1 \rightarrow F' = 2$ transition. One part of the repumper beam is used for $F = 1 \rightarrow F' = 2$ transition (opportunistically controlled by an AOM) which is necessary for the optical pumping phase. Note the both the repumper and the cooling AOMs controlling the frequencies of the MOTs must compensate the frequency shift introduced by the AOMs controlling the switching of the MOTs and displaced after the MOPA. The MOTs cooling and repumping lights, with typical ratio between the two powers 3:1, are aligned in a polarizer cube and sent to the mixing cube in front of the MOPA where they are mixed with the potassium beams (see Fig. (2.4)).

2.2.3 Potassium laser set-up

In Fig. (2.6) we show the scheme used for generating the lights necessary for cooling potassium atoms. Differently from rubidium, the hyperfine splitting of the ground state is only 1.28 GHz so that we are able to produce all the frequencies

we need thanks to one single laser source, a home-made Ti:Sa, pumped by a doubled Nd:Yag (Millennia X, Spectra Physics) [75]. The frequency of the Ti:Sa is stabilized with respect to one atomic line of ^{39}K by means of standard saturated spectroscopy. In the following we consider both the cases of the boson ^{41}K and of the fermion ^{40}K . The beam exiting from the Ti:Sa laser is splitted in two parts, one for the cooling and the other for the repumping, with a controllable ratio typically of the order of 4:1. The cooling part is then divided in other two beams, one for the MOT and the other for the imaging, push beam and the optical pumping (see Fig. (2.6)). The cooling frequency for the MOTs is red shifted respect to the closed transition $F = 9/2 \rightarrow F' = 11/2$ (^{40}K), or $F = 2 \rightarrow F' = 3$ (^{41}K) with ($\Delta \simeq -3\Gamma$) and it is controlled by an acusto-optic modulator. The light for the imaging, is instead resonant with $F = 9/2 \rightarrow F' = 11/2$ (^{40}K), $F = 2 \rightarrow F' = 3$ (^{41}K), while the one for the push beam must be slightly blue shifted respect to $F = 9/2 \rightarrow F' = 11/2$ (^{40}K), $F = 2 \rightarrow F' = 3$ (^{41}K), and, at the end, the one for the optical pumping is resonant with $F = 9/2 \rightarrow F' = 9/2$ (^{40}K), or $F = 2 \rightarrow F' = 2$ (^{41}K) transition. We generate the frequency for the repumper with three different AOMs which produce the light resonant with the $F = 7/2 \rightarrow F' = 9/2$ (^{40}K) or $F = 1 \rightarrow F' = 2$ (^{41}K) transitions. Also in this case, we need to separately produce the light for the MOTs, and the ones used for the pushing and the optical pumping. In particular, the potassium pushing beam (in both cases, rep + cool.) is mixed with the one of rubidium inside a fiber. The cooling and the repumping light for the two MOTs are mixed inside a polarizer cube and then injected into the MOPA. As it was pointed out in the introduction of this chapter, the standard laser cooling techniques do not work properly in the case of ^{41}K . In particular, it is not possible to achieve in the MOT stage temperature lower than the Doppler temperature $T = 150 \mu\text{K}$, since Sub-Doppler cooling is not efficient. The frequency configuration by which we observe a more efficient cooling and a higher number of atoms captured in the MOT is when the cooling and the repumper light are separated by the hyperfine splitting of the ground state, 254 MHz. In this way [73] it is possible to achieve temperatures of the order of $200 \mu\text{K}$. In the case of the fermionic potassium the situation is completely different. Indeed we easily obtain in the MOT temperatures of the order of $50 \mu\text{K}$ much lower than the Doppler limit. This difference between ^{41}K and ^{40}K is one of the reasons why was easier to cool down "sympathetically" the fermionic potassium than the bosonic isotope. Indeed a lower initial temperature allows a better transfer in the magnetic trap and also a more efficient initial cooling with rubidium.

2.3 Experimental procedure

The four frequencies are simultaneously injected into the MOPA. As shown in Fig. (2.4), at the exit of the amplifier, the spatial mode of the beam is cleaned by means of a spatial filter (the pinhole radius is $50 \mu\text{m}$) and then the beam is splitted in two parts, for generating the different pairs of beams for the first and second

MOT. The final size of the each beam, set to 1.5 cm by different telescopes, is limited by the dimensions of the half and quarterwave plates placed in the set-up. In the case of the first MOT, we use two pairs of retroreflected beams along the $x - y$ spatial directions and two independent beams along the z direction (the direction of the gravity). The second MOT configuration is instead realized using 6 beams in all the three directions, whose intensity can be independently regulated by means of polarizing cubes and halfwave plates. Typically these ratios are set to maximize the loading of the MOT but also the *mode-matching* (see W. Ketterle in [5]) with the magnetic trap. For this reason, we can electronically control few halfwave plates of the second MOT, whose angle can be varied during the phase of the compression of the atoms inside the magnetic potential. In this way, by having a better overlap between the center of the MOT and the center of the quadrupole, we can increase the number of transferred atoms.

The first MOT is loaded by vapour background pressure (10^{-9} Torr) from metallic samples of ^{87}Rb , of bosonic ^{41}K (enriched to 99%) and of the fermionic ^{40}K (enriched to 5%). We typically are able to load in the MOT about 10^9 atoms of rubidium together with some 10^7 of ^{41}K or with some 10^5 of ^{40}K . The atoms are transferred in the second MOT where the vacuum is kept to 10^{-12} Torr, for limiting collisions with the background atoms, which would definitely reduce the lifetime of the trapped samples. As it is possible to see in Fig. .(2.3), the two cells are connected by a tube 30 cm long, in which is inserted a small $r = 4$ mm cylindrical tube (the *transfer tube*), which allows to maintain the differential vacuum between the two cells, controlled by two separate ion pumps.

We transfer the atoms of the two species from the first to the second MOT in two different ways. The loading of Rb is achieved by continuously pushing [77], [78] the atoms, while K atoms are transferred by pulsing the push beam. In the case of Rb the frequency of the pushing beam is on the red (2Γ) of the $F = 2 \rightarrow F' = 3$ transition and the typical power we use is around $400 \mu\text{W}$. In about 20 s of loading we are able to transfer and then to recapture in the second MOT about 10^9 Rb atoms at a temperature of $50 \mu\text{K}$.

In the case of K, we instead pulse the push beam on the first MOT every 200 ms, taking care the quadrupole field of the first MOT is switched off during each shot. Furthermore, we found that a better transferring is obtained when the power of the repumper light is reduced of about $1/3$ respect its usual value, and when the frequency of the cooling light is slightly more on the red respect to the MOT detuning. Differently from [79], we need both the frequencies (cooling and repumping light) in the push beam. The frequency of the cooling is almost resonant with the $F = 9/2 \rightarrow F' = 11/2$ (^{40}K), $F = 2 \rightarrow F' = 3$ (^{41}K), while the repumping is resonant with $F = 7/2 \rightarrow F' = 9/2$ (^{40}K), $F = 1 \rightarrow F' = 2$ (^{41}K) transitions. The typical power is about 1 mW: $600 \mu\text{W}$ are dedicated to the cooling component, and the remnant $400 \mu\text{W}$ to the repumper light. The potassium atoms travel in the transfer tube, guided by hexapole magnetic field (which does not affect the loading of rubidium) and they are recaptured in the second MOT. We can typically transfer about 10^6 atoms of ^{41}K and 10^5 atoms of

^{40}K , in about 10 s of loading. The push beam is focalized just before the second MOT, differently from the case presented in [77], [78]. However the continuous transferring of rubidium is not affected by this and it is still quite efficient.

We have experimentally found out that the best experimental procedure is to load separately potassium and rubidium atoms in the MOTs. Infact, we first inject inside the tapered amplifier almost only the rubidium frequencies loading in this way the two magneto-optical traps of Rb, then we add potassium atoms by injecting the potassium lights in the MOPA (the ratio between potassium and rubidium lights in this stage is about 10:1). In the case of rubidium the total power we typically measure after the spatial filter is about 200 mW, whose 60 mW are dedicated to the first MOT and 70 mW to the second one, while for potassium we use about 240 mW divided in 70 mW and 80 mW for the first and the second MOT respectively.

It is important to note that during the loading of potassium, we have two different situations, when we work with the boson ^{41}K or with the fermion ^{40}K . As said, we can select the ratio between the different frequencies we inject in the MOPA. During the loading of rubidium, we have less than 5 % of the potassium light in the amplifier, and the contrary occurs when potassium is loaded. In the case of the pair ^{41}K - ^{87}Rb during the loading of potassium we have losses (that can be of even 50%) in the rubidium sample which are caused essentially by nonlinear processes in the tapered amplifier when K-Rb frequencies are both injected. Indeed, we observe sidebands on the cooling light of rubidium ($|F = 2\rangle \rightarrow |F' = 3\rangle$). Since the hyperfine splitting of potassium ground state is 254 MHz, one of these sidebands is resonant with the $|F = 2\rangle \rightarrow |F' = 2\rangle$ transition of rubidium, reducing the efficiency of the rubidium MOT. In case of the ^{40}K - ^{87}Rb mixture, since the ground state splitting of K is 1.285 GHz, we do not observe any losses in the rubidium MOT when also the potassium light is injected in the MOPA.

2.3.1 Magnetic trapping of the mixture

Evaporative cooling is the only technique by which it is possible to achieve high density and the ultracold temperatures which are the necessary conditions for quantum degeneracy in a dilute gas. The first requirement of evaporative cooling is the trapping of the atoms in a conservative potential, in which to start to perform the evaporation. To this purpose, it is possible to confine the atoms either in a far-detuned optical trap, or in a pure magnetic trap. The main feature of the optical potentials is that they can be almost spin-independent, in the sense that all the internal Zeeman sublevels of the atoms can be trapped. By playing with the geometrical configuration and with the parameters (intensity and detuning) of the laser beams, it is possible to achieve high confinement and thus high density of the sample. However, the fact that the optical trap is insensitive to the internal state of the atoms has a drawback: it is not possible to remove selectively atoms from the confining potential by inducing transition to untrapped states by means of

some external e-m field. This means that for forcing the evaporation of the atoms, the only solution is to slowly open the confining potential, allowing the escape of the most energetic atoms. Despite of many attempts only in few experiments [80], [10], it was possible to achieve the BEC regime. Their success is due to the particularly high phase-space density they can obtain during the loading of the atoms in the tight optical potential.

Magnetic potential are instead selective in the internal Zeeman state of the atoms. In this case, as briefly reported in section (1.2.1), it is possible to write the interaction energy between the atomic magnetic moment and the external field is as

$$U(\vec{r}) = m_F g_F \mu_B B(\vec{r}) \quad (2.1)$$

where m_F is the projection of the quantum angular momentum, g_F is the Lande' factor and μ_B is the Bohr magneton. The atoms are trapped in a minimum of the field only if this interaction energy increases when the magnitude of the magnetic field increases. In other words only the magnetic states that have magnetic moments antiparallel respect to the direction of the field can be trapped. The states which have this property are named low-field seekers. For this reasons the sample must be completely polarized before transferring it into the magnetic potential. This optical pumping phase is particularly important in the experimental procedure, since it determines the effective number of atoms which are available for the evaporation. In the case of the mixtures it results even more crucial, since a non perfect polarization can lead to large losses in the sample. The minimum of the magnetic field that the atoms see must be different from zero (see W. Ketterle *et al.* in [5]). Indeed crossing the region of weak and zero magnetic field the atoms make a transition to untrapped states and they are lost from the trap (*Majorana spin flips*). Many different geometrical configurations have been proposed and realized so far [5] in order to avoid this losses and create the optimized conditions for the trapping.

In our case we have decided to work with a very simple and compact coils configuration, first realized by T. Esslinger [81], and that it is named QUIC (Quadrupole Ioffe-Pritchard Configuration). As shown in Fig. (2.7) it consists of three coils, two of which generate the quadrupole field needed for the MOT stage (Anti-Helmoltz configuration) and a third one (pinch coil) which is orthogonal to the quadrupole axis. The axial field generated by the pinch coil is in the opposite direction with respect to the radial field of the quadrupole, giving rise to a harmonic potential which presents a minimum different from zero, spatially separated with respect to the quadrupole axis. In particular, in our case, the minimum of the field B_0 (*bias field*) is about 1 Gauss and it can be experimentally varied by changing the distance between the pinch coil and the center of the quadrupole or by adding an external magnetic field. One of the main advantage of this kind of trap is that is particularly compact and it can be fed with low current. Indeed, we have found that an excellent operation is obtained with a current flow of 30 A, which corresponds to a dissipated power of about 900 Watt. However for avoiding not desired

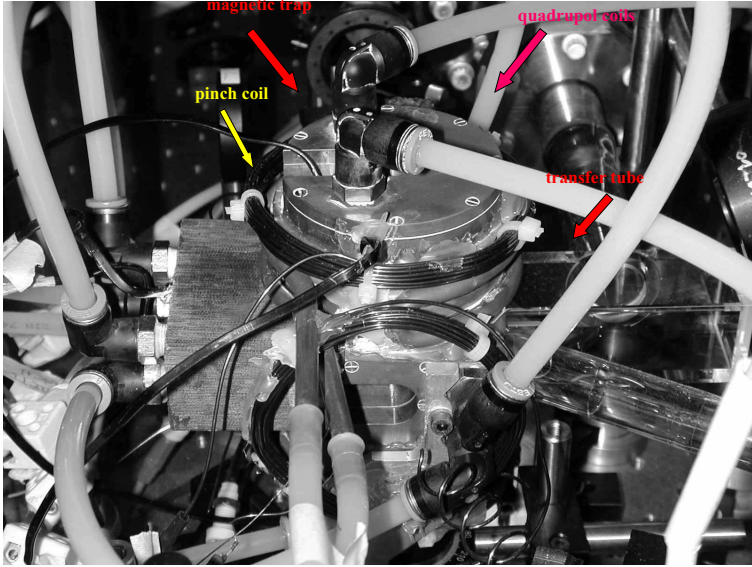


Figure 2.7: Picture of the QUIC trap used in the experiment.

heating, every coil is water cooled. The experimental procedure for transferring the atoms in the QUIC trap is controlled by the circuit shown in Fig. (2.8). During the MOT stage the current can flow only in the quadrupole circuit, keeping closed both IGBT quic and IGBT quad and open IGBT pinch. Then, before transferring the atoms in the QUIC, we compress the atoms in the quadrupole ramping the current to 30 A. Then we slowly close the IGBT pinch while slowly opening the IGBT quad. The duration of this procedure, which can last from 500 to 800 ms, gives the velocity by which we transfer the atoms from the quadrupole trap to the final magnetic trap. At this point the polarized atoms (see next paragraph) are magnetically trapped in the QUIC.

This field geometry generates a cylindrical magnetic potential with the weak axis directed along the pinch direction (the weak-axis of the trap). The expression for the magnetic potential near the minimum is given by:

$$U(z, r) \simeq \mu \left[B_0 + \frac{1}{2} B'' z^2 + \frac{B'^2}{2B_0} r^2 \right] \quad (2.2)$$

From (2.2), it is possible to derive the expressions for the oscillation frequencies of the trap, related to the curvature B'' , to the gradient B' and to the bias field B_0 by:

$$\omega_z = \sqrt{\frac{\mu B''}{m}} \quad \text{and} \quad \omega_r = \sqrt{\frac{\mu B'^2}{m B_0}} \quad (2.3)$$

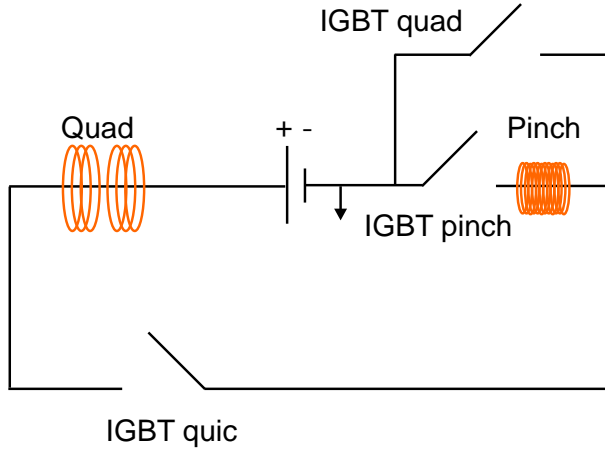


Figure 2.8: Scheme for controlling the QUIC trap

In our case, the bias field is $B_0 \simeq 1$ Gauss, the gradient is $B' \simeq 170$ Gauss/cm, while the curvature is $B'' \simeq 240$ Gauss/cm². The trap frequencies that we have measured $\omega_z \simeq 2\pi \times 16.3$ Hz and $\omega_r \simeq 2\pi \times 197$ Hz in the case of rubidium, and $\omega_z \simeq 2\pi \times 23.7$ Hz and $\omega_r \simeq 2\pi \times 286$ Hz in the case of potassium are in agreement with the prediction of (2.3). The difference between the oscillation frequencies of K and Rb is due to the different masses of the two atoms (the ratio between the frequencies scales as $\sqrt{m_{Rb}/m_K}$). We also note that the radial frequency is directly related with the bias field, $\omega_r \propto 1/B_0^{1/2}$. We can vary the value of B_0 by means of extra-coils and in fact we will use this feature for parametrically heat the atoms in the trap. The magnetic trap is switched off by opening the IGBT quic in a time of the order of some μ s. Before setting the magnetic trap in its ultimate position, near the glass cell, we have checked for the presence of eddy currents after the switching of the field. In fact we did observe some residual current which were responsible of a delay in the switching off of the magnetic field of some ms. By replacing the copper support of our pinch coil with one done by bakelite, a good thermal conductor but still good electrical insulator, we are now able to switch off completely our magnetic field in about 100μ s.

2.3.2 Optical pumping procedure

Before to be transferred in the magnetic trap, the atoms must be polarized in the low-field seekers sublevels which are efficiently trapped in the magnetic potential. In our experiment, we must distinguish two different situations, the ^{41}K - ^{87}Rb mixture and the ^{40}K - ^{87}Rb mixture.

In the first case, the nuclear spin is $I = 3/2$ for both potassium and rubidium, thus the Zeeman structure of these atoms is the same. We have decided to trap both potassium and rubidium in the $m_F = 2$, $F = 2$ state which is the state more coupled to the magnetic field. For preparing the mixture in this specific

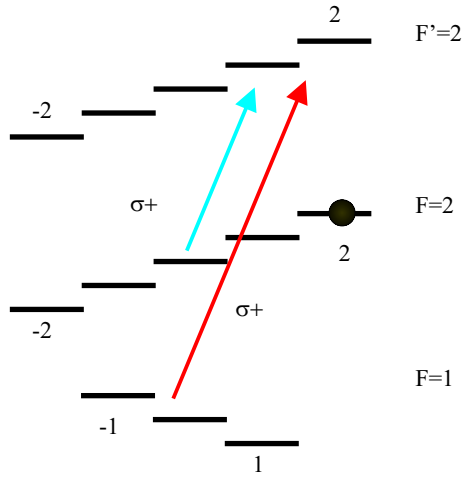


Figure 2.9: Scheme of the optical pumping procedure in the case of ^{41}K - ^{87}Rb . The atoms are polarized in the $|F = 2, m_F = 2\rangle$ state. Rb Zeeman levels structure is shown.

Zeeman sublevel, we use an optical pumping phase (OP) which is performed by applying to the sample pulses of light with opportune polarization and frequency. The atoms initially trapped the MOT are almost equally distributed in all the Zeeman sublevels of the $F = 2$ state. Consequently, without the optical pumping phase, we would trap in the magnetic trap in the $|F = 2, m_F = 2\rangle$ state only about $1/5$ of the total number of atoms. The experimental procedure for the OP phase is the following (see Fig. (2.9)). We start with the samples trapped in the magneto-optical trap then we switch off both the MOT gradient and the MOT laser beams and we apply an opportune bias magnetic field (some Gauss) which defines the polarization axis for our atoms. At this point we shine simultaneously two short light pulses polarized σ_+ polarization, one in resonance with the transition $F = 2 \rightarrow F' = 2$ and the other with $F = 1 \rightarrow F' = 2$. The length of the two pulses is slightly different and it is optimized in the experimental running. Typically the $F = 2 \rightarrow F' = 2$ pulse lasts hundreds of μs , while the second one can last even

some ms. The power of these beams is approximately 150 μW and 100 μW respectively. All the parameters (bias magnetic field, intensity and frequencies of the beams) are directly set by improving the number of atoms trapped in the QUIC trap.

In the case of the ^{40}K , the situation is different, since the nuclear spin is $I = 4$. This implicates that there are more Zeeman sublevels trappable for both the $F = 7/2$ and $F = 9/2$ states. In our situation, we trap potassium atoms in the level $|F = 9/2, m_F = 9/2\rangle$ which corresponds to the maximally coupled state. For getting the fully polarized sample, we proceed as before with two pulses resonant with the $F = 9/2 \rightarrow F' = 9/2$ and $F = 7/2 \rightarrow F' = 9/2$ transitions and polarized σ_+ . In the case of a mixture composed by different atomic species, the importance of an effective optical pumping is not only a better transfer of the cold sample into the magnetic potential, as it occurs for single species, but it also affects the efficacy of the sympathetic cooling.

Consider indeed the specific case of trapping potassium ^{41}K and ^{87}Rb atoms. As mentioned above, in this case both atomic species are simultaneously trapped in the stretched state $|F = 2, m_F = 2\rangle$ state. In the magnetic trap, if the system is completely polarized, the only collisional process which involve one potassium and one rubidium atom is: $|2, 2\rangle_{\text{Rb}} + |2, 2\rangle_{\text{K}} \rightarrow |2, 2\rangle_{\text{Rb}} + |2, 2\rangle_{\text{K}}$. This kind of collisions is completely elastic, i.e. the internal state of the atom does not change during the collisions. For this reason it does not lead to any losses. Suppose now that, due to an imperfect OP phase, we have some residual rubidium atoms in the trappable state $|2, 1\rangle$ (the same in the case of potassium, but in our particular case, since the number of rubidium atoms loaded in the magnetic trap is much bigger than the potassium one, this effect is negligible). The collisional process $|2, 1\rangle_{\text{Rb}} + |2, 2\rangle_{\text{K}}$ is no more completely elastic. Indeed, since only the total m_F must be conserved during the collisions, more than one final channels for this collisional process exists. For example, after the collision, the rubidium atom can be transferred in the $|1, 1\rangle$ state of the ground state. The hyperfine splitting energy between the $F = 1$ and $F = 2$ levels of Rb (~ 6.8 GHz) is likely to be stored by potassium and the rubidium atoms as kinetic energy, causing big losses in the sample. This specific losses processes take name of *hyperfine changing collisions* and in the experiment we have determined the rate at which they occur [55]. The same inelastic process is likely to happen in the mixture ^{40}K - ^{87}Rb , if the sample is not initially perfectly polarized in the $|2, 2\rangle_{\text{Rb}} + |9/2, 9/2\rangle_{\text{K}}$ states.

2.3.3 Imaging the atoms

The optimization of most of the experimental parameters is done by looking at the number of atoms loaded in the MOTs, that we measure from their fluorescence. We can monitor the shape of both the MOTs by means of two cheap CCD cameras, while for estimating the number of atoms we use two calibrated photodiodes. Once the atoms are in the magnetic trap, we determine their number and their temperature by using a standard absorption imaging technique. Through a system

of lenses, we image the shadow of the trapped cloud on a resonance probe beam on a CCD camera. In fact, after the switching off of the magnetic trap, we let the atoms expand for a suitable time for avoiding problems related with the high density of the sample. From the analysis of these images, we can extract all the interesting physical properties of the system, such as density and momentum distribution. Indeed, the relation between the intensity of the laser beam and the density of the atomic sample is given by:

$$I_T(x, z) = I_0(x, z) \exp\left[\sigma \int dy n(x, y, z)\right] \quad (2.4)$$

where n is the atomic density, σ the cross section for the absorption and the integration is along the beam direction. The quantity $\sigma \int dy n(x, y, z)$ is called optical density (OP) of the system and it is what is directly measured in the experiment. The experimental procedure for measuring the optical density of the cloud is the following: we first take an image without any light going on to the CCD camera (background image (I_b), it takes into account the intrinsic noise of the camera). Then we take the image with atoms (signal image, I_T), and at the end a third image without atoms (reference image, I_0). The optical density is given by:

$$OP = -\ln \frac{I_T - I_b}{I_0 - I_b} = \sigma \int dy n(x, y, z) = n(x, z) \quad (2.5)$$

Our CCD camera is produced by Theta System and it is based on a frame transfer

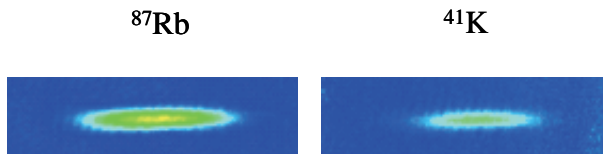


Figure 2.10: Simultaneous images of potassium and rubidium atoms after 200 μ s of ballistic expansion. Note how the shape of the clouds reflects the cylindrical symmetry of the trapping potential.

chip composed by 1024×1024 pixels with dimensions $7.5 \times 7.5 \mu m$. The optical system we use for imaging the atoms into the CCD is composed by two lenses that give an overall magnification factor of 1.75. We have directly measured the magnification by studying the ballistic trajectory of the released rubidium BEC trapped in the magnetic field independent state $m_F=0$.

Since the optical transitions of potassium and rubidium are ~ 13 nm apart, it is possible to image simultaneously the two clouds without affecting the other one. In order to do that, we first shine a short pulse (40 μ s) of potassium light resonant with $F = 9/2 \rightarrow F' = 11/2$ (^{40}K) or $F = 2 \rightarrow F' = 3$ (^{41}K). The CCD, externally controlled by a TTL trigger, starts to transfer the image in the dark region of the

chip: at this point we flash the rubidium light resonant with the $F = 2 \rightarrow F' = 3$ transition imaging also the rubidium cloud. The delay between the two pulses is determined by the requirement of two spatially separate images of the two clouds and it typically ranges between hundreds of μs and some ms.

Sympathetic cooling of potassium and K-Rb interactions

In this chapter we show the effectiveness of the sympathetic cooling technique between potassium and rubidium atoms. In particular, we present the results that we have obtained in the case of the boson-boson mixture composed by ^{41}K - ^{87}Rb atoms. By means of elastic collisions with the evaporatively cooled rubidium, it has been possible for the first time to reach Bose-Einstein condensation in a sample of potassium atoms. We have deduced, through accurate collisional measurements, the interaction properties of all the potassium-rubidium isotopic pairs.

3.1 Evaporative cooling of rubidium atoms in the mixture

The aim of this experiment is to cool down potassium by means of sympathetic cooling with rubidium: once the atoms of both species are trapped in the magnetic potential, evaporative cooling is selectively performed only on the Rb component, leaving the K atoms to be cooled by this thermal bath of rubidium. In most of the experiments, the evaporation is performed by coupling the trapped state to untrapped ones by means of an RF field, since the typical Zeeman splitting between the levels is of the order of tens of MHz for the typical value of magnetic field (B_0 of the order of few Gauss).

In our specific situations, however, this is not always the case. For understanding this point, it is necessary to distinguish the two different situations we have dealt in the experiments, schematically sketched in Fig. (3.1). The first case is the mixture composed by ^{41}K - ^{87}Rb atoms. These two species have the same nuclear spin, thus the same Zeeman structure. For this reason it is not possible to proceed with the evaporation of the rubidium atoms by means of the standard RF coupling since,

also the potassium atoms would be removed from the trap. The evaporation

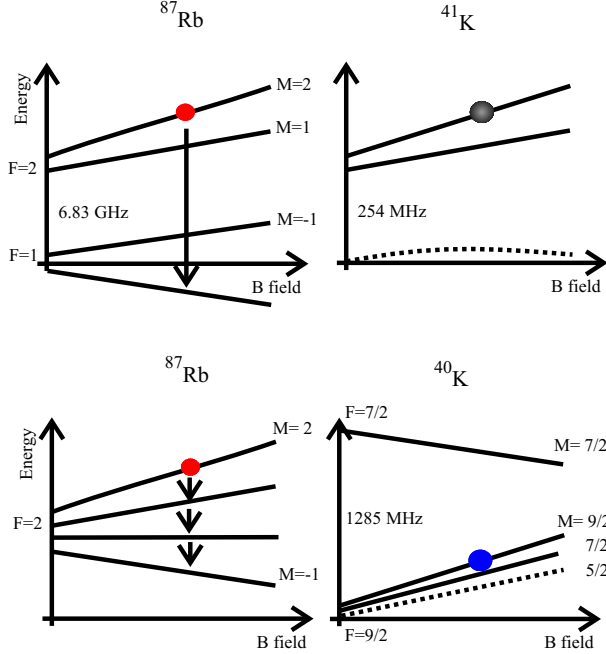


Figure 3.1: Evaporation schemes for potassium rubidium mixtures. In the case of ^{41}K - ^{87}Rb , the atoms of both species are optically pumped in the $|F = 2, m_F = 2\rangle$ states. However, due to the same Zeeman structure, the evaporation of rubidium is performed by means of μ -wave knife at 6.8 GHz. In the other case, ^{40}K atoms are pumped in the $|F = 9/2, m_F = 9/2\rangle$ state, while rubidium ones, trapped in the $|F = 2, m_F = 2\rangle$ state, are evaporated from the trap by RF knife.

of Rb is then performed by using a μ -wave knife at 6.8 GHz, that couples the $|F = 2, m_F = 2\rangle$ state with the untrapped $|F = 1, m_F = 1\rangle$ state of the ground state. The ^{40}K - ^{87}Rb mixture is easier to handle, since the two Zeeman structures are completely different. It is therefore possible to evaporate rubidium atoms with a standard RF knife, that couples the various Zeeman sublevels of the $F=2$ hyperfine level of Rb.

In the following of this chapter we will discuss the property of the ^{41}K - ^{87}Rb mixture, that was the first studied in our experiment.

3.1.1 Cooling the potassium atoms to quantum degeneracy

After being optical pumped in the $|2, 2\rangle$ state, potassium and rubidium atoms are trapped in the magnetic trap, where the evaporative cooling on Rb is performed.

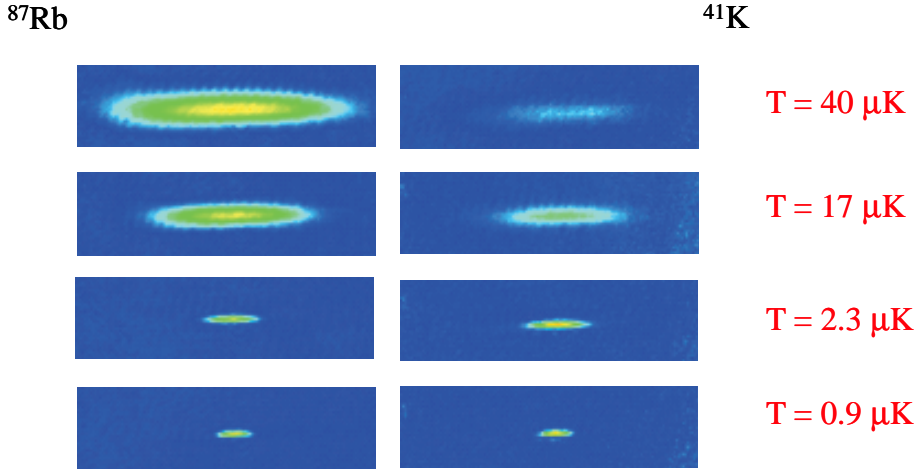


Figure 3.2: False colour absorption images of potassium and rubidium in different stages of the evaporation ramp. The density of potassium increases lowering the temperature, while the rubidium one remains almost constant during all the evaporation.

The typical number of atoms we can load inside the QUIC trap is 2×10^8 and 2×10^6 for Rb and K respectively. The temperature of both species is quite high, ranging from 200 to 300 μK , essentially due to the heating during the compression phase in the quadrupole. In Fig. (3.2) we show the simultaneous images of potassium and rubidium taken at different stages of the μ -wave evaporation.

We do observe a strong increase of the density of potassium, while decreasing the temperature of the sample from 40 μK to 900 nK: indeed we measure an increase of more than two orders of magnitude during the evaporation going from $4 \times 10^9 \text{ cm}^{-3}$ to $6 \times 10^{11} \text{ cm}^{-3}$. In Fig. (3.3a) we report the evolution of the temperature of the potassium and rubidium versus the microwave cut. During all the evaporation ramp the potassium and rubidium temperatures remain always the same, indicating that potassium atoms are really efficiently cooled by the thermal contact with rubidium. The efficacy of sympathetic cooling is the direct consequence of the large interspecies interaction between ^{41}K - ^{87}Rb atoms. In Fig. (3.3b) we show the evolution of the numbers of atoms during the evaporation ramp. The population of rubidium decreases as expected and we can note some losses also in the potassium essentially due to some inelastic processes, probably depending from the high densities of both the samples. If we now look more in detail at Fig. (3.3) we see that when the number of K and Rb atoms become comparable, the efficiency of the cooling is reduced. Indeed, when the two populations become similar then also the thermal capacities do the same and consequently the efficacy of the sympathetic cooling is likely to be smaller (see section 1.2.2).

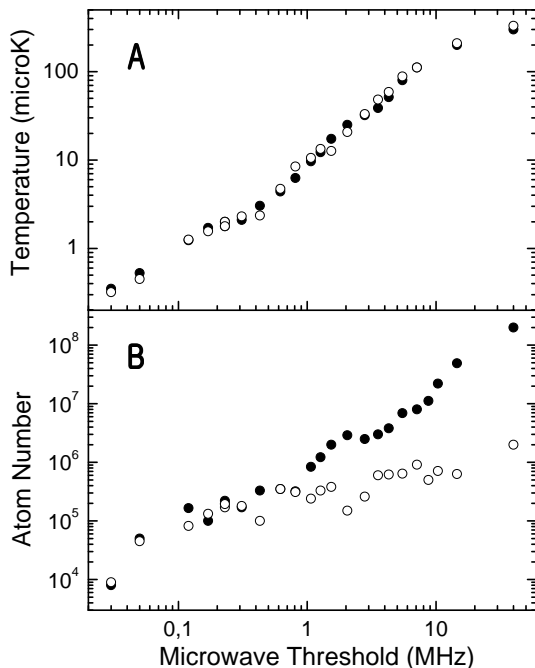


Figure 3.3: Evolution of the temperature (a) and of the number of atoms (b) of potassium (o) and rubidium (●) as a function of the μ -wave cut of Rb.

However, if we now evaporate more deeply the rubidium distribution we finally achieve the Bose-Einstein condensation for ^{41}K [11]. We have experimentally found that the evaporation ramp by which it is possible to achieve the potassium BEC has to be essentially composed by two parts. In the first stage we are forced to evaporate rapidly the rubidium atoms in order to eliminate some residual population of Rb trapped in the $|2, 1\rangle$ state which induces large losses in the potassium sample (see also 4.1). When the temperature of both species is below the microKelvin, we instead have to decrease the rate of evaporation since the number of atoms and thus the thermal capacities of K and Rb become more comparable. The typical duration of the ramp is about 50 s.

In Fig. (3.5) we report the density profiles of the potassium sample crossing the transition temperature T_C . The critical temperature $T_C = 150nK$ is determined by fitting with Gaussian the thermal wings of the bimodal distribution. The condensate fraction is instead reproduced by an inverted parabola, solution of the GPE equation in the Thomas-Fermi approximation (1.3.2). The typical number of atoms in the condensate is about $N = 10^4$. By plugging the detected number of atoms in the BEC and our experimental parameters in the relation:

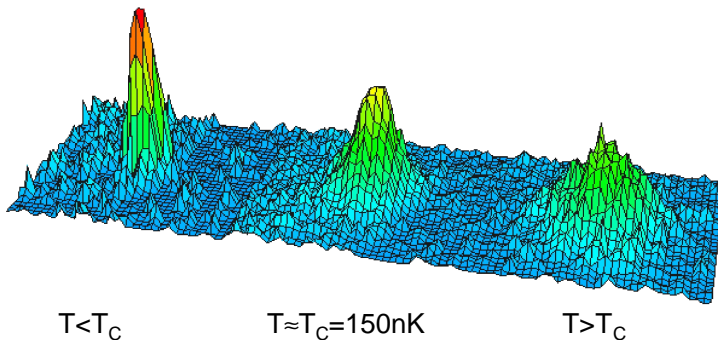


Figure 3.4: False colour density profile of the ^{41}K cloud after 15 ms of ballistic expansion. From right to left we can observe the transition from a thermal gas at $T > T_C$, to a partially condensed sample at $T \simeq T_C$ and to a pure potassium BEC at $T < T_C$. The critical temperature, $T \simeq 150$ nK, is determined by fitting the thermal wings of the bimodal distribution.

$$T_C = \frac{\hbar\varpi}{k_B} (N/1.202)^{1/3} \quad (3.1)$$

we find $T_C = 160$ nK, in good agreement with the measured value. When potassium reaches the degenerate regime, Rb is completely evaporated. In fact the first achievement of potassium BEC was possible thanks to the inelastic losses which, at very low temperature (see Fig. (3.3)), reduce the number of K atoms. Indeed if this did not occur, when the number of potassium and rubidium atoms becomes similar, sympathetic cooling would have not been efficient and the temperature of K would have not been decreased further. The lifetime of the condensate of K is about 500 ms, the same than the lifetime of our Rb BEC. It is limited by the background heating in the magnetic trap, 100 nK/s.

3.2 Measuring K-Rb ultracold interactions

In the first chapter of this thesis, we have discussed the collisional properties of a dilute system composed by atoms at ultralow temperature. The main result we have found out was that, when the temperature of the sample is sufficiently low (tens of μK), all the interactions properties can be completely described by a single parameter, the scattering length a . Indeed, the magnitude of the scattering length gives the strength of the interaction, since the collisional cross-section is simply $\sigma \propto a^2$. The knowledge of the interaction properties of atoms of the same alkali specie was the subject of an intensive study in these last ten years, both theoretically and experimentally [82]. Particularly important is the possibility

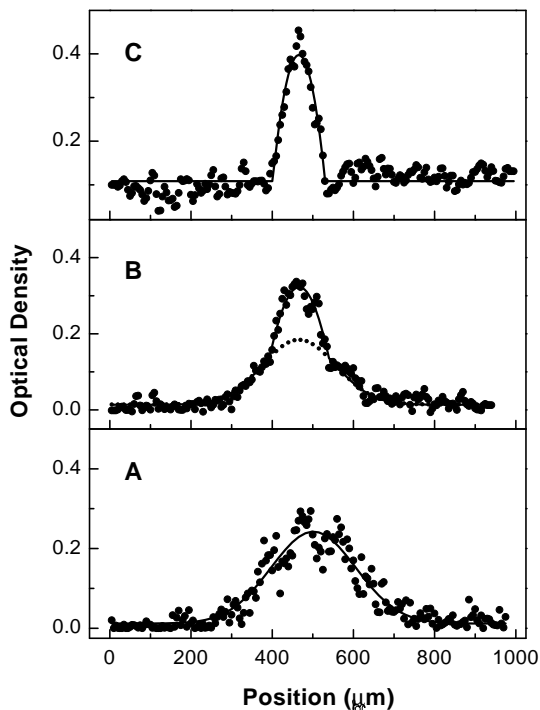


Figure 3.5: From A to C: density profiles of potassium cloud crossing Bose-Einstein condensation at a critical temperature $T \simeq T_C = 150$ nK. The lines are the best fit with Gaussian in the case of thermal component and with an inverted parabola for the condensate fraction.

of directly controlling the interaction between the atoms, by using magnetically tunable Feshbach resonances [83–85], that recently has allowed the formation of stable BEC for even for species like ^{85}Rb [7; 72] and ^7Li [25; 28; 29] for which the negative sign of the scattering length was a limiting factor.

The situation is completely different in the case of ultracold mixtures composed by atoms of different species, since no experimental data, neither theoretical studies were available. This is true also in the case of potassium rubidium mixtures. Indeed when we have started the experiment there were no predictions about the efficiency of sympathetic cooling between these two species. This lack of knowledge has motivated our decision of performing accurate collisional measurements on the mixture in order to determine the scattering length between K and Rb atoms [55]. Actually, by such a investigation on the pair ^{41}K - ^{87}Rb , we could have important predictions even for the other interesting K-Rb mixture, the one composed by ^{40}K - ^{87}Rb atoms, predictions subsequently confirmed by direct experimental ob-

servations [15]. In the following of this section, we will discuss the two independent methods that we have performed for determining the magnitude and the sign of ^{41}K - ^{87}Rb scattering length, and which give results in good agreement one with the other.

3.2.1 Thermalization by elastic interspecies collisions

As discussed in (2.3.1), potassium and rubidium atoms oscillate inside the magnetic trap at different frequencies due to the different masses. In particular, rubidium sample oscillates at 16.3 Hz axially and at 197 Hz radially, while potassium oscillates at 23.7 Hz and 286 Hz, respectively. This feature allow us to selectively heat rubidium atoms by superimposing a 10% modulation on the trapping potential at twice the radial frequency of Rb [11; 55]. This modulation of the radial confinement is achieved by modulating the magnetic field along the axial direction (the pinch direction) acting directly on the current of the compensation coils along the same direction. Indeed, if we look at that the expression for the magnetic potential around its minimum (2.3.1):

$$U(z, r) \simeq \mu \left[B_0 + \frac{1}{2} B'' z^2 + \frac{B'^2}{2B_0} r^2 \right] \quad (3.2)$$

we see that the oscillation frequencies of the trap are related to the curvature B'' , to the gradient B' and to the bias field B_0 by:

$$\omega_z = \sqrt{\frac{\mu B''}{m}} \quad \text{and} \quad \omega_r = \sqrt{\frac{\mu B'^2}{m B_0}} \quad (3.3)$$

therefore the square of radial frequency ω_r is proportional to $1/B_0$: by modulating B_0 we modulate the radial confinement at the same frequency. If the modulation is at twice the radial oscillation frequency of Rb, we selectively heat the rubidium cloud by parametric heating [86; 87]. After the driven excitation, we have observed experimentally how the total system (potassium + rubidium) evolves to the new equilibrium condition, by means of interspecies elastic collisions. In Fig. (3.6) we show the evolution of potassium temperature versus time after a 10% modulation for 100 ms at $2\omega_r$ of Rb. The initial temperature of the mixture in this case is $T = 1.6 \mu\text{K}$. While rubidium temperature decreases, we observe a corresponding increase in the one of potassium, until the two samples reach a common equilibrium value. Since this new equilibrium condition is reached by means of interspecies elastic collisions, the analysis of the thermalization process gives information on the collisional cross-section. Indeed, as shown in Fig. (3.6), the thermalization process is well described by an exponential decay, whose measured time constant τ is related to the elastic cross-section by:

$$\frac{1}{\tau_{mix}} = \frac{\xi}{\alpha_s} \bar{n} \sigma v_{rel} \quad (3.4)$$

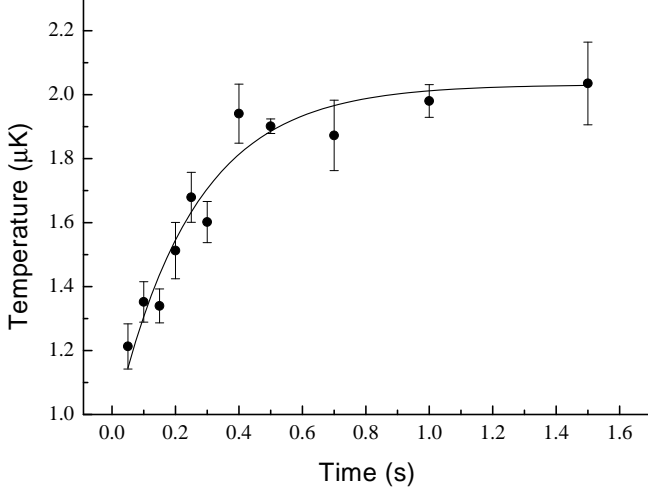


Figure 3.6: Evolution of the mean temperatures of the K sample after 100 ms of selective heating of Rb. Each datapoint is the average of five measurements, and the error bar displays the corresponding statistical fluctuation. The continuous line is the best fit to an exponential function; the time-constant is inversely proportional to the K-Rb elastic collisional rate.

where σ is the collisional cross-section ($\sigma 4\pi a_{K-Rb}^2$), considering only the s-wave scattering contribution to the cross-section, while v_{rel} and \bar{n} are the relative velocity between two colliding atoms and the effective average density given by,

$$v_{rel} = \sqrt{\frac{8k_B T}{\pi m}} \quad \bar{n} = \left(\frac{1}{N_{Rb}} + \frac{1}{N_K} \right) \int d^3r n_{Rb} n_K \quad (3.5)$$

The factor $\xi = 4(m_{Rb}m_K/(m_{Rb} + m_K)^2)$ takes into account the different masses of potassium and rubidium atoms, while the numerical coefficient α_s is the average number of s-wave collisions necessary for the thermalization: $\alpha_s \simeq 2.7$. From the analysis of our experimental data, we have found that $|a_{K-Rb}| = 170 \pm 35 a_0$.

Since the direct measured quantity is proportional to the square of the scattering length a , from this kind of measurement we do not have any information about its sign. As remarked in the previous chapter, while the magnitude of the scattering length determines the efficiency of the sympathetic cooling at high temperatures, the sign is crucial when the system reaches the degenerate regime, when the mean-field interaction between the atoms becomes important.

However, by repeating series of thermalization measurements, varying the tem-

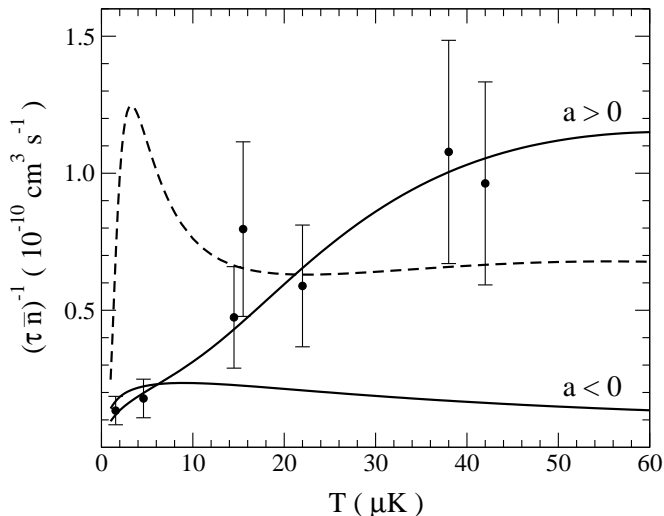


Figure 3.7: Dependence on temperature of the elastic collision rate $1/(\tau\bar{n})$. The points are the experimental data, and the error bars represent a 40% uncertainty on the number of atoms. The solid lines are the best fit to the model described in the text for positive and negative triplet scattering lengths, corresponding to $a = 163 a_0$ and $a = -209 a_0$, respectively. The dashed line corresponds to $a = 140 a_0$.

perature of the mixture, we were able to also extract the sign of the scattering length between ^{41}K - ^{87}Rb atoms.

The temperature dependence of the scattering cross-section can be extract in the effective range theory [20; 22] from the following equation:

$$\sigma_s \simeq \frac{4\pi a^2}{(1 - 1/2r_s a k^2)^2 + a^2 k^2} \quad (3.6)$$

where r_s is the effective range of the potential and the temperature dependence of the scattering cross-section enters in the wave-vector k . In Fig. (3.7) we show the measured elastic-collision rate $1/(\tau\bar{n})$ as a function of temperature in the range $(1.6 - 45) \mu\text{K}$. The measurements were performed on samples with a typical ratio $N_K : N_{Rb} = 1:2$, and with a total number of atoms ranging from 2×10^5 at $T = 1.6 \mu\text{K}$ to 2×10^6 at $T = 45 \mu\text{K}$. The general model we have used for describing the thermalization processes shown in Fig. (3.7) extends the one presented in [88] to the case of energy dependent collisional cross-sections by considering contributions from higher partial waves than s -wave. In our case, we have checked that in our temperature range, the only important contributions to the scattering rate are due to s - and p -wave collisions. Then it is possible to write the thermalization rate

(the thermalization time per unit atomic density) in the following way:

$$\frac{1}{\tau \bar{n}} = \frac{\xi}{2\alpha_s k_B T} \left[\langle \sigma_s v_{rel} E \rangle + \frac{\alpha_s}{\alpha_p} \langle \sigma_p v_{rel} E \rangle \right], \quad (3.7)$$

where, as above $\alpha_s \simeq 2.7$ is the average number of s -wave collisions necessary for rethermalization, v_{rel} is the relative velocity of a colliding pair and E is the relative collision energy. We obtain the ratio $\frac{\alpha_s}{\alpha_p} = \frac{3}{5}$ upon integration over all collision directions. The factor $\xi = 4\mu/M$, with M and μ the total and the reduced mass respectively, gives a reduction $\xi \simeq 0.87$ of the thermalization efficiency with respect to the case of equal masses. Finally, the averages $\langle \cdot \rangle$ are performed on a classical Maxwell-Boltzmann distribution of relative velocities.

The partial cross sections are obtained from a numerical solution of the scattering equations using standard propagation algorithms. The molecular Hamiltonian for collisions of atoms with hyperfine structure includes the kinetic energy of the relative motion, the hyperfine atomic energy and the adiabatic Born-Oppenheimer (ABO) $^1\Sigma^+$ and $^3\Sigma^+$ symmetry potentials. The latter have been constructed by smoothly matching the short-range *ab initio* potential of [89] onto a long-range analytic potential $V = V_d \pm V_{ex}/2$. Here $V_d = -C_6/R^6 - C_8/R^8 - C_{10}/R^{10}$ is the dispersion potential and V_{ex} is the exchange potential. An accurate van-der-Waals coefficient C_6 is taken from [90], C_8 and C_{10} from [91] and the analytic form of V_{ex} from [92]. The molecular potential is made flexible by adding a short-range correction to the adiabatic potentials (see [93]). This procedure allows us to tune singlet and triplet scattering lengths to agree with the data.

The experimental data are fitted using a min- χ^2 procedure. Since collisions between atoms prepared in a doubly-polarized spin state are single-channel collisions involving only the $^3\Sigma^+$ symmetry potential, the scattering length a is the only free parameter in the model [94]. Our main results are shown in Fig. (3.7). The best agreement is obtained for a positive scattering length $a = 163 a_0$, while the best-fit curve for negative a fails to fit the experiment at high temperature (solid lines in Fig. (3.7)). Actually, for $a < 0$ the cross-section drops with energy from its threshold value $\sigma_s = 4\pi a^2$ at lower collision energies than it does for $a > 0$. Moreover, the curve for $a = 163 a_0$ has a significant contribution from a broad p -wave shape-resonance near the top of the centrifugal barrier which further increases the rate at high T . This resonance rapidly shifts at lower energies for decreasing a (dashed line in Fig. (3.7)). This circumstance and the *absence* of observed resonant features sets a tight lower bound $a \approx 150 a_0$ on the confidence interval for a , while the upper bound is looser. Actually, scattering lengths $a \approx 200 a_0$ having only a minor p -wave contribution still agree well with the data.

3.2.2 Dipolar oscillations

As we have seen, we have determined the magnitude and the sign of the triplet scattering length between ^{41}K - ^{87}Rb atoms, by means of series of thermalization measurements performed on the mixture at different temperatures. The value we have finally found is $a = +163_{-12}^{+57} a_0$. For having an independent estimation of a , we have studied the damping of the dipole oscillations on a sample composed by about 8×10^4 K atoms and 1.5×10^5 Rb atoms, at $T = 1.7 \mu\text{K}$, where the only s -wave scattering contribution is relevant. We have induced dipole oscillations suddenly shifting the trapping potential, by varying the current in the pinch coil for about 30 ms (half of an oscillation period), after the conclusion of the evaporation ramp. After the displacement, the atoms start to oscillate inside the magnetic trap along the weak axis of the trap around the potential minimum. In Fig. (3.8), we show the evolution of the center of mass oscillations versus the time after the displacement. As it is possible to see from the figure, after the first oscillation, in which the potassium and rubidium atoms oscillate at their own "bare" frequency (24 Hz and 16.3 Hz respectively), the dipolar oscillations become rapidly coupled and damped by the interaction between the atoms. In particular, the motion of potassium atoms (the lighter element) is strongly affected by the presence of rubidium, as showed by the appearing of beatings.

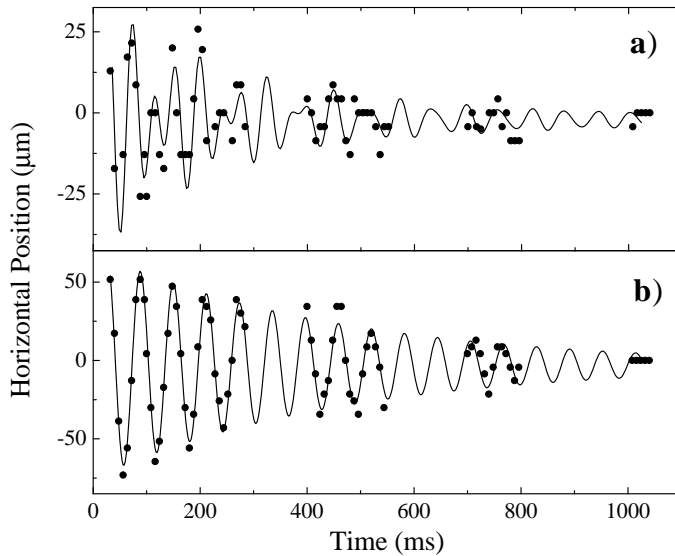


Figure 3.8: Dipole oscillations of the K (a) and Rb (b) clouds along the weak trap axis. The solid lines are a best fit to the model presented in the text. The faster damping and the beatings observed in the K motion are due to the smaller mass of the K sample.

The motion of the two center of mass is well described by the solutions of the following coupled differential equations [95; 96]:

$$\begin{aligned}\ddot{z}_1 &= -\omega_1^2 z_1 - \frac{4}{3} \frac{M_2}{M} \frac{N_2}{N} \Gamma (\dot{z}_1 - \dot{z}_2) \\ \ddot{z}_2 &= -\omega_2^2 z_2 + \frac{4}{3} \frac{M_1}{M} \frac{N_1}{N} \Gamma (\dot{z}_1 - \dot{z}_2),\end{aligned}\tag{3.8}$$

where the labels 1 and 2 denote K and Rb respectively, $M = M_1 + M_2$, $N = N_1 + N_2$, $\Gamma = \bar{n}\sigma_s v$ is the instantaneous s -wave collision rate, v is the rms relative velocity, and \bar{n} is the atoms density defined above. The coupled equations (3.8) indicate that, in the collisionless regime, in which the collisional rate Γ is much smaller than the oscillation frequency in the trap ω , $\Gamma \ll \omega$, the motion of the two clouds is a superposition of two different normal modes at the bare frequency of potassium and rubidium. Since the mass of Rb is almost twice the one of potassium, K motion is more influenced by the presence of Rb and it is faster damped respect to Rb one. By fitting our experimental results with the solution of (3.8), we can extract the collisional rate $\Gamma = 5.2 \pm 0.7 \text{ s}^{-1}$ and the value of the magnitude of the triplet scattering length $|a| = 170^{+35}_{-35} a_0$, where the uncertainty is dominated by that on the atom number ($\pm 50\%$). As it is possible to see, this result is in good agreement with the one we have found by the thermalization measurements.

3.3 Potassium-rubidium interactions

From the measurements we have presented so far, we are able to extract the magnitude and the sign of the scattering length between ^{41}K - ^{87}Rb atoms. In particular, since we started always with a sample fully polarized, in the stretched state $|F = 2, m_F = 2\rangle$ state, we can have information only about the triplet scattering length a . In order to determine also the singlet scattering length a_1 we have performed some inelastic measurements. We have transferred some population of Rb atoms in the trapped state $|F = 2, m_F = 1\rangle$, and we have studied the trap losses due to the collisions of this atoms with the K in the $|F = 2, m_F = 2\rangle$ state. In details, we have started with a mixture composed by 3×10^4 K atoms and a larger number of Rb atoms (1.2×10^5), both in $|2, 2\rangle$ state, at a temperature $T = 1.8 \mu\text{K}$. We have then transferred a small fraction (20%) of rubidium in $|2, 1\rangle$ using a radio-frequency sweep and we have studied the subsequent decay of K. The decay of potassium in this state turned out to be much faster than the usual decay of the fully polarized system ($\tau = 70\text{s}$). Indeed, the mixture composed by rubidium in $|F = 2, m_F = 1\rangle$ state and potassium in $|F = 2, m_F = 2\rangle$ is no more stable (see 2.3.2). In particular, we can have the following inelastic processes $|2, 1\rangle + |2, 2\rangle \rightarrow |2, 2\rangle + |1, 1\rangle$ and $|2, 1\rangle + |2, 2\rangle \rightarrow |1, 1\rangle + |2, 2\rangle$ that cause large losses in the trap. Since the Zeeman structure is the same for both species, during the RF sweep, we could also transfer some potassium atoms in the $|2, 1\rangle$ state. How-

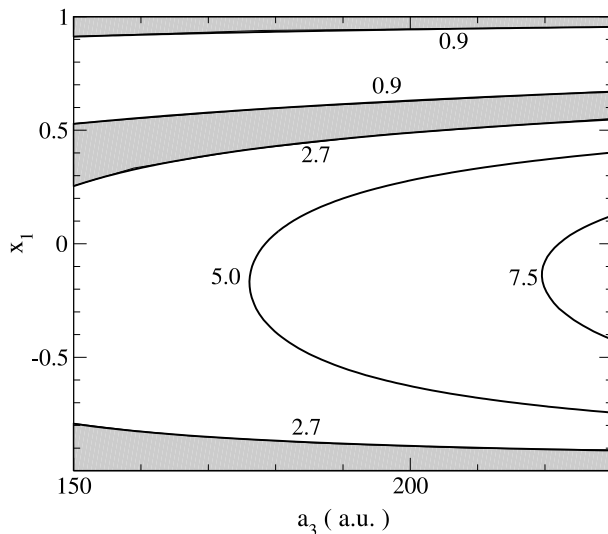


Figure 3.9: Contour plot of the calculated inelastic collisional rate G in units of $10^{-11} \text{ cm}^3 \text{ s}^{-1}$ vs the triplet scattering length a and the reduced singlet scattering length $x_1 = 2/\pi \arctan(a_1/a_{sc})$, where $a_{sc} = 72 a_0$. The shaded regions correspond to the rate determined in the experiment.

ever, this population did not contribute significantly to the losses of potassium and rubidium, being the number of K atoms transferred in this state negligible respect to the initial number of rubidium atoms in the $|2, 2\rangle$. It is possible to describe the evolution of the population of potassium atoms in $|2, 2\rangle$ state by solving the rate equation:

$$\dot{n}^K(t) = -G n_{|2,2}^K(t) n_{|2,1}^{Rb}(t) \quad (3.9)$$

with the constraint $N_{|2,2}^K(t) - N_{|2,1}^{Rb}(t) = \text{const}$. Here n is the spatial density,

N the atom number and G is the rate constant for inelastic collisions between K in $|2, 2\rangle$ and Rb in $|2, 1\rangle$. From this model, we have extracted the inelastic collisional rate $G=1.8(9)\times 10^{-11} \text{ cm}^3 \text{ s}^{-1}$. If we compare this experimental result with a numerical calculation, we can determine a range of values for the singlet scattering length a_1 , given our interval of a values. As shown in Fig.(3.9), we can have two range of values for a_1 , that are compatible with our measured inelastic rate G . Indeed both $a_1 > 30 a_0$ and $a_1 < -210 a_0$ are compatible with our data, excluding, in this way, excluding a broad region of strong suppression of inelastic processes centered at $a_1 \sim a$, as in the case of ^{87}Rb [5]. Thanks to these collisional measurements, by mass scaling, it has been possible to draw down a picture of the triplet scattering length of all the K-Rb possible pairs [55].

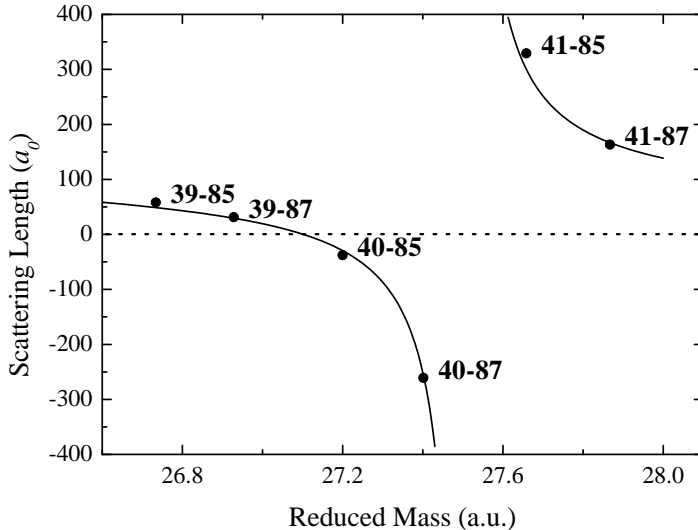


Figure 3.10: Triplet s -wave scattering lengths for collisions between potassium-rubidium isotopes. The values are derived by mass scaling from the directly measured ^{41}K - ^{87}Rb scattering cross-section.

In Fig. (3.10) we present the triplet interactions versus the reduced mass for all the potassium-rubidium mixtures. It is worth to comment these results. First of all the measured repulsive character of the ^{41}K - ^{87}Rb triplet interaction indicates that it is possible to form a stable binary Bose-Einstein condensate. Indeed in the case of a negative inter-species scattering length much larger in magnitude than the single-species ones, the mean-field interaction would lead to the collapse of the condensates [103], since the magnitude of the ^{41}K - ^{87}Rb scattering length is larger than the intraspecies ones (see (1.4.1)). Among all the other possible combinations, the more interesting one is the ^{40}K - ^{87}Rb : the value of the triplet scattering length we can infer from these measurements made on the ^{41}K - ^{87}Rb pair is $-261^{+170}_{-159} a_0$. Therefore, we can expect that sympathetic cooling of fermionic K with ^{87}Rb is highly efficient. Moreover, the attractive character of the interaction prevents phase separation of the two components once the degenerate regime has been reached [37], thus insuring an efficient thermalization even in this regime.

CHAPTER 4

Bose-Bose degenerate mixture

In the previous chapter, we have demonstrated the possibility of cooling down to quantum degeneracy a sample of ^{41}K atoms, by means of sympathetic cooling with rubidium atoms. The efficacy of sympathetic cooling is supported by a large inter-species collisional rate. We have directly measured the ^{41}K - ^{87}Rb triplet scattering length and we have found a quite large value $a \simeq 163 a_0$. The positive sign assures the possibility of forming a stable binary BEC with these two species. In this chapter, we report on the experimental observation of this double BECs system, and show how the feature of superfluidity affects the dynamics of such a system, inducing scissors-like oscillations of the BECs inside the magnetic potential.

4.1 Producing the degenerate mixture

As discussed previously, in our first attempts we were not able to see the simultaneous formation of potassium and rubidium condensates: typically ^{41}K could reach the degenerate regime, only when all rubidium atoms were evaporated from the trap. The reasons for this failure depend essentially from two different factors that however are strictly related.

First, as mentioned in (2.3), during the loading of potassium in the second MOT we have observed large losses in the rubidium sample, due to non linear processes occurring in the MOPA. In particular, when all the four frequencies were injected in the amplifier, we have seen the formation of sidebands on the cooling light of rubidium ($|F = 2\rangle \rightarrow |F' = 3\rangle$ transition). Since the hyperfine energy splitting of ^{41}K is 254 MHz one of this two sideband was resonant with the $|F = 2\rangle \rightarrow |F' = 2\rangle$ transition reducing, in this way, the efficiency of the rubidium

MOT. For this reason we had a limitation in the maximum number of potassium and rubidium atoms loaded in the second MOT. Indeed a too long potassium loading caused large losses (even of the 50%) in the rubidium sample, not allowing the formation of a BEC of ^{87}Rb , while a shorter transferring of K atoms did not permit the observation of the potassium condensate.

On the other side, we have noted how the good polarization of the system was really important for avoiding losses in the sample. However, despite of our efforts, at the beginning, we were never able to produce a fully polarized mixture in the $|2, 2\rangle$ state. Indeed we could always reveal a small component of rubidium atoms trapped in the $|2, 1\rangle$ state, not cleaned up by the μ -wave evaporation. This residual population in the $|2, 1\rangle$ state could induce losses in the potassium sample. We have tried to get rid of these atoms in the $|2, 1\rangle$ state, by forcing the first part of the evaporation of rubidium. Infact, at high temperatures ($T \geq 100 \mu\text{K}$) it is possible to remove efficiently from the potential both the $|2, 1\rangle$ and the $|2, 2\rangle$ components. However, when the temperature of the system approaches to about $40 \mu\text{K}$ the $|2, 1\rangle$ is no more eliminated from the trap. Furthermore, since the value of the bias field for the $|2, 1\rangle$ state is just the half of the one for the $|2, 2\rangle$ state, it is not possible to cut completely the population in the $|2, 1\rangle$ state without before eliminating all the atoms in the $|2, 2\rangle$.

The only way for evaporating all the atoms trapped in the $|2, 1\rangle$ state was to apply a second μ -wave knife, always operating on the rubidium sample at 6.8 GHz but directly coupling the $|2, 1\rangle$ with the $|1, 0\rangle$ and $|1, 1\rangle$ states of the ground state. In this way we could eliminate almost all the population of rubidium in the $|2, 1\rangle$ level, and after an suitable evaporation ramp lasting 50 s, we could finally have the right numbers of atoms of both the species for the observation of the binary BEC [12].

Actually, by means of this double evaporation scheme, we could soon observe the formation of the binary BEC [12]. In Fig. (4.1a-b) we show the transition between a Bose-Einstein condensate interacting with a thermal gas of Rb to a binary BEC. The typical number of atoms is about 10^4 for both the species, and since the critical temperatures, for similar number of atoms, depend only from the mass, $T_C \propto \varpi \propto M^{-1/2}$, this means that the condensation regime is reached before for the potassium sample at $T \simeq 120 \text{ nK}$ and then for the rubidium at $T \simeq 80 \text{ nK}$.

We were able to detect the two condensates simultaneously by absorption imaging after 13 ms of free ballistic expansion; the two images are taken with a temporal delay of $700 \mu\text{s}$, by pulsing the potassium light at 766.7 nm and the rubidium at 780 nm for about $30 \mu\text{s}$. As it is possible to note from Fig. (4.1 b), due to the lighter mass potassium expands faster than rubidium as appears from the different aspect of the two clouds.

By studying the two condensates at different expansion times, we could get information on the size and on the relative positions of the two samples inside the magnetic potential. By comparing our experimental results with an analytic model for the ground state of a binary BEC in the Thomas-Fermi approximation [4], we

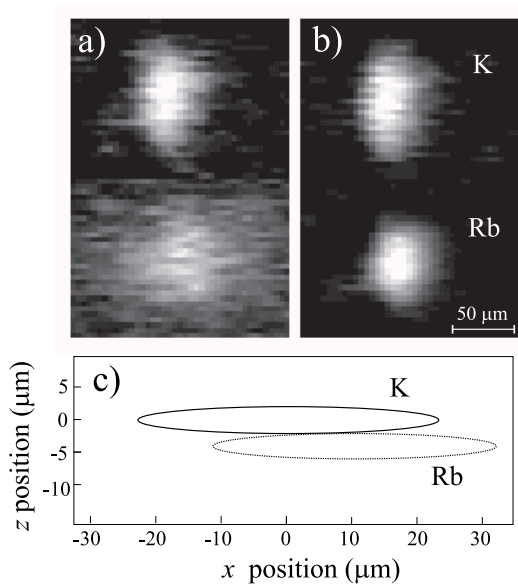


Figure 4.1: Absorption imaging of a binary ^{41}K - ^{87}Rb Bose-Einstein condensate after 13 ms of ballistic expansion: a) at $T \simeq 100$ nK the Rb sample is still thermal; b) at $T \leq 80$ nK both species are condensed. c) Enlarged view of the density profile of the binary BEC in the magnetic trap.

have found that the radii of the K (Rb) condensates are $r_x = 23 \mu\text{m}$ ($r_x = 22 \mu\text{m}$) along the weak axis of the trap, and $r_z = 2 \mu\text{m}$ ($r_z = 1.9 \mu\text{m}$) in the other two directions. As sketched in Fig. (4.1c), the two centers are displaced along the z axis due to the gravity (gravitational sag) of about $\delta z = 3.6 \mu\text{m}$. Furthermore, due to a misalignment of our magnetic trap, the weak axis of the trap (x - direction) forms an angle of about 20 mrad with respect to the gravity and thus the two centers are displaced of about $\delta x = 10 \mu\text{m}$ also along this direction. We have measured the temperature of the mixture from the Gaussian tails of the thermal component of each condensate. Due to the resolution of our imaging system, we were able to detect a minimum thermal fraction of 30 % in each condensate. This detectable thermal component fixes our minimum measurable temperature to $T = 0.65 T_C$. In the case of the K condensate, the minimum temperature that we could measure was about 80 nK which is just the critical temperature of rubidium. This means that even if the overlap region between the two samples in the magnetic potential is not very large, as we can see from Fig. (4.1c), the thermal contact and consequently sympathetic cooling is assured by the two thermal clouds, which even in the degenerate regime continue to have good spatial overlap. The lifetime of this double BECs was about 500 ms, as in the case of individual BECs of potassium

and rubidium, limited by the background heating of our magnetic potential (100 nK/s).

4.2 Stability of the degenerate mixture

The stability of this binary condensate is assured mostly by the large and repulsive character of the ^{41}K - ^{87}Rb interaction. For understanding this, we write down the equations in mean-field approximation describing the ground state of such a system [104]:

$$\left[-\frac{\hbar^2}{2m_1} \nabla^2 + U_1(\mathbf{r}) + g_{11}|\psi_1|^2 + g_{12}|\psi_2|^2 \right] \psi_1 = \mu_1 \psi_1 \quad (4.1)$$

$$\left[-\frac{\hbar^2}{2m_2} \nabla^2 + U_2(\mathbf{r}) + g_{21}|\psi_1|^2 + g_{22}|\psi_2|^2 \right] \psi_2 = \mu_2 \psi_2 \quad (4.2)$$

where we defined:

$$g_{11} = \frac{4\pi\hbar^2 a_{11}}{m_1} > 0 \quad (4.3)$$

$$g_{22} = \frac{4\pi\hbar^2 a_{22}}{m_2} > 0 \quad (4.4)$$

$$g_{12} = 2\pi\hbar^2 a_{12} \left(\frac{m_1 + m_2}{m_1 m_2} \right) \quad (4.5)$$

The interaction between the two condensates is described by the term $g_{12} = 2\pi\hbar^2 a_{12}(m_1 + m_2)/m_1 m_2$, i.e. it is proportional to the interspecies scattering length a_{12} . The study of the stability of a mixture composed by two interacting Bose gases has been reported in many theoretical works [97–104]. In particular, M. Modugno and F. Riboli in [104] have considered, in the mean-field approximation, the general case of two condensates composed by different atomic species (with different mass and in different hyperfine states) confined in a magnetic trap. They have included in their model also the presence of the gravity and the possibility of having the eigenaxes of the potential tilted with respect to the gravity direction, as we actually find in our experiment. By an appropriate coordinate transformations, it is possible to model this complicated problem in a much simpler form, reducing it to the study of the intersections of spheres each representing in the Thomas-Fermi limit, the regions of existence of the BECs. Following [104], we can rewrite the equations (4.1) and (4.2) as:

$$V_1(\mathbf{x}) + u_{11}|\psi_1|^2 + u_{12}|\psi_2|^2 = \mu_1 \quad (4.6)$$

$$V_2(\mathbf{x}) + u_{21}|\psi_1|^2 + u_{22}|\psi_2|^2 = \mu_2 \quad (4.7)$$

where the reduced coupling constants u_{ij} are

$$u_{11} = 4\pi \frac{a_{11}}{a_{ho}} \quad (4.8)$$

$$u_{12} = 2\pi \frac{a_{12}}{a_{ho}} \left(1 + \frac{m_1}{m_2}\right) = u_{21} \quad (4.9)$$

$$u_{22} = 4\pi \frac{a_{22}}{a_{ho}} \frac{m_1}{m_2} \quad (4.10)$$

We can consider the solutions of (4.6) and (4.7) either in the overlapping regions or in the regions where the two wavefunction describing the condensates do not overlap. In the first case, the solutions of the GPE system are:

$$|\psi_1|^2 = \alpha_1 (R_1^2 - r^2 - (z - z_{c1})^2) \quad (4.11)$$

$$|\psi_2|^2 = \alpha_2 (R_2^2 - r^2 - (z - z_{c2})^2) \quad (4.12)$$

where we have defined the radii R_i

$$R_1^2(\mu_1, \mu_2) = \frac{2(\mu_1 - \gamma_2 \mu_2)}{1 - \eta \gamma_2} + \frac{\eta \gamma_2}{(1 - \eta \gamma_2)^2} dz^2 \quad (4.13)$$

$$R_2^2(\mu_1, \mu_2) = \frac{2(\mu_2 - \gamma_1 \mu_1)}{\eta - \gamma_1} + \frac{\eta \gamma_1}{(\eta - \gamma_1)^2} dz^2 \quad (4.14)$$

the position of the centers along z

$$z_{c1} = \frac{-\eta \gamma_2}{1 - \eta \gamma_2} dz \quad (4.15)$$

$$z_{c2} = \frac{\eta}{\eta - \gamma_1} dz \quad (4.16)$$

and the normalization factors α_i

$$\alpha_1 = u_{22} \frac{1 - \eta \gamma_2}{2\Delta} \quad (4.17)$$

$$\alpha_2 = u_{11} \frac{\eta - \gamma_1}{2\Delta}. \quad (4.18)$$

and $\gamma_1 \equiv u_{21}/u_{11}$, $\gamma_2 \equiv u_{12}/u_{22}$ and $\Delta = u_{11}u_{22} - u_{12}^2$.

As we can see from (4.11) and (4.12), the density $n_i(r) = |\psi_i|^2$ of each condensate is represented by spatial regions delimited by spherical surfaces of radii R_i whose magnitudes depend only on the interaction parameter u_{ij} . Since $|\psi_i|^2 \geq 0$ then we must have

$$\alpha_1 [R_1^2 - r^2 - (z - z_{c1})^2] \geq 0 \quad (4.19)$$

$$\alpha_2 [R_2^2 - r^2 - (z - z_{c2})^2] \geq 0 \quad (4.20)$$

and therefore the overlap region between the two BECs is the intersection between two spherical surfaces Σ_i which are defined by the equations $R_i^2 = r^2 + (z -$

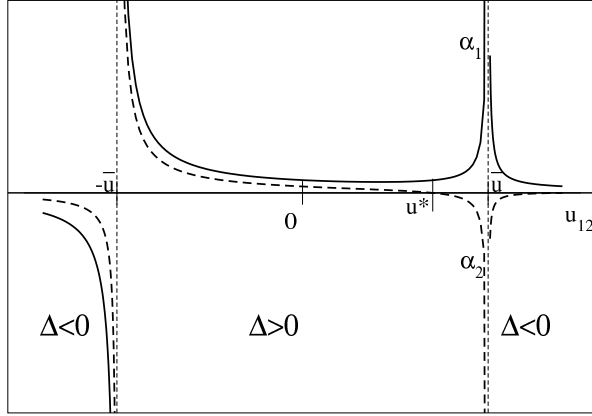


Figure 4.2: Plot of the normalization factors α_1 (continuous line) and α_2 (dashed line) of the interacting wave functions as a function of u_{12} (in arbitrary units). The region for $\Delta < 0$ and $u_{12} < -\bar{u}$ corresponds to the physical situation of the collapse between the two condensates, while if $-\bar{u} < u_{12} < \bar{u}$, $\Delta > 0$, the two BECs can have some overlap region, depending on the value of the parameters \bar{u} and u_{12} . Phase-separation instead occurs if $u_{12} > \bar{u}$, $\Delta < 0$. The quantity u^* is defined as $u^* = \min(u_{11}, u_{22})$.

z_{ci}^2), and identified by the sign of the coefficient α_i : for $\alpha_i > 0$ the region to be considered is the one inside the surface Σ_i , for $\alpha_i < 0$ the one outside.

In the regions where the two wavefunctions do not overlap the solutions of (4.6) and (4.7) are:

$$|\psi_{01}|^2 = \frac{1}{2u_{11}} (2\mu_1 - r^2 - z^2) \quad (4.21)$$

$$|\psi_{02}|^2 = \frac{\eta}{2u_{22}} \left(\frac{2\mu_2}{\eta} - r^2 - (z - dz)^2 \right). \quad (4.22)$$

Also in this case, the solutions are represented by the intersection of two spherical surfaces, defined by: $R_{0i}^2 = r^2 + (z - z_{ci}^0)^2$, with $R_{01}^2 = 2\mu_1$, $R_{02}^2 = 2\mu_2/\eta$, $z_{c1}^0 = 0$ and $z_{c2}^0 = dz$.

By imposing the continuity condition of the wavefunction at the boundary between the overlapping and the nonoverlapping regions, we can distinguish three different situations defined by the value of the u_{12} parameter, which is directly related to the interspecies scattering length a_{12} . Defining the parameter $\bar{u} \equiv \sqrt{u_{11}u_{22}}$ we have the following cases:

- (i) $u_{12} < -\bar{u}$, $\Delta < 0$. For this range of values, we have no overlapping solution. From Fig. (4.2) we see that both α_i are negative and it is possible to show that the only region of overlap between the two BECs could be constructed by

putting a hole in the condensate, where both the condensates wavefunctions ψ_i would be vanishing. This has obviously no physical meaning and in fact what actually happens is that when u_{12} approaches $-\bar{u}^+$ the condensates eventually collapse [98; 103].

- (ii) $-\bar{u} < u_{12} < \bar{u}$, $\Delta > 0$: in this range the two condensates can coexist and overlap in some region of space if $|dz| < R_{10} + R_{20}$.
- (iii) $u_{12} > \bar{u}$, $\Delta < 0$: in this case the strong mutual repulsion leads to a phase separation between the two condensates [37; 99; 100].

In our specific situation, we can calculate the parameters Δ and \bar{u} , by considering the values of the potassium-rubidium scattering lengths, $a_K=60 a_0$ [105] and $a_{Rb} = 99 a_0$ [106], and $a_{K-Rb} = 163 a_0$. We find that the ^{41}K - ^{87}Rb mixture verifies the condition $u_{12} > \bar{u}$, $\Delta < 0$. This means that we are in a regime of phase-separation between the two condensates [37]. Indeed if the interspecies scattering length was negative, $a_{KRb} = -163 a_0$, we would not observe the stable binary condensates, because $u_{12} < -\bar{u}$, $\Delta < 0$. In fact, in this case the attractive mean-field interaction between atoms of the two BECs would overwhelm the repulsion between atoms of the same specie, leading to the collapse of the system. Our observation of the stable binary BEC of ^{41}K and ^{87}Rb confirms our estimation of the magnitude and of the sign of the triplet scattering length that we made by collisional measurements.

4.3 Dynamics of binary potassium-rubidium BECs: collision-induced scissors mode

As we have discussed before, the overlap region between the two condensates in the trap is likely to be quite small, essentially due to the repulsive character of the interaction between the two species, that causes phase-separation [37] between the two degenerate clouds, and due the gravitational sag. In this conditions, only the residual thermal component of both BECs is assuring the thermal contact among the two clouds. To observe some effects due to the large interspecies interaction, we have forced the dynamical overlap between the two condensates, by exciting dipolar oscillations [12]. These oscillation were excited by reducing the radial confinement of the trap by almost 25 % for 2 ms, controlling the current in the compensation coils along the weak axis of the trap. Indeed, by varying the current inside this coils, it is possible to change the value of the bias field B_0 , and subsequently to vary the value of the radial frequency of the trap ($\omega_z \propto 1/B_0^2$), leading to a vertical oscillatory motion of the whole sample (2.3.1).

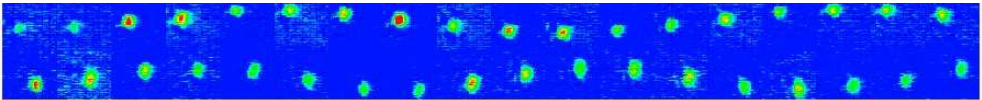


Figure 4.3: Dipolar oscillations of potassium (top) and rubidium (bottom) Bose-Einstein condensates. The absorption images are taken after 13 ms of free expansions.

After the modification of the magnetic potential, we have left the system evolve in the trap some time and then we have imaged the two clouds simultaneously by usual absorption imaging technique. Typical recorded images are shown in Fig. (4.3). In this case, we have let the two BECs expand for 13 ms before pulsing the imaging lights. The time delay between the two pulses was $700 \mu\text{s}$. The numbers of atoms of condensates were typically 6×10^3 and 10^4 for K and Rb, respectively, and we could not detect any thermal component in both the cases.

In Fig. (4.4a-b) we report the center of mass motion of the potassium and rubidium versus evolution time inside the magnetic trap. We have described our system in the mean-field approximation by considering two coupled time-dependent Gross-Pitaevskii equations (GPE), whose numerical solution is represented by the continuous line in Fig. (4.4a-b). As it is possible to see, our experimental data are pretty well reproduced by this simulation. It is worth to note that the motion of the center of mass is not strongly affected by the large mean-field repulsion between the two condensates, since we do not observe almost any damping in the first oscillations of the two clouds. Damping and coupling are instead observed on much longer time scale (more than 100 ms), when anyway we suspect that some thermal components starts to interfere in the motion of the two BECs. The theoretical analysis of the system allows us to reconstruct the motion of the con-

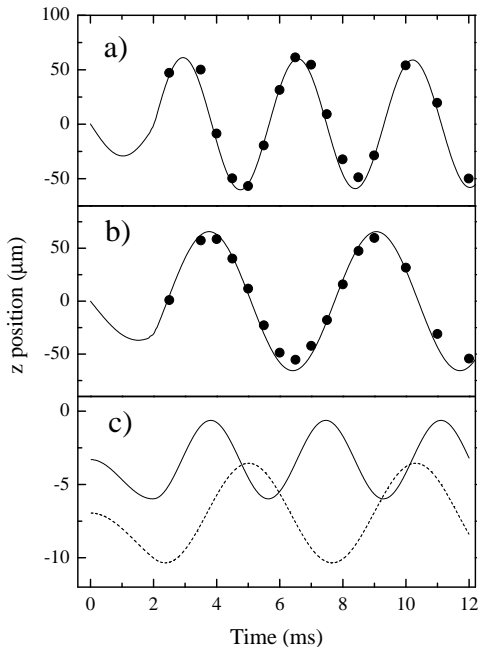


Figure 4.4: Dipolar oscillations of the K and Rb condensates along the z axis, induced by a modification of the radial trap confinement. Center-of mass position of a) K and b) Rb after the ballistic expansion; the dots are the experimental data, while the continuous lines are a simulation using the GPE. c) Calculated evolution of the center-of-mass position for K (continuous line) and Rb (dotted line) in the trap.

condensates in the magnetic trap, as reported in Fig. (4.4c). The initial positions of the two clouds in the trap is determined by the gravity that pulls down the rubidium condensate more than the potassium one. As soon as the potential is modified, the two BECs start to oscillate in the trap, each one at its own frequency, $\nu_r(\text{Rb}) = 190$ Hz and $\nu_r(\text{K}) = 275$ Hz. Due to this frequency shift, after some ms, the two clouds will completely superimpose, i.e. the two BECs collide. Since the two condensates are displaced also along the x direction, see Fig. (4.1), the two clouds are likely to exchange angular momentum as a consequence of these off-collisions. We have actually observed this kind of behaviour, by looking at the shape of the BECs in function of the time after the excitation of the dipolar motion.

In Fig. (4.5) we show the absorption images of potassium and rubidium condensates at evolution times corresponding to the collisions between the two BECs. It is possible to note that the two clouds effectively rotate around their vertical

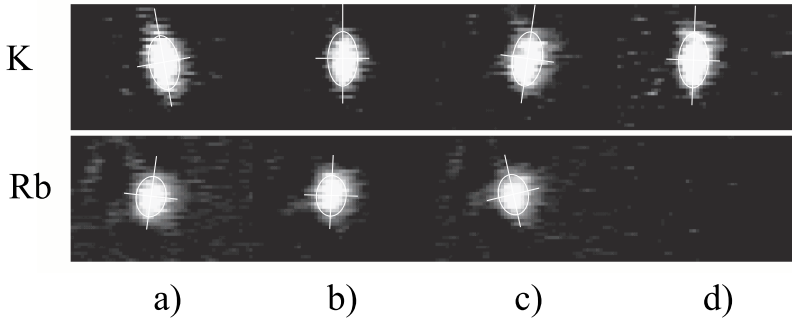


Figure 4.5: Collision-induced rotation of the binary BEC during the dipolar oscillations. The first three images correspond to an evolution time in the trap: a) 8 ms; b) 8.5 ms; c) 9 ms. In d) the evolution time is 8 ms like in a), but the Rb BEC has been removed before the excitation of the dipolar oscillations; no rotation is observed in this case.

axis. In the case of potassium, this phenomena appears more evident, since its shape is more elongated in the vertical direction due to faster expansion. Since the optical transitions of K and Rb are 13 nm far, it is possible to eliminate from the trap selectively only one of the two condensates, studying in this way, the free evolution of the center of mass without any collisions with the other specie. When we have performed such a measurement, shown in Fig. (4.5d) for potassium, we have not observed any rotation. We have been able to explain this behaviour by considering the GPE approach: in this mean-field approximation, each BEC sees the other one as a time-dependent perturbation of its trapping potential [107; 108]. Since the axial symmetry of the potential is broken due to the misalignment of the magnetic trap, the BECs acquire a macroscopic angular momentum.

When we have repeated the same experiment using, this time, ultracold but still thermal samples, we have not detected any rotation of the clouds. This can be understood qualitatively in the following way. In general, when describing the interaction between trapped atoms it is possible to distinguish two different regimes [109]. The first regime is called *collisionless regime* and it is characterized by a scattering rate much lower than the oscillation frequency of the atoms in the trap, $\Gamma \ll \omega$, where $\Gamma = n\sigma v$, as introduced in the previous chapter. In this case, the atoms inside the sample behave as individual particles, so then the scattering process are essentially uncorrelated two body events. On the other side, when the scattering rate becomes much larger than the trapping frequency, $\Gamma \gg \omega$ (*hydrodynamic regime*), the collisional rate is so high that the system responds to external perturbations as a whole (this regime is also called first sound regime). With our experimental parameters we are in the collisionless regime: this means that the collisions between the two thermal clouds are completely uncorrelated two-body processes, ruling out the possibility of a macroscopic exchange of momentum.

In the case of two classical gases in the hydrodynamic regime, we could observe such exchange of angular momentum but, in this regime the center-of-mass motion would be damped on the timescale of the trap period, differently from what we observe for the two condensates.

The observed exchange of angular momentum and the following oscillation of the angle (scissors mode) are direct consequences of the superfluid nature of the condensates. Indeed, as suggested by S. Stringari et al. [110] the scissors mode are a feature of superfluid systems, since they are solutions of the hydrodynamic equations which, in the a Thomas-Fermi approximation describe the condensate [4],

$$\frac{\partial \rho}{\partial t} + \nabla \cdot (\rho \mathbf{v}) = 0 \quad (4.23)$$

$$m \frac{\partial \mathbf{v}}{\partial t} + \nabla \cdot \left(\frac{\mathbf{v}^2}{2m} + U(\mathbf{x}, t) + g\rho \right) = 0, \quad (4.24)$$

where $S(\mathbf{x}, t)$ and $\rho(\mathbf{x}, t)$ are related to the condensate wavefunction by $\psi(\mathbf{x}, t) = \sqrt{\rho(\mathbf{x}, t)} e^{iS(\mathbf{x}, t)/\hbar}$. In fact the observation of such oscillation mode [111] was another demonstration of the superfluidity of a Bose-Einstein condensate.

In our experiment, these scissors mode are excited by means of off-axis collisions between the two BECs and not by a direct rotation of the trapping potential as presented in [111]. An interesting issue of a rotating BEC is the evolution of the angle during the expansion of the cloud. Indeed, as it was pointed out recently [112; 113], a rotating condensate expands in a completely different way with respect to a non rotating one. The reason of this peculiar behaviour is in the quenching of the moment of inertia of the superfluid. Indeed, if we consider [113] a BEC rotating, for example, in the $x - y$ plane, we can write the general expression for its momentum of inertia as:

$$\Theta = \Theta_{rig} \frac{\langle x^2 - y^2 \rangle^2}{\langle x^2 + y^2 \rangle^2} \quad (4.25)$$

where $\Theta_{rig} = Nm \langle x^2 + y^2 \rangle$. Due to the irrotational nature of the superfluid ($\nabla \times \bar{v} = 0$), the moment of inertia of the condensate is quenched with respect to the rigid body value Θ_{rig} . While the condensate expands, its aspect ratio evolves due to the mean-field interaction between the atoms. After a certain time, typically given by $\tau = 1/\omega_{fast}$, the condensate will reach a minimum deformation, $x \simeq y$. But since it is also rotating, when $x \simeq y$, the momentum of inertia vanishes. The angular momentum conservation law implies that the angular velocity must increase in order to compensate the decrease of Θ .

On the other hand, the angular velocity can not increase too much, due to the energy conservation. This means that the system cannot reach a complete symmetric configuration ($\langle x \rangle = \langle y \rangle$.) during the expansion but it can reach a minimum deformation which depends form the initial angular velocity Ω_0 .

The total angle α described by the condensate during the expansion depends from the initial angular velocity and this angle can be only smaller than $\pi/2$, differently respect to the case of an ideal gas, for which it always reach $\pi/2$ value [113]. As soon as the aspect ratio of the BEC approaches to one, the condensate has to increase its angular velocity (see above) and at the same time the angle will slowly evolves towards the asymptotic value of $\alpha = \pi/2$.

In our experiment, we could study the evolution of the angle versus the dwelling time in the trap, fixed the expansion time to 13 ms. Due to the different trapping

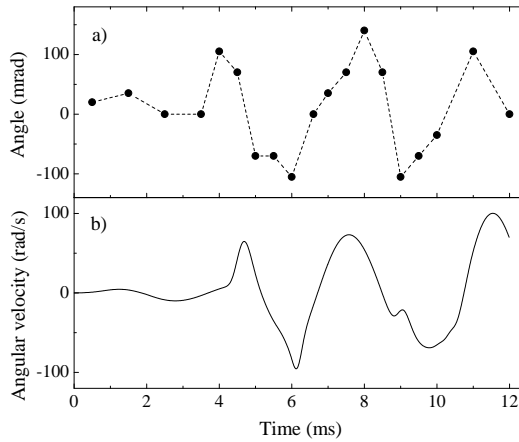


Figure 4.6: a) Evolution of the angle of rotation of the K BEC from the vertical direction, after a 13 ms ballistic expansion. The dotted line is a guide to the eye. b) Numerical simulation using the GPE of the angular velocity of the condensate at release from the trap.

frequencies between potassium and rubidium, the K condensate, after 13 ms has yet reached almost its asymptotic angle, while Rb one is in the region of high angular velocity, as it was possible to verify by directly solving the Thomas-Fermi hydrodynamic equations [113]. In Fig.(4.6 a), we report the evolution of the K angle versus the time in the trap, after 13 ms of expansion: it is possible to see the condensate starts to oscillate just after 4 ms, which corresponds to the time when it is likely to happen the first collision between the two BECs (see Fig.(4.4c). Since these scissors mode are induced by collisions between the two clouds, we do not have a pure sinusoidal behaviour that is observed in [111]. By simulating our experiment by means of time-dependent GPE model, we have calculated the angular velocity of the condensate at the release from the trap. The result is shown in Fig.(4.6b), where we can see that the angle after the expansion turns out to be proportional to the angular velocity of the condensate in the trap.

4.3.1 Expansion of a rotating BEC

We have studied in more detail the expansion of a rotating BEC. The experimentally easier situation was to study the scissors mode excited on our ^{87}Rb condensate. Since the QUIC trap is a magnetostatic trap, we could not excite the scissors mode by rotating directly the potential as reported in [111]. In fact we could excite the scissors mode in a quite peculiar way: we have taken advantage of the fact that the gravity breaks the symmetry of our potential, leading to some anharmonicity of our magnetic minimum. More in detail, we have found that our eigenaxes of our magnetic trap are rotated in the plane perpendicular with respect to the gravity (plane $x - y$).

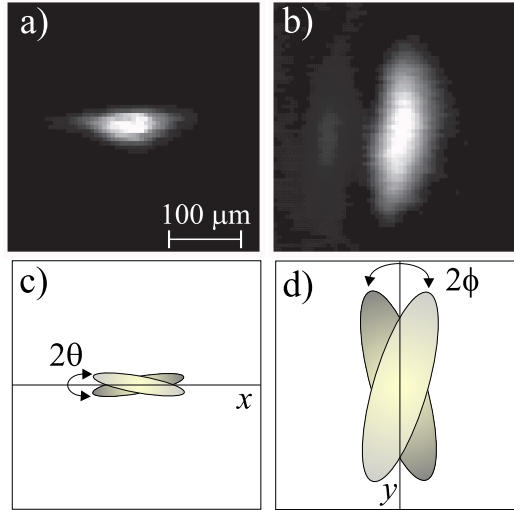


Figure 4.7: Absorption images of a rotating, elongated Rb condensate during the ballistic expansion. In a) the BEC has just been released from the trap ($t_{exp} = 2$ ms), and in b) it has expanded for 23 ms. The other two pictures, not to scale, show the corresponding evolution of a scissors mode. The initial oscillation about the horizontal x -axis (c) is transformed in an oscillation about the vertical y -axis for long expansion times (d).

By exciting dipolar oscillations along the weak axis of the trap (x direction), we were able to produce a rotation in the condensate, as soon as it crossed for the first time the trap minimum. By varying the amplitude of the dipolar oscillations, we could excite an almost pure scissors mode with an initial angle of $\theta_{in} \simeq 15$ mrad. In Fig. (4.7) we show a typical absorption image of the rotating rubidium BEC after 2 ms (a) and 23 ms (b) of ballistic expansion respectively. As remarked above, a rotating condensate shows peculiar features during the expansion that are directly related to its superfluidity. In particular if the condensate is rotating in the $x - y$ plane, with its long axis forming an angle θ_{in} with the x -axis, at

the release from the trap it will start to expand along the short direction. When the aspect ratio of the cloud approaches unity, the rotating BEC will increase its angular velocity for compensating the decrease of the momentum of inertia. At this point the condensate will continue to expand in the other longer direction, as shown in Fig. (4.7c d). In Fig. (4.8) we show the evolution of the rotation angle

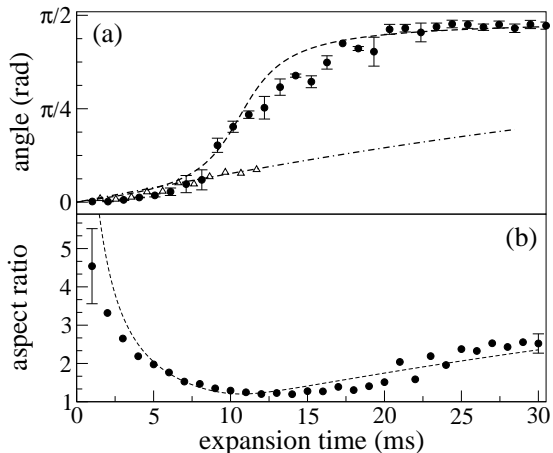


Figure 4.8: a) Evolution of the rotation angle for a condensate (circles) and a thermal cloud (triangles) released with small angular velocity from an elongated trap. b) Evolution of the aspect ratio of the rotating condensate. When the aspect ratio gets close to unity the angular velocity shows a rapid increase. The lines represent the theoretical predictions.

versus the expansion time τ_{exp} . These measurements were performed by fixing the dwelling time of the condensate in the trap, in order to have the same evolution time of the scissors mode. We also show for comparison the same measure done on a thermal cloud. As it is possible to see, at short τ_{exp} , the classical and the Bose gas behave in the same way. In both cases, the expansion is determined by the initial angular velocity Ω_0 . Anyway, as soon as the aspect ratio of the BEC evolves, see Fig. (4.8b), the quenching of its momentum of inertia affects more and more its expansion behaviour that becomes non-classical. Indeed its rotation undergoes a fast acceleration followed by an evolution towards an asymptotic value of the angle, which is smaller than $\pi/2$. Our experimental data are well reproduced by solving the hydrodynamic equation for a superfluid [114], as appear from the dotted lines in figure. From this model, it was also possible to identify three different regimes for the expanding scissors mode, depending on the expansion time τ_{exp} . In the case of $\tau_{exp} < 1/\omega_x$, the behaviour of the Bose gas is quite similar to a classical gas, characterized by an almost sinusoidal scissors mode; if $\tau_{exp} \simeq 1/\omega_x$, the rotation angle is always near to $\pm\pi/4$, depending from the sign of the angular velocity at the release. In this case the oscillation of the angle is near to a square wave, with

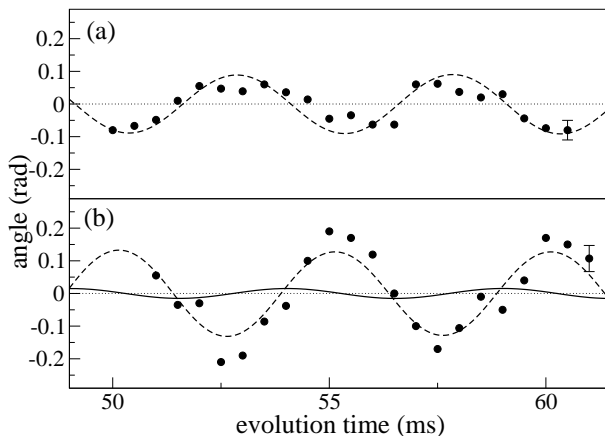


Figure 4.9: Evolution of the scissors mode during the ballistic expansion. In a) the angle $\theta(t)$ after a short expansion of 4 ms (circles) is compared to theory (dashed line) to extrapolate the oscillation in the trap. In b) we compare the latter (continuous line) to the oscillation $\phi(t)$ after a longer expansion of 23 ms (circles). The data show an enhancement of the scissors mode, as expected from theory (dashed line).

the same phase of the angular velocity in the trap. The last situation happens when $\tau_{exp} > 1/\omega_x$: the BEC has reached almost its asymptotic angle $\pi/2$, and at this point it is more convenient describe the angle of the condensate with respect to the vertical axis than with respect the x-y plane. In this last case we find that the sinusoidal scissors mode is repristined with a time-dependence that can be written as:

$$\begin{aligned} \phi(t; t_{exp}) &= \theta_0(t) + F(t_{exp})\Omega_0(t) \\ &= \theta_{0i} \sqrt{1 + \omega_{sc}^2 F^2(t_{exp})} \cos(\omega_{sc}t + \varphi), \end{aligned} \quad (4.26)$$

where F is a non-trivial function of the expansion time and of the trap geometry, and φ is a phase shift. This means that after passing the non classical region $\tau_{exp} \simeq 1/\omega_x$, the condensate does not lose the memory of its initial angular velocity, and it starts to behave again as a classical gas. We could experimentally observe these different regimes, by studying the scissors mode at different expansion time: just after the release from the trap, we have measured a sinusoidal behaviour of the scissors oscillation. When τ_{exp} is closer to 12 ms ($\simeq 1/\omega_x$), we really see a square-wave oscillation, while at longer expansion times, the scissors mode show again the sinusoidal behaviour. In Fig. (4.9), we compare the experimental evolution of the scissors mode with the one predicted from the theory, at two different expansion times. In particular, in (a) we show the behaviour at $\tau_{exp} = 4$ ms from which we can reconstruct the scissors mode in the trap. In (b), we compare

such a motion with the experimental oscillation after 23 ms of expansion. As it is possible to observe the scissors mode at long expansion time is clearly amplified and phase-shifted with respect to the one calculated in the trap. If we calculate the amplification factor $F\omega_{sc}$ (see eq.(4.26)), for $\tau_{exp} = 23$ ms we see that it is almost 10.6: this means that the evolution of the scissors mode outside the trap is a replica of that of the angular velocity in the trap. This is what we have seen above in the case of the scissors mode induced by the collisions between the two condensates. Indeed, in also in that case we observed a proportionality between the evolution of the angle and the angular velocity of the BEC at the release from the trap (see Fig. (4.6)).

CHAPTER 5

Fermi-Bose degenerate mixture

In the previous chapter we have shown how, thanks to the large interspecies scattering length, it has been possible to achieve a binary BEC of K and Rb. The stability of such a system is assured by the large and repulsive interaction between ^{41}K and ^{87}Rb . This achievement has confirmed the result of our previous collisional measurements on the pair ^{41}K - ^{87}Rb . We have also predicted a value for the scattering length between the fermionic isotope ^{40}K and rubidium. The predicted large and negative value, $a = -261 a_0$ allows an efficient sympathetic cooling between these two species also in the degenerate regime.

In this chapter we discuss the experimental realization of such a degenerate mixture composed by a Fermi gas of ^{40}K and a Bose-Einstein condensate of ^{87}Rb atoms. Potassium atoms are cooled to quantum degeneracy by thermal contact with evaporatively cooled rubidium, and the minimum temperature we can measure is about 0.2 the Fermi temperature T_F . We see that the main consequence of this large and attractive interaction between ^{40}K - ^{87}Rb atoms is the possibility of observing the collapse of the whole system.

5.1 Motivations and experimental procedure

Evaporative cooling is the standard technique by which it is possible to bring a dilute atomic gas to quantum degeneracy. We have seen that it exploits the thermalization between the trapped atoms after the removal from the trap of the more energetic ones by RF (μ -wave) knife. The thermalization occurs by elastic collisions so that the interaction properties of the system play a relevant role in the efficacy of the cooling. On the other hand, at very low temperatures, only s-wave

scattering amplitude contributes significantly to the collisional cross-section, being the other contributions (p -wave, d -wave, etc..) suppressed. A system composed by identical fermions is thus completely non interacting. Since elastic collisions between the fermionic atoms are forbidden, the evaporative cooling scheme cannot work at all, differently to the case of bosonic systems which are instead efficiently cooled to quantum degeneracy. It is possible to circumvent this limitation in cooling fermions by trapping simultaneously two separate spin states, as demonstrated in [24; 25]. Evaporative cooling is then performed on both the components, since s -wave collisions between different atoms are allowed. The other scheme, successfully carried out at ENS [29], at Rice University [28] and at MIT [30], is to mix the fermionic gas with a bosonic one. It has been possible to realize systems composed by a Fermi gas interacting with a Bose-Einstein condensate. With respect to the previous scheme, sympathetic cooling offers the unique possibility of cooling the fermionic clouds well below the Fermi temperature. Indeed, as discussed in (1.3.1), once the degeneration regime is reached, Pauli blocking reduces the elastic scattering processes between the fermions [42], limiting in this way the minimum temperature achievable. Pauli blocking is less relevant when considering mixtures composed by bosons and fermions. The minimum temperature that is possible to reach corresponds to the minimum temperature achievable for the bosonic component, and it is determined by the ratio between the two heat capacities.

In our specific case, we mix together ^{40}K and ^{87}Rb . The main difference of our mixture with respect to the others available [25; 28–30], is the large and attractive character of the interspecies scattering length of ^{40}K - ^{87}Rb . This feature allows a very efficient sympathetic cooling of potassium even in the degenerate regime since the two clouds are supposed to maintain always a good thermal contact. The behaviour is expected to be different for the mixtures of ^6Li - ^7Li [53] and of ^6Li - ^{11}Na [54] where phase-separation between the two components should be observed.

The set-up and the experimental procedure for loading K and Rb in the magnetic trap is the same that we have described previously. There are however some differences that it is worth to point out, in order to understand why sympathetic cooling turned out to be so efficient. The first difference stands in the fact that ^{40}K can be much efficiently cooled already in the MOT stage, with respect to ^{41}K . Indeed Sub-Doppler cooling mechanisms work properly for ^{40}K , allowing temperatures of the order $60\ \mu\text{K}$, and temperature in the QUIC trap of about $100\ \mu\text{K}$ to be compared with $200\text{-}300\ \mu\text{K}$ we have measured for ^{41}K . Another advantage of working with ^{40}K is that we do not have any losses of rubidium during the loading of potassium in the second MOT. Indeed the nonlinear processes which were present into the tapered amplifier when both potassium and rubidium lights were injected are absent, since the hyperfine splitting of ^{40}K is $\simeq 1.28\ \text{GHz}$. We can typically load in the QUIC trap about 10^5 atoms of ^{40}K and 5×10^8 ^{87}Rb at a temperature of $100\ \mu\text{K}$. Potassium and rubidium atoms are magnetically trapped in the states $|9/2, 9/2\rangle$ and $|2, 2\rangle$ respectively: these states experience the same trapping potential with frequencies $\nu_a = 24\ \text{Hz}$ and $\nu_r = 317\ \text{Hz}$ for

K and $\nu_a = 16.3$ Hz and $\nu_r = 215$ Hz for Rb. Once the atoms of both species are trapped in the magnetic potential, we perform evaporative cooling only on the rubidium component. Differently from the ^{41}K - ^{87}Rb mixture when we were forced to use μ -wave knife for cutting the rubidium distribution, it is possible to use the more conventional RF evaporation that couples the various Zeeman sublevels of the $F = 2$ rubidium ground state, since, the nuclear spin of potassium is $I = 4$. With an evaporation ramp lasting around 25 s we are able to cool below $1 \mu\text{K}$ a sample composed by 2×10^4 K atoms and 10^5 Rb atoms and we have observed that the temperature of potassium cloud follows the one of rubidium, indicating a large interaction between the two species. We probe the two clouds by two-colour absorption imaging, using two delayed pulses at 766.7 nm for K and at 780 nm for Rb, whose duration is about $30 \mu\text{s}$ each.

5.2 Measuring the interaction: parametric heating and dipolar oscillations

We have directly measured the scattering length between ^{40}K and ^{87}Rb , by performing rethermalization measurements on a thermal sample at $T = 400$ nK typically composed by 1.2×10^4 K atoms and 4×10^4 rubidium atoms [15]. As discussed in the case of ^{41}K - ^{87}Rb mixture, the idea is to drive out of the initial equilibrium the system by modulating the trapping potential at twice the radial oscillation frequency of rubidium ($\nu_h \simeq 420$ Hz). After this selective parametric heating phase, we have studied the subsequent heating of potassium, mediated by the elastic collisions with the rubidium component. From the analysis of the experimental data, similar to the one presented in (3.2.1), we have derived a quite large value for the triplet scattering length between ^{40}K and ^{87}Rb , $|a| = 330_{-100}^{+160} a_0$, where the uncertainty is due to the uncertainty of 40% on the number of atoms and on the measure of the thermalization time τ (10%). If we now compare this experimental result with the value we inferred by mass scaling from collisional measurements performed on the ^{41}K - ^{87}Rb mixture, $a = -261_{-159}^{+170} a_0$, we find good agreement between the two. In particular, the measurement of a such large value for $|a|$ also seems to confirm the *attractive* character of the interaction, since a positive scattering length would have been compatible only with a much smaller magnitude. Due to this large value of the scattering length, we could not repeat the same procedure performed on ^{41}K - ^{87}Rb mixture (3.2.1), when by studying the thermalization rate as a function of the temperature of the mixture, we were able also to determine the sign of the scattering length. In the case of ^{40}K - ^{87}Rb the scattering cross-section is in the Wigner regime [22], i.e. it assumes the constant value $\sigma = 4\pi a_{KRb}$ independently from the temperature and the equation (1.1.1) is no more useful.

In order to have another estimation of ^{40}K - ^{87}Rb scattering length, we have decided to study the damping of the dipolar oscillations of thermal K-Rb sample [96]. As discussed previously, we can excite dipolar oscillations along the weak axis of the trap (pinch axis) by suddenly displacing the minimum of the trapping potential, varying the ratio of the current flowing in the trap coils. By an appropriate choice of the experimental parameters, such as the amplitude of the oscillation and the timing of the displacement, we have excited only pure dipolar oscillations, not involving any apparent deformation of the shape of the two clouds as instead occurred in (4.3.1). The mean relative velocity between the two centers of mass, $5 \mu\text{m/ms}$, assured that the two clouds were almost always overlapping during the oscillation dynamics. In Fig. (5.1), we report a typical measurement, performed on a thermal system composed by 8×10^3 of K and 8×10^4 Rb atoms at a temperature $T = 300$ nK. The effect of the interaction between potassium and rubidium clearly appears from the observed damping in the motion of both species. The coupled center-of-mass motion can well be reproduced by a classical model of two harmonic oscillators coupled by a viscous damping. For sake of clarity, we rewrite

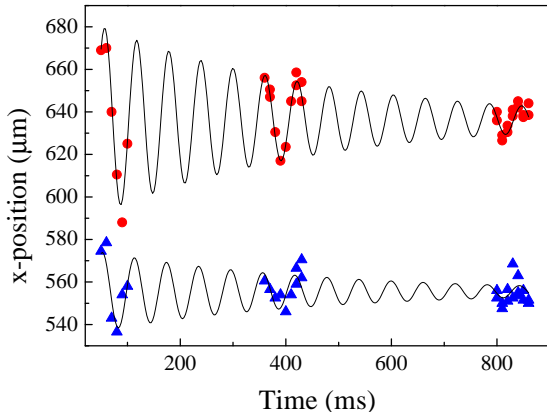


Figure 5.1: Coupled dipolar oscillations of 8×10^3 thermal K (triangles) and 8×10^4 Rb (circles) atoms along the horizontal axis at $T=300$ nK. The two clouds oscillate at the same frequency, signature of the hydrodynamic regime. The solid curves are the best fit to the model presented in the text.

here the equations of motion for K and Rb clouds (3.2.1):

$$\begin{aligned}\ddot{x}_{Rb} &= -\omega_{Rb}^2 x_{Rb} - \frac{4}{3} \frac{M_K}{M} \frac{N_K}{N} \Gamma (\dot{x}_{Rb} - \dot{x}_K) \\ \ddot{x}_K &= -\omega_K^2 x_K + \frac{4}{3} \frac{M_{Rb}}{M} \frac{N_{Rb}}{N} \Gamma (\dot{x}_{Rb} - \dot{x}_K),\end{aligned}\quad (5.1)$$

where M is the total mass $M_K + M_{Rb}$ and N the total number of atoms $N_K + N_{Rb}$, and Γ is the rate of K-Rb two-body elastic collisions, given by:

$$\Gamma = \bar{n} \sigma v_{th} \quad (5.2)$$

where $v_{th} = \sqrt{8k_B T / \pi M}$ is the rms relative thermal velocity and $\bar{n} = (\frac{1}{N_{Rb}} + \frac{1}{N_K}) \int d^3 r n_{Rb} n_K$ is the averaged density. In particular the motion of potassium and rubidium is described by two normal modes, whose frequency and damping depend on the scattering rate Γ . From this kind of analysis, it is possible to extract the value of the collisional cross-section $\sigma = 4\pi a^2$, and therefore the magnitude of the triplet scattering length. To this purpose, we have performed several measurements of this kind by varying the temperature of the mixture in the range $T=300-500$ nK, the total number of atoms of K and Rb in the range $N = 10^4 - 10^5$ and the ratio N_{Rb}/N_K from 2.5 to 7.5. Then we have made a weighted average of the resulting values, obtaining for a the following value: $a=410_{-80}^{+90} a_0$. Here again the uncertainty is dominated by a 40% uncertainty on the number of atoms

of both species. As we can see, this result turns out to be in good agreement with the other we have obtained by rethermalization measurements, although it gives an even more large magnitude of the scattering length.

5.2.1 From hydrodynamic to collisionless regime

If we now look in more detail at the evolution of the center-of-mass motion of potassium and rubidium shown in Fig. (5.1), we note that the two clouds oscillate at the same frequency, $\nu = 18$ Hz. We remember that along the weak axis of the trap the "bare" oscillations frequencies are predicted to be $\nu = 16.3$ Hz and $\nu = 24$ Hz for Rb and K respectively. The explanation of this behaviour can be found by considering the dependence of the dynamics of the center of mass on the collisional properties of the whole system. Indeed, as briefly mentioned in (4.3), depending on the magnitude of the scattering rate Γ with respect to the oscillation frequency ω , the system is said to be either in the collisionless ($\Gamma \ll \omega$) or in the hydrodynamic regime ($\Gamma \gg \omega$) [109]. We have seen that the center-of-mass motion can be described by a classical model of two coupled harmonic oscillators that oscillate at two normal modes and the center-of-mass motion is a superposition of these two modes. The frequency and the damping time τ of these modes depend on collisional rate Γ . At low collisional rate ($\Gamma \ll \omega$) the two clouds oscillate each at its own bare frequency, and the ratio between the damping time scales as the inverse ratio of the total mass of each sample. When the collisional rate increases, the damping time of the two normal modes decreases, and the frequencies of the modes shift to an intermediate value. If finally the collisional rate becomes larger than the oscillation frequency of the trap ($\Gamma \gg \omega$) the system enters in the hydrodynamic regime. In particular, the motion is still described by two normal modes, one corresponding to an "in-phase" motion of the two clouds, and the other one to the "out-of-phase" oscillation. The latter one is overdamped and its frequency decreases when increasing the scattering rate Γ . This means that the two samples start to oscillate at an intermediate frequency which depends on the ratio between the masses. In this regime the damping time τ increases linearly with the collisional rate, differently from the collisionless regime where it decreases as $1/\Gamma$ [109]. In the experiment we have found that potassium and rubidium clouds oscillate at the same frequency, almost in phase and with a long damping time [96]. In Fig.(5.2), we show the oscillations of a thermal sample composed by 2×10^4 K and 2×10^5 Rb atoms at $T=300$ nK. The measured collisional rate is 650 s^{-1} , and the corresponding damping time is almost three times the damping time of the measure presented in Fig. (5.1) since in that case the total number of atoms was 1/3 of this last one. This result confirms that our system is in the hydrodynamic regime, since the damping time increases linearly with the collisional rate Γ , which is proportional to the density of the sample.

It is worth to compare the experimental result of the ^{40}K - ^{87}Rb mixture with the one obtained for the ^{41}K - ^{87}Rb system (3.2.2). Both measurements were performed with similar number of atoms and almost at the same temperature. While

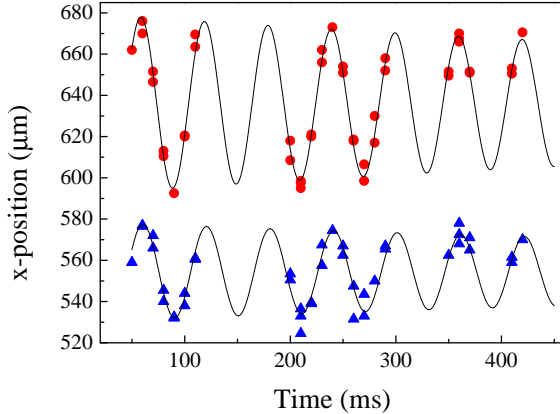


Figure 5.2: Coupled dipolar oscillations of 2×10^4 thermal K (triangles) and 2×10^5 Rb (circles) atoms along the horizontal axis at $T=300$ nK. Also in this case, the two clouds oscillate at the same frequency, indicating that the system is in the hydrodynamic regime. The solid curves are the best fit to the model presented in the text.

^{40}K and ^{87}Rb samples oscillate at the same frequency with long damping time, in the other case, potassium and rubidium oscillate at different frequencies. In particular, while the rubidium motion is only marginally affected by the presence of potassium, the one of K is largely modified by the interaction with the other specie and we can see the appearing of beatings at the frequency of rubidium. The fact that ^{40}K - ^{87}Rb mixture is in the hydrodynamic regime, while the ^{41}K - ^{87}Rb is in the collisionless regime depends only on the different magnitude of the triplet scattering length, that for ^{40}K - ^{87}Rb is almost 3 times larger.

We have repeated these dipolar oscillation measurements also in the case of a degenerate system, composed by a Fermi gas of ^{40}K interacting with a BEC of ^{87}Rb : as we will discuss later, in this case we have found that the quantum statistics strongly affects the collisional dynamics of the system which enters in the collisionless regime.

5.3 ^{40}K - ^{87}Rb degenerate mixture

By proceeding with the evaporation of the rubidium component, we have observed the formation of a degenerate Fermi gas of ^{40}K atoms coexisting with a Bose-Einstein condensate of ^{87}Rb .

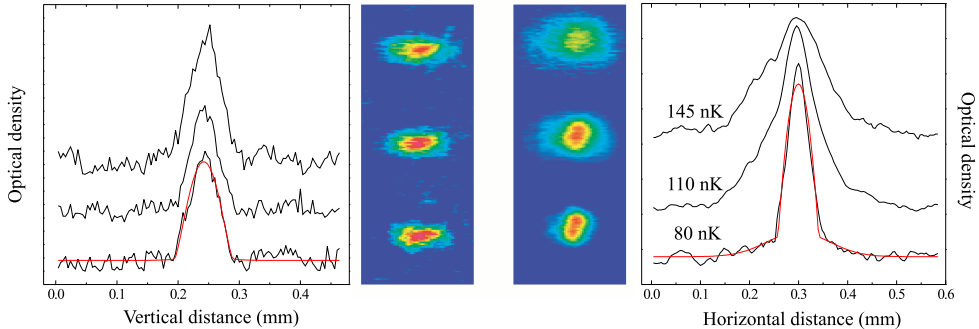


Figure 5.3: Simultaneous onset of Fermi degeneracy for ^{40}K (left) and of Bose-Einstein condensation for ^{87}Rb (right). The absorption images are taken for three decreasing temperatures, after 4.5 ms of expansion for K and 17.5 ms for Rb, and the sections show the profile of the momentum distributions.

In Fig. (5.3), we show a series of absorption images of the mixture at three different stages of the evaporation ramp corresponding to three different temperatures of the system. The images are taken after a ballistic expansion appropriate to measure the momentum distribution of the samples and in particular the expansion time is 4.5 ms for K and 17.5 ms for Rb. Sections of such images are also reported: they are taken along the vertical direction for K, and along the horizontal direction for Rb. With our experimental parameters, we have a Fermi temperature $T_F=250$ nK and a critical temperature for BEC $T_c=110$ nK for a sample composed by 10^4 and 2×10^4 atoms, respectively, that correspond to peak-densities of the order of $n \simeq 10^{14} \text{ cm}^{-3}$ for Rb and $n \simeq 5 \times 10^{12} \text{ cm}^{-3}$ for K. The fact that the Fermi temperature is higher than the critical temperature for Bose condensation arises from the difference in mass, $m_{Rb} \simeq 2m_K$, and from equations (1.32) and (1.55). We have determined the temperature of the whole system by measuring the temperature of the thermal wings of the Bose gas, assuming thermal contact between the two components. As the temperature is decreased by almost a factor of two (from top to bottom in Fig. (5.3)), we have observed the formation of a rubidium BEC, shown by the appearance of a narrow peak in the momentum distribution, while the width of the fermionic component remains almost constant, due to the Fermi pressure. By fitting the coldest K cloud with a Thomas-Fermi profile [38] we have obtained a radius $R=52 \mu\text{m}$, which is consistent to within 10% with the minimum radius allowed by Fermi statistics: $R = R_F \sqrt{1 + \omega_r^2 \tau^2}$, where

$R_F = \sqrt{2k_B T_F / (M\omega_r^2)}$ is the Fermi radius and τ is the expansion time.

The condensate in Fig. (5.3) contains less than 40% of thermal fraction, indicating that the temperature of the Fermi gas is about $T=80$ nK, corresponding to $0.3 T_F$. In Fig. (5.4) we show the evolution of the Gaussian $1/e$ width of the

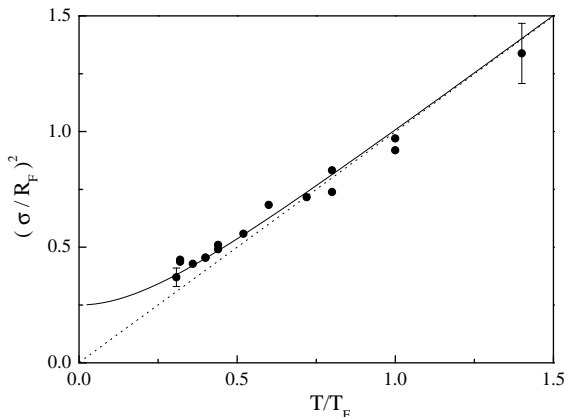


Figure 5.4: Gaussian $1/e$ radius of the radial distribution of K atoms, versus the reduced Fermi temperature. The temperature is given by the Rb sample and $T_F=250$ nK. The solid line is the theoretical prediction for an ideal Fermi gas, while the dotted line is the classical behaviour.

fermionic sample as a function of temperature. As expected from classical theory, the square of the width, normalized to R_F , scales linearly for $T > T_F$, indicating thermal equilibrium between K and Rb. On the other hand, below T_F , the data deviate from the behaviour expected for a classical gas, and indeed they are better reproduced by the prediction of the model for an ideal Fermi gas [38].

By measuring the size of both the degenerate clouds after the expansion, we have determined the size and the positions inside the magnetic trap, for the typical number of atoms 10^4 and 2×10^4 for potassium and rubidium respectively. We have to note that in our magnetic trap, the centers of mass of the two species are displaced due to the different gravitational sag for K and Rb. However, such displacement, $\Delta z = 2.9 \mu\text{m}$, is not sufficiently large to affect the geometrical overlap of the two degenerate components, since the radial sizes of the Fermi and Bose gases are $R_F=5.1 \mu\text{m}$ and $R_B=2 \mu\text{m}$, respectively. Therefore, the BEC is completely immersed in the Fermi sea, with a ratio of the two volumes of approximately 1:16. The lifetime of the mixture is around 1 s. which is also the lifetime of the Bose condensate.

As we have remarked previously, we expect the sign of the ^{40}K - ^{87}Rb scattering length to be positive, resulting in an attractive interaction between potassium and rubidium atoms. We have seen a first evidence of this attractive interaction by

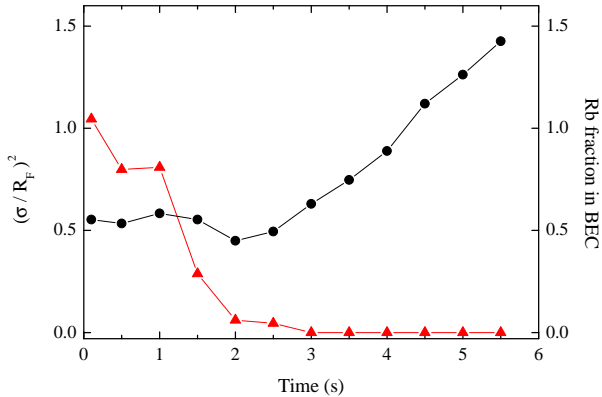


Figure 5.5: Evidence of thermal exchange between the two degenerate gases. The Gaussian width of ^{40}K (circles) increases only when ^{87}Rb atoms (triangles) are almost completely evaporated from the trap, as explained in the text. The solid lines are a guide to the eye.

leaving the degenerate mixture in the magnetic trap for a relatively long time after the end of the evaporation and studying the evolutions of the temperatures of both the components. The Rb temperature was kept constant by means of a radio-frequency shield, but the background heating (≈ 100 nK/s) caused by fluctuations in the magnetic field, continuously removed atoms from the BEC. This is illustrated in Fig. (5.5), together with the simultaneous behaviour of K. The evolution of the width of the fermionic distribution indicates that K starts to heat up only when Rb is almost completely evaporated from the trap. Although, as shown in Fig. (5.4) the Gaussian width is not a sensitive "thermometer" at low temperatures, the results reported in Fig. (5.5) are significant. Indeed, should K be thermally decoupled from Rb, its heating at the observed rate would manifest already after 1 s even in the extreme case of an initial temperature $T \ll T_F$.

5.3.1 Dipolar oscillations in the quantum degenerate regime

In (5.2.1) we have shown how the large interspecies scattering length affects dramatically the dynamics of the dipolar oscillation of thermal potassium and rubidium atoms. In particular we found that the interaction is so large that the system is in the hydrodynamic regime, characterized by a scattering rate bigger than the oscillation frequency of the atoms in the trap ($\Gamma \gg \omega$).

Once observed the degenerate mixture, we have decided to repeat such measurements on the degenerate samples. Since in our system the Fermi temperature is always higher than the critical Bose temperature, we first have considered a mixture composed by a Fermi gas interacting with a thermal cloud of rubidium

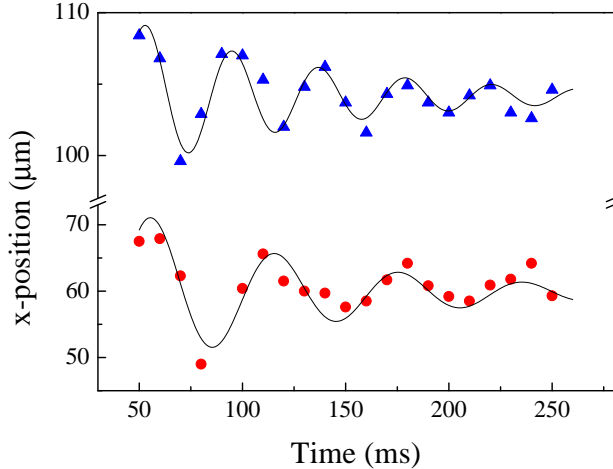


Figure 5.6: Coupled dipolar oscillations of degenerate K (triangles) and thermal Rb (circles) along the horizontal axis in the collisionless regime at $T=120$ nK. The solid lines are the best fit to the model presented in the text.

[96]. In Fig. (5.6) we show the evolution of the center of mass of potassium and rubidium after the excitation of the dipolar motion at $T = 120$ nK, when we have a Fermi gas of potassium of $\sim 10^4$ atoms and a thermal cloud of rubidium composed by 3×10^4 atoms. As it is possible to see, in this case the two samples oscillate at their "bare" frequency ($\omega_K \approx 2\pi \times 24 \text{ sec}^{-1}$, $\omega_{Rb} \approx 2\pi \times 16.3 \text{ sec}^{-1}$). This observation indicates that the system is in the collisionless regime ($\Gamma \ll \omega$). We indeed obtain for the scattering rate Γ , $\Gamma=60(10)$ Hz, which is significantly smaller than the one expected for a non-degenerate sample containing the same number of atoms at $T=100$ nK, $\Gamma=100$ Hz.

The observed reduction of the scattering rate is an effect related to the degenerate regime of the potassium component. In section (1.3.1), we have discussed the consequences of the Fermi statistics on the scattering properties of the Fermi gas, pointing out that as soon as the degenerate regime is reached, Pauli blocking inhibits the elastic scattering events involving the fermionic atoms. In our particular case, in which we have collisions between a Fermi gas and thermal gas of rubidium only the fermions in the outer shell of the Fermi sphere, having an energy $E=E_F-E_{CM}$ can scatter with bosons and participate to the damping. Here E_{CM} is the collision energy of fermions and bosons in the center-of-mass frame

$$E_{CM} = 1/2\mu\langle v^2 \rangle, \quad (5.3)$$

where μ is the reduced K-Rb mass. An upper value for E_{CM} for the typical

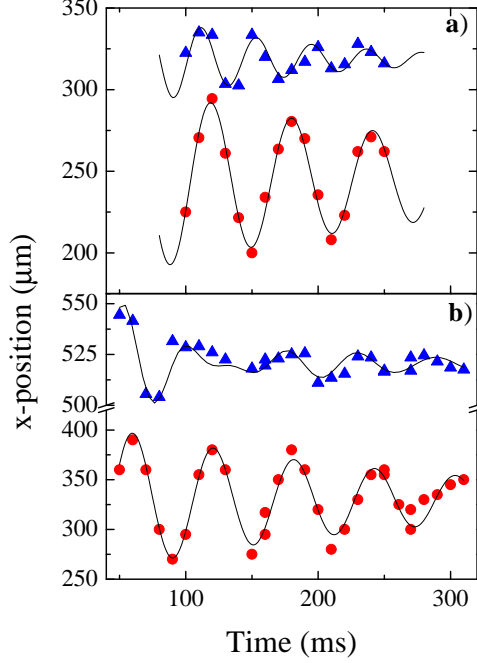


Figure 5.7: Coupled dipolar oscillations of degenerate K (triangles) and Rb (circles) clouds along the horizontal axis: (a) in the intermediate regime at $T \approx 0.84 T_c$ nK and (b) in the collisionless regime at $T < 0.7 T_c$ nK. The solid lines are the best fit to the model presented in the text.

experimental parameters is $E_{CM} \approx 50$ nK, which is significantly smaller than the typical Fermi energy $E_F = 300$ nK. At $T = 0$ K, just half of the fermions could participate to scattering process with boson however a finite temperature reduces Pauli blocking because of the smearing of the Fermi distribution. As shown in [41], for this excitation energy Pauli blocking should nevertheless produce a significant reduction of Γ also at the temperature $T = 0.4 T_F$ of the experiment, as we have observed indeed.

We have performed these oscillation measurements also on a fully degenerate mixture, composed by a Bose-Einstein condensate and a Fermi gas: in this case, depending on the degree of degeneration of the Bose gas, we have observed the transition from the hydrodynamic to the collisionless regime [96] In Fig. (5.7a) we show the strongly damped Rb and K oscillations in this transition region: such transition corresponds to a passage from a synchronous motion in which the two

clouds oscillate at an intermediate frequency to an uncoupled motion at the two bare frequencies. Here the dipole oscillations are excited for a mixed sample with $N_K=2.5\times 10^4$ K atoms and $N_{Rb}=3.9\times 10^4$ at $T=0.84T_c=118$ nK. In Fig. (5.7b) we instead report a measurement performed with a BEC at lower a temperature $T < 0.7T_c$. Here the two samples oscillate at their bare frequencies, indicating that we are in the collisionless regime. Notice that the minimum measured temperature is fixed to $T=0.7T_c$ by the minimum detectable uncondensed Rb component.

We have to point out that this variation in the collisional rate that we have observed, reflects the transition from the classical to the quantum regime. Indeed, for explaining the measured behaviour we have to consider both the superfluid nature of the BEC and the Pauli blocking. Collisions between the BEC and fermions are indeed suppressed if the momentum exchanged in the collision is below $M_{Rb}c$, where c is the sound velocity $c=\sqrt{4\pi\hbar^2 a_{Rb}n_0/M_{Rb}^2}$. We have to stress that the large reduction of Γ when lowering the temperature from T_c to $0.85 T_c$, cannot be reproduced by the classical prediction. Since the change in temperature between these two measurements is negligible for fermions, such a reduction of the collisional rate cannot be ascribed to Pauli blocking in the Fermi gas, and it can actually be the consequence of superfluidity in the BEC.

However, a complete description of this behaviour requires a model which takes into account the quantum nature of the system. Indeed the model of the two classical coupled harmonic oscillators does not consider the damping mechanisms which are likely to occur in the degenerate regime, such as Landau damping [115–117] and the breaking of the superfluidity of the BEC [118] which can largely influence the dynamics of the system.

5.4 Mean-field interaction in the degenerate mixture

So far, we have described the interaction between potassium and rubidium atoms only by the scattering length a_{BF} , that directly gives information on the collisional cross-section between these two atomic species. To gain a more quantitative insight into the quantum nature of the mixture, it is necessary to consider a more complicated many-body approach. In section (1.4.2), however, we have remarked that the ground state of a degenerate mixture composed by a Fermi gas interacting with a Bose condensate can be well described in the mean-field approximation [17; 37] by the following equations:

$$n_F(\mathbf{r}) = \frac{\sqrt{2m_F^3}}{3\pi^2} [\mu_F - U_F(\mathbf{r}) - \frac{4\pi a_{BF}}{m_{BF}} n_B(\mathbf{r})]^{3/2} \quad (5.4)$$

$$\left[-\frac{1}{2m_B} \nabla^2 + U_B(\mathbf{r}) + \frac{4\pi a_{BF}}{m_{BF}} n_F(\mathbf{r}) + \frac{4\pi a_B}{m_B} \phi^2(\mathbf{r})\right] \phi(\mathbf{r}) = \mu_B \phi(\mathbf{r}) \quad (5.5)$$

where $\phi_B(\mathbf{r}) = \sqrt{n_B(\mathbf{r})}$, $M_{BF} = 2m_F m_B / (m_B + m_F)$ is twice the reduced mass of the pair. As we have already addressed, the mean-field interaction on the

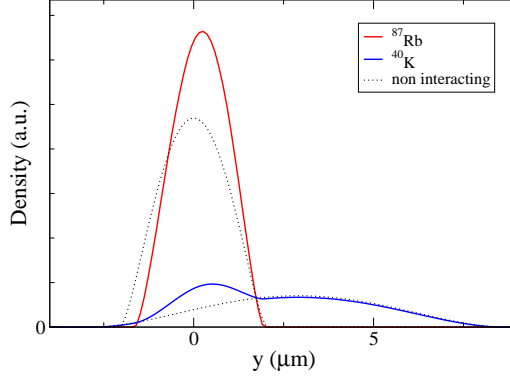


Figure 5.8: Density profiles of the Bose-Einstein condensate of ^{87}Rb and of the Fermi gas of ^{40}K . The dotted lines correspond to the noninteracting case. The effect of the interaction between fermions and bosons is an increase of the peak-density of both species in the overlap region (continuous lines). The curves are the result of mean-field calculations with our experimental parameters.

j^{th} specie is described by the term $4\pi a_{ij}/m_{BF} n_i$, proportional to the scattering length a_{ij} and to density of the i^{th} specie. This means that a large scattering length and a high density of both species can deeply modify the behaviour and even the characteristic properties of each component. We have also to remark that, in the case of fermions, we do not have any self mean-field contribution, due to the fact that we are dealing here with a system composed by identical fermions, that do not interact at this ultralow temperatures. We have solved these coupled equations plugging in the typical number of atoms of the Fermi gas and of the condensate, our trapping frequencies and our estimation of the interspecies scattering length, $a_{BF} = -410 a_0$. We have first studied the situation in which we neglect the interaction between the two components, $a_{BF} = 0$. In Fig. (5.8) the dotted curves show the calculated density profiles along the direction of the gravity of both the clouds in this non interacting case. The number of atoms that we have considered here are 10^4 and 3×10^4 , for potassium and rubidium respectively. As it is possible to see, the two sample are simply displaced along the gravity due to the gravitational sag, induced by the different mass of K and Rb and, as we expect, the peak-density of the Fermi gas is much lower than that of the condensate, due to the Fermi pressure which oblige the fermionic system to a much larger shape and consequently lower density with respect to the BEC (1.3.1).

If we now switch on the attractive interaction $a_{BF} = -410 a_0$, the situation

changes, as clearly appear from the continuous lines in Fig. (5.8). The first thing we can note is that, since the interaction between potassium and rubidium is attractive, we do not see any phase-separation between the two clouds. They still keep good spatial superposition and, despite of the gravitational sag, the BEC is completely immersed in the Fermi "sea".

The most relevant consequence of the interaction is, anyway, the large increase of the density of both the species in the overlap region. This increase is evident for both the component, but larger in the case of potassium since the effective influence of the interaction depends from the density of the other specie, and the mean density of a Bose-Einstein condensate ($n \simeq 10^{14}$) is typically two orders of magnitude larger than the one of a Fermi gas ($n \simeq 10^{12}$).

5.4.1 Evidence of the mean-field interaction: study of the expansion of the clouds

In order to observe the effect of such a large mean-field interaction on the mixture, we have studied in detail the expansion of the two degenerate samples in presence or not of the other component. Before discussing our experimental results, it is worth to recall here very briefly the main features of the expansion of a pure Bose-Einstein condensate and of a non interacting Fermi gas, that we have discussed in (1.3.2) and in (1.3.1). In the case of a condensate, the expansion is determined essentially by the repulsive mean-field interaction between the bosons that, as soon as the trapping potential is turned off, is transformed in kinetic energy [4]. In particular, for an anisotropic potential, the most confined directions expand faster than the other one, resulting in an inversion of the initial ellipticity of the condensate. The evolution of the radii of the BEC is given by the following expressions,

$$\begin{aligned} R_r(t) &= R_r(0)\sqrt{1 + \tau^2} \\ R_a(t) &= R_a(0) (1 + \lambda^2[\tau \arctan \tau - \ln\sqrt{1 + \tau^2}]) \end{aligned} \quad (5.6)$$

where where $\tau = \omega_r t$ and $\lambda = \omega_a/\omega_r$. The aspect ratio of the condensate, R_r/R_a , initially smaller than one, crosses unity at about $\tau \simeq 1/\omega_r$. This behaviour is very different from the expansion of a thermal gas trapped in the same potential which is completely isotropic (the aspect ratio goes asymptotically to one).

Conversely, the expansion of a non interacting Fermi gas is quite similar to the one of a classical gas, since the mean-field interaction is not present. The evolution of the radii can be easily calculated in the semiclassical approximation [40], giving for the aspect ratio the following result:

$$\mathfrak{R} = \sqrt{\frac{r_a^2}{r_r^2}} = \frac{1}{\lambda} \sqrt{\frac{1 + \omega_a^2 t^2}{1 + \omega_r^2 t^2}} \quad (5.7)$$

At long expansion time, the aspect ratio of the Fermi gas approaches asymptotically to one, as in the case of a thermal gas. Let us consider how the mutual interaction modifies the expansion of the two degenerate gases. The expansion of a quantum degenerate boson fermion mixture has been recently studied in detail by H. Hu et al. in [119]. In particular, they have applied their general results to our specific ^{40}K - ^{87}Rb mixture, by considering our experimental parameters and our estimation of the interspecies scattering length. In this work they have shown that the attractive interaction between potassium and rubidium atoms gives rise essentially to two separate effects that affect in different way the expansion of the degenerate mixture. The first consequence is the modification of the density

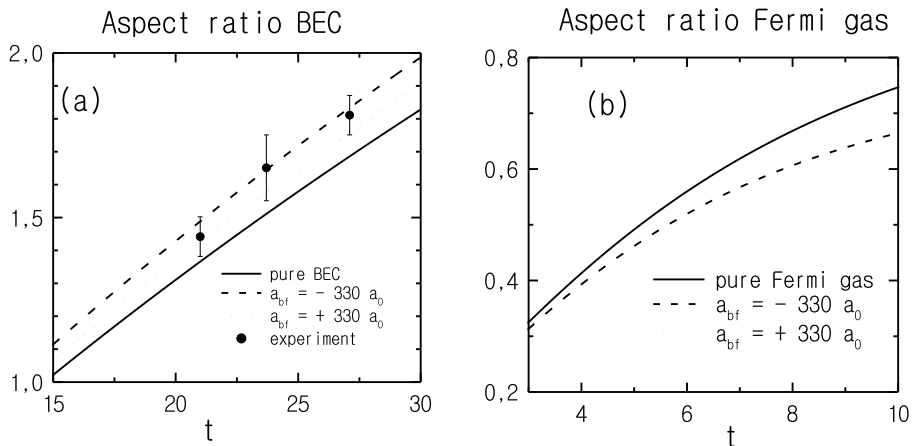


Figure 5.9: Theoretical predictions for the evolution of the aspect ratio of the Bose-Einstein condensate of ^{87}Rb (a) and of the Fermi gas of ^{40}K (b) as a function of the dimensionless parameter $\tau = \omega_r t$. The calculated curves [119] refer to an interaction between fermions and bosons of $a = \pm 330 a_0$. The different behaviour between an attractive and repulsive interaction is evident. In the case of the expansion of the Bose gas a comparison with the experimental results is shown.

profiles of the two clouds in the trapping potential, as we have already mentioned above. In particular, we have noted that the attractive character of the ^{40}K - ^{87}Rb interaction induces an increase of the density of both the condensate and the Fermi gas in the overlap region, as it is possible to see in Fig (5.8). This enhancement of the density is likely to be seen by the atoms as an effective tighter confining potential with higher oscillation frequencies. This *static effect* depends only on the interaction between the atoms in the trap and it leads to a faster expansion for both BEC and Fermi gas. The second consequence of the mean-field interaction takes place instead during the expansion of the degenerate clouds and it can be seen as a *dynamical effect*. What they have suggested is that the condensate and

the Fermi gas also interact during the first moments after the release from the trap. Anyway, the result of this further interaction goes opposite with respect to the one described above. Indeed, due to the attractive sign of the scattering length, both species are slowed down during the expansion. This slowing effect becomes more important the smaller is the relative velocity between the two clouds.

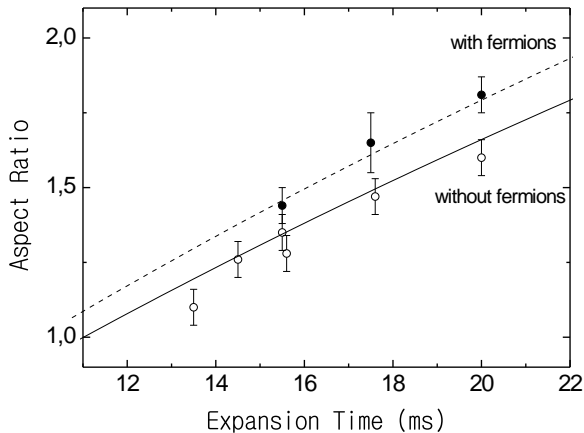


Figure 5.10: Evolution of the ^{87}Rb BEC with and without degenerate fermions. As predicted from the theory discussed in the text, in presence of the Fermi gas of ^{40}K , the condensate expands faster. The continuous lines are the theoretical predictions corresponding to our experimental parameters.

As a result, the actual expansion of the two Fermi and of the Bose is determined by the competition of these two contributes. In Fig (5.9), we show the results of this theoretical model. We plot the evolution of the aspect ratio of the BEC and of the Fermi gas as a function of the dimensionless parameter $\tau = \omega_r t$. In particular in Fig (5.9a) is reported the predicted expansion of the a Bose condensate, for a boson-fermion interaction of $a_{BF} = \pm 330 a_0$: in the case of attractive interaction with the degenerate fermionic cloud, the expansion of the condensate is predicted to be faster than the non interacting one. This behaviour is explained by taking into account the mechanisms that we have discussed before. Indeed, if from one side the static effect wants to accelerate the evolution of the aspect ratio of the cloud, on the other side the dynamical one decreases it, since during the first moments of the expansion the bosons still feel an attractive 'potential' of fermions. Anyway it turns out that for the BEC, the static effect of the mean-field attraction dominates with respect to dynamical one, leading to a faster expansion

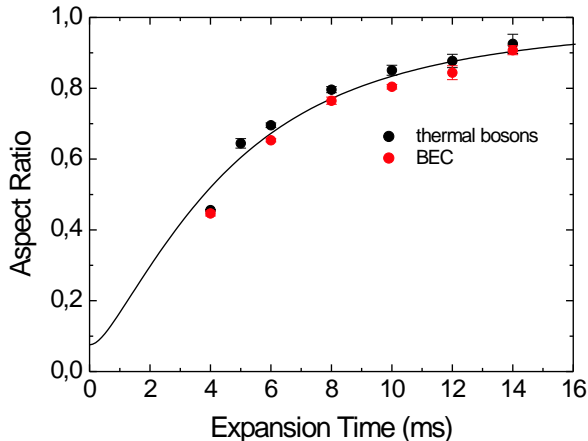


Figure 5.11: Evolution of the aspect ratio of Fermi gas in presence of a thermal gas of bosons (black dots) and of a BEC (red dots). The black line is the theoretical prediction for a non interacting Fermi gas, calculated with our parameters. As it is possible to see, the evolution in presence of the Bose condensate is slower due to the attractive ^{40}K - ^{87}Rb interaction.

with respect to the one expected for a pure condensate. It also appears from the figure, that in the case of repulsive interaction between bosons and fermions, the evolution of the aspect ratio is slower than in the attractive case. This can be understood by considering that in case of repulsion between the two species, the phase-separation would wash out the static contribution to the expansion, reducing in this way the velocity of the expansion. In the experiment, we have really observed this behaviour, as shown in Fig. (5.10), where we plot the evolution of the aspect ratio of the rubidium condensate in function of the expansion time when potassium degenerate gas is present (upper curve) or absent (lower one). It is possible to note the difference between the two situations that indicates that the resulting effect of the interaction between bosons and fermion actually reveals in a faster expansion of the condensate.

In Fig. (5.9b), it is instead presented the theoretical result for the expansion of the Fermi gas. In the case of an non interacting Fermi gas, we see that evolution of the aspect ratio follows the one of a classical gas, approaching one for long expansion times. The interaction with a Bose gas changes the picture: in particular, in the figure, are reported the two opposite situations for the mixture ^{40}K - ^{87}Rb of repulsive and attractive interaction with $a_{BF} = \pm 330 a_0$. If the scattering length is positive, we have that the behaviour of the radii of the degenerate fermionic

sample is very similar to the case of the "free" Fermi gas, even if for $\tau \geq 8$ the interacting case shows up a faster dynamics. More dramatic it is the change in the case of an attractive interaction. Indeed in this latter case, theory predicts an evident decrease of the velocity of the expansion of the Fermi gas due to the attraction with the Bose-Einstein condensate. In Fig (5.11), we show the experimental data to be compared with the theoretical results of Fig. (5.9b). As it is possible to see, we actually see the predicted reduction in the evolution of the aspect ratio. The theoretical explanation of this behaviour is again in the competition between the *static* and the *dynamical* effect of the mean-field attraction, as we have seen in the case of the expansion of the condensate. In this case, case however, the *dynamical* mechanism always dominates the *static* one, leading to an aspect ratio that is less than the one of a non interacting Fermi gas.

5.5 Collapse of the Fermi gas

As we have discussed in the previous section, the main effect of the large attractive mean-field interaction between potassium and rubidium atoms in the mixture is to increase the peak-density of both species in the overlap region, as it is possible to obtain by directly solving the two coupled equations (1.72), (1.73). Before proceeding in the discussion, it is worth to remember that both the Fermi gas of ^{40}K and the Bose-Einstein condensate of ^{87}Rb are stable systems against collapse induced by mean-field interaction. The stability of the fermionic gas is indeed assured essentially by its non interacting nature, since it is composed by identical fermions, and by its relatively high kinetic energy. In particular, this can be described in terms of an outward Fermi pressure which arranges the fermions in the trap in a relatively large spatial distribution compared to the one of a Bose-Einstein condensate. This pressure is a general property of any degenerate Fermi system, as in the case of the white dwarfs and neutron stars, in which it counteracts the gravitational force. The stability of a Bose-Einstein condensate is instead assured by the positive sign of the intraspecie scattering length, that corresponds to a net repulsive interaction between the atoms composing the system.

On the other side, the stability of a system composed by a Fermi gas interacting with a Bose condensate depends essentially by the quantity $U_{BF} = 4\pi a_{BF}/m_{BF} n_i$. Once fixed the value of the scattering length a_{BF} , it is possible to vary U_{BF} , by changing the number of atoms and therefore the densities of both species. As we have discussed in (5.3), we were able to produce a stable degenerate mixture typically composed by some 10^4 atoms of ^{40}K and ^{87}Rb atoms and in this case we have measured a lifetime of the system of about a second, limited only by the background heating of our magnetic trap. However, if the number of atoms of both species exceed some critical number, the theory [17] predicts that the mixture is not more stabilized by the kinetic energy and by the repulsive boson-boson interaction and due to the attractive interaction between fermions and bosons it can lower its energy by continuously increasing the density in the overlap region until it collapses. In the case of a spherical trap, R. Roth et al. [17], have derived the expression for the critical particle number N_{cr} as a function of the scattering length a_{BF} :

$$N_{cr}^{1/6}(a_B, a_{BF}, l) = \frac{0.863}{|a_{BF}/l|^{0.281}} + \frac{0.087(a_B/l)^{1.91}}{|a_{BF}/l|^{3.49}} \quad (5.8)$$

where $l = (m\omega)^{-1/2}$ is the harmonic oscillator length. If $N_B = N_F \geq N_{cr}$ the system is no more stable against the collapse induced by the mean-field interaction. In Fig. (5.12), we report the behaviour of the critical number of atoms in

function of the boson-fermion scattering length a_{BF} in the case of spherical trapping potential and for different values of the boson-boson interaction a_B (image taken by [17]). In our discussion we are interested only in considering the solid

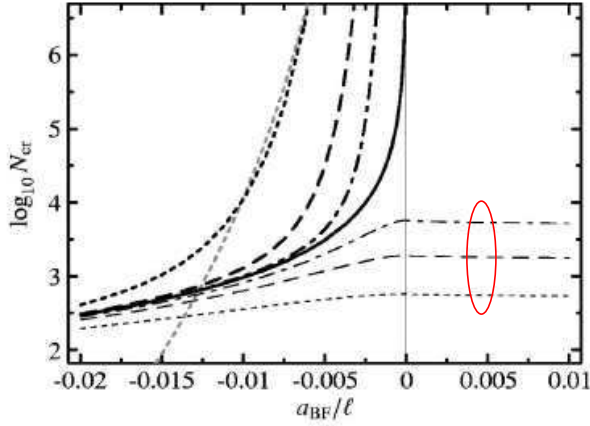


Figure 5.12: Logarithm of the critical number in function of the interspecies boson-fermion scattering length a_{BF} for different values of the boson-boson scattering length a_B , rescaled to the harmonic oscillator length l [17]. The curves inside the red circle refer to the case of negative boson-boson scattering length. The case of ^{40}K - ^{87}Rb mixture corresponds to a critical number of about 4.5×10^4 atoms ($a_{BF}/l \simeq -0.016$ and $a_B/l \simeq 0.004$). Calculations made in the case of anisotropic potential confirm this predictions.

and the thick lines that correspond to $a_B/l \geq 0$, as we have in the case of rubidium where $a_B \simeq 0.004$. In the ideal case of zero boson-boson interaction (solid line in the figure), we would have that, in our case ($a_{BF}/l \simeq -0.016$), the system would be stable only for $N_{Rb} = N_K \leq 3 \times 10^3$ atoms. The fact that the bosons repel each others in the trap leads to a higher stability of the system that becomes unstable only if the number of atoms of both species is larger than 3×10^4 . These results are valid in the case of a spherical trap. If we include the actual anisotropy of our trapping potential [120], we have that the predicted critical number of atoms for the collapse are of the order of $N_{cr}(Rb) \simeq 10^5$, and $N_{cr}(K) \simeq 10^4$.

Since we could not change the value of the interspecies scattering length, we have improved the loading of the atoms of both species in the magnetic trap, taking particularly care of the optical pumping phase and we have optimized the evaporation ramp in order to reach the critical number of atoms and to observe the instability.

By doing this, we were actually able to reach the onset of condensation of Rb with samples typically larger than previously, composed by 3×10^5 rubidium and 3×10^4 potassium atoms. To approach the collapse, the idea was to slowly add rubidium condensate atoms in the mixture, by lowering the trap depth at constant rate, and to observe the possible decay of the potassium atoms during this procedure. In Fig. (5.13), we show the evolution of the number of potassium and rubidium atoms during the final stage of the evaporation ramp. As it is

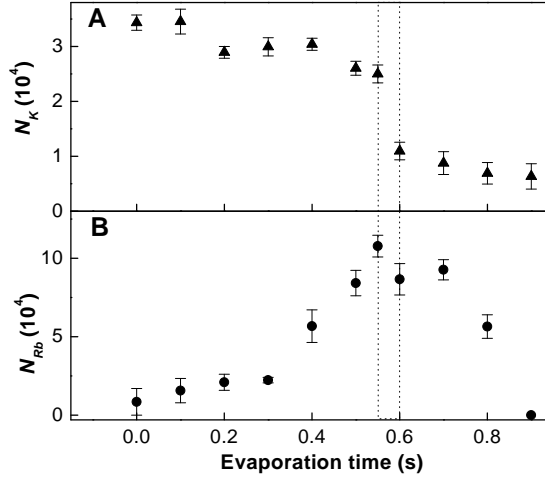


Figure 5.13: Evolution of the number of potassium atoms N_K (A) while the number of condensed rubidium atoms N_{Rb} (B) is increased by further evaporation after the onset of BEC. When the number of Rb is increased above 10^5 , we observe the collapse of the Fermi gas indicated by the fact that more than half of the fermions disappear from the trap.

possible to note, while the condensate is still forming, we can see some inelastic losses in the K sample, however on the same time scale of the evaporation. But, as soon as the condensate is completely formed, we observe a sudden drop in the K number of atoms, that becomes less than one half its original value. In order to understand what was going on, we have first tried to determine the time scale of this loss process: what we have found is that the duration of this strong reduction in the potassium population was much shorter than the time scale of all the other loss mechanisms we could observe in the trap. Indeed, when we have repeated the measurement, spanning the time interval between 0.55 and 0.6 s (Fig. (5.13)), due to the small shot-to-shot fluctuations of the atom numbers, we have always measured either a larger ($N_K = 2 \times 10^4$) or smaller ($N_K \leq 10^4$) Fermi gas. This indicates that these inelastic losses happens on a time $\tau \ll 50$ ms. When we have studied the dynamics of this phenomenon by varying the number of atoms of both species, we have discovered the existence of a threshold in the population of both K and Rb.

In Fig. (5.14), we report the measurements performed by halving either the population of K or of Rb. In both cases, we do not observe any sudden drop in the number of atoms of the potassium component, but only a much slower decay, if compared to the one shown in Fig. (5.13). Indeed, for the largest Fermi gas we can produce, typically $N_K \simeq 2 \times 10^4$, we do not see any dramatic variation in the K component if the number of atoms of rubidium is lower than $N_{Rb} \simeq 10^5$, and

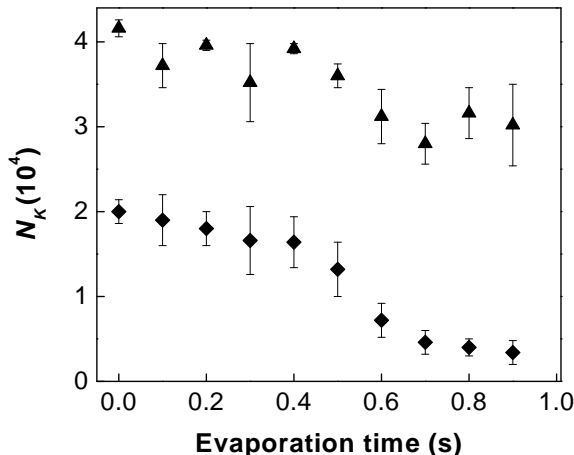


Figure 5.14: Evolution of the number of potassium atoms N_K using the same evaporation procedure described in the text but halving the initial number of atoms. In particular, the triangles refer to a lower initial number of bosons, while the rhombuses to a lower number of fermions.

the same happens for $N_K \leq 1.8 \times 10^4$ even if we produce the largest BEC we can achieve composed by $N_{Rb} \simeq 1.5 \times 10^5$.

Another evidence of this threshold behaviour is shown in Fig. (5.15), in which we present the evolution of the number of potassium atoms in function of the number of rubidium in the condensate. It is clearly possible to observe a forbidden region for N_K between 2×10^4 and 0.5×10^4 , with a threshold for N_{Rb} given by $N_{th} = 9 \times 10^4$.

All these features described so far, such as the fast dynamics, the threshold in the numbers of atoms and the gap in the population of the potassium sample, varying the number of Rb atoms, show that the phenomenon we have observed in the experiment is the collapse of the Fermi gas of ^{40}K , driven by the interaction with the Bose condensate of ^{87}Rb . Indeed, the critical number of atoms for which we do observe the disappearance of the fermionic sample $N_K \simeq 2 \times 10^4$ and $N_{Rb} \simeq 10^5$, are compatible with the predicted values we obtain from the mean-field theory, when considering our estimation of the K-Rb scattering length $a_{BF} = -410 a_0$. In other words, as the theory predicts [17], the mutual attraction between potassium and rubidium atoms is likely to lead to an considerable increase in the density of both samples in the overlap region. In the case of the Fermi gas, even if this superposition region is small with respect to its whole volume, this effect is enhanced because the typical density of the BEC n_B is much larger than the

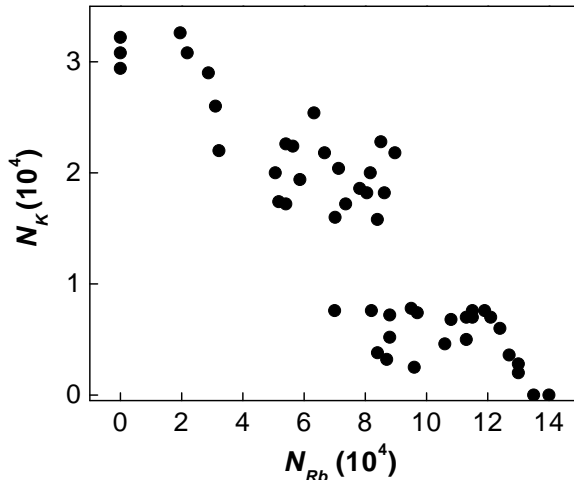


Figure 5.15: Evolution of the number of atoms N_K of the Fermi gas in function of the number of atoms in the condensate N_{Rb} . The threshold in N_{Rb} is clear from the gap of data in the range from $0.8 \times 10^4 N_K < 1.5 \times 10^4$.

one of the Fermi gas n_F , $n_B/n_F \simeq 100$. We can say that in this mixture the attractive interaction between potassium and rubidium atoms is sufficiently strong to overwhelm the Fermi pressure that usually stabilizes the Fermi gas.

We must remark that the theory predicts the simultaneous collapse of the Bose-Einstein condensate: actually, in the experiment, we have observed that the BEC appears only marginally affected by the collapse of the Fermi gas. Indeed, by looking at Fig. (5.13), it is possible to measure an effective depletion of the condensate only of the order of 2×10^4 atoms.

However this observation can be explained by considering the microscopic dynamics of the collapse. Indeed, the collapse of the Fermi-Bose mixture is likely to be halted at some stage by some inelastic processes which are favoured by the high density in the overlap region. These losses reduce the number of atoms below the critical values. This behaviour is confirmed by the observation that we have a comparable decrease in both potassium and rubidium sample, and these inelastic losses are likely to be due to interspecies collisions. In order to identify the possible kind of inelastic processes that are involved during the collapse, we have measured the losses of potassium in function of the density of the rubidium sample in case of a nondegenerate mixture at $T = 300$ nK. We have observed losses in the K sample only if the rubidium is present and in particular we have seen that this loss rate scales quadratically with the density of Rb. In Fig. (5.16),

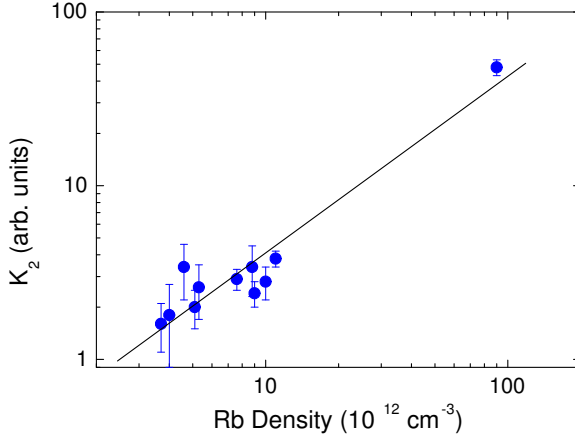


Figure 5.16: Dependence of the 2-body collisional rate K_2 versus the density of rubidium. In the case of 2-body losses, we would expect a constant dependence from the rubidium density, while, as it is possible to see, the behaviour seems to indicate that the collisional process that we have observed in the experiment is a 3-body recombination.

we show the dependence of the 2-body K_2 scattering coefficient in function of the density of rubidium. If the losses mechanism were a real 2-body scattering, we would expect a constant behaviour. As it is possible to see, this is not the case. In fact K_2 shows a linear dependence from the rubidium density, indicating that the underlying collisional process is more likely to be a 3-body K-Rb recombination. Indeed if we plot the dependence of the 3-body K_3 scattering coefficient as a function of the temperature of the sample, Fig. (5.17), we see a constant behaviour. In particular, since no s -wave scattering between two fermions is possible in our system, these 3-body losses must involve two Rb atoms and one K atom, with the possible formation of K-Rb molecules. We have also determined the coefficient rate $K_3 = \dot{N}_K / (N_K n_{Rb}^2) = 2 \pm 1 \times 10^{-27} \text{ cm}^6 \text{ s}^{-1}$.

If we now look in more detail at Fig. (5.13), we can observe that this prediction of 3-body recombination mechanism meets the experimental results of the losses during the collapse. Indeed, we see a drop in the number of atoms of potassium, during the collapse, from the initial value of about 2.5×10^4 to slightly more than 10^4 . At the same time, the condensate number changes from 10^5 to about 7×10^4 , corresponding to losses twice as large as the one for potassium.

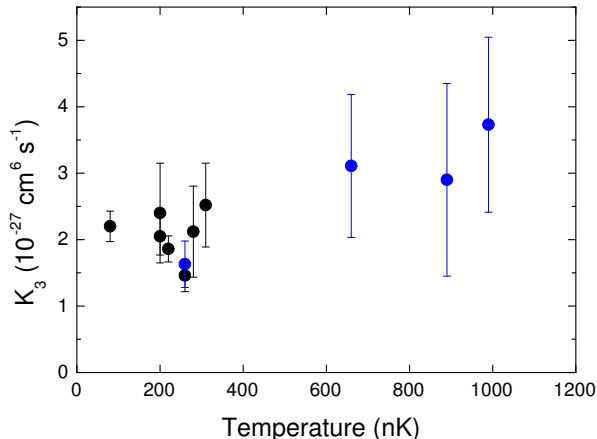


Figure 5.17: 3-body recombination rate as a function of the temperature of the mixture. The observed constant behaviour indicates the absence of collisional resonances. From the measurements we estimate $K_3 = 2 \pm 1 \times 10^{-27} \text{ cm}^6 \text{ s}^{-1}$.

5.5.1 Determination of the scattering length by the collapse

We have used our observation of the collapse of the Fermi gas for better determining the value of the ^{40}K - ^{87}Rb scattering length, assuming valid the mean-field approximation for this system [17]. In Fig. (5.18), we show the regions of stability of the mixture in the (N_K, N_{Rb}) plane, with N_K and N_{Rb} the numbers of atoms of both species, obtained by solving the equations (1.72), (1.73). The system is stable below the critical curves and becomes unstable crossing them. The instability rises up when the solutions of of the mean-field equations (1.72), (1.73) diverge. Indeed this divergence of the solutions corresponds to an increase of the density of both species in the overlap region that leads to the collapse of the system. In this way it is possible to draw the curves reported in the figure that delimit the area of stability for the mixture. Since in the experiment we can measure the number of atoms with an uncertainty of about the 40%, we can have an estimation even of the uncertainty of the value of the scattering length. In particular, since the dependence of the scattering length from the number of atoms turns out to be $a_{BF} \propto N^{-1/10}$, it is possible to determine the value of the scattering length with higher precision with respect to the collisional measurements when $a_{BF} \propto N^{-1/2}$, since the experimental uncertainty that we have in the determination of N_K and N_{Rb} it is almost completely washed out. In this way, we can derive a new

value for a_{BF} given by $a_{BF} = -395_{-15}^{+15} a_0$, which is in good agreement with $a_{BF} = -410_{-80}^{+90} a_0$ determined before.

5.5.2 Beyond the mean-field description of the mixture

As remarked several times in the previous discussion, we have always considered appropriate for analyzing our experimental results the mean-field approach which is summarized by the equations (1.72) and (1.73). In this approximation, the single atom evolves in the mean field generated by all the other atoms.

The general Hamiltonian of a system composed by a Fermi gas interacting with a Bose-Einstein condensate [17], from which equations (1.72) and (1.73) are derived, has the following form:

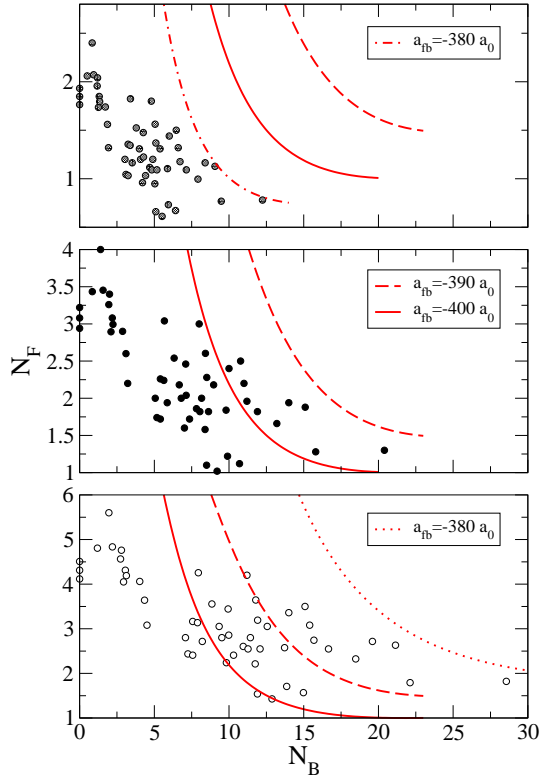


Figure 5.18: Regions of stability of ^{40}K - ^{87}Rb degenerate mixture in the (N_K, N_{Rb}) plane. The numbers of atoms of potassium and rubidium are taken from the experiment, while the theoretical curves are derived in the mean-field approximation. From this analysis we can estimate for the ^{40}K - ^{87}Rb scattering length the following value $a_{BF} = -395_{-15}^{+15} a_0$.

$$\begin{aligned}
T_B &= - \int d\mathbf{r} \Phi^\dagger(\mathbf{r}) \frac{\hbar^2 \nabla^2}{2m_B} \Phi(\mathbf{r}) \\
V_B &= \int d\mathbf{r} \Phi^\dagger(\mathbf{r}) V_B \Phi(\mathbf{r}) \\
T_F &= - \int d\mathbf{r} \Psi^\dagger(\mathbf{r}) \frac{\hbar^2 \nabla^2}{2m_F} \Psi(\mathbf{r}) \\
V_F &= \int d\mathbf{r} \Psi^\dagger(\mathbf{r}) V_F \Psi(\mathbf{r}) \\
W_{BB} &= \frac{1}{2} \int \int d\mathbf{r} d\mathbf{r}' \Phi^\dagger(\mathbf{r}) \Phi^\dagger(\mathbf{r}') U_{BB} \Phi(\mathbf{r}') \Phi(\mathbf{r}) \\
W_{BF} &= \int \int d\mathbf{r} d\mathbf{r}' \Phi^\dagger(\mathbf{r}) \Psi^\dagger(\mathbf{r}') U_{BF} \Psi(\mathbf{r}') \Phi(\mathbf{r})
\end{aligned} \tag{5.9}$$

where T_B and T_F are the boson and the fermion kinetic energy, V_B and V_F the trapping potential and $\Phi(\mathbf{r})$ and $\Psi(\mathbf{r})$ the boson and the fermion field operator. The density of the bosons and of the fermions is defined:

$$\begin{aligned}
n_B(\mathbf{r}) &= \langle g | \Phi^\dagger(\mathbf{r}) \Phi(\mathbf{r}) | g \rangle \\
n_F(\mathbf{r}) &= \langle g | \Psi^\dagger(\mathbf{r}) \Psi(\mathbf{r}) | g \rangle
\end{aligned} \tag{5.10}$$

where we defined $|g\rangle$ the ground state of the system, whose energy is $E_0 = \langle g | H | G \rangle$. The Hamiltonian (5.9) can be rewritten in the following form:

$$H = H_B + H_F + H_I \tag{5.11}$$

The interaction between the Fermi and the Bose gas is described by H_I ,

$$H_I = \int \int d\mathbf{r} d\mathbf{r}' \Phi^\dagger(\mathbf{r}) \Psi^\dagger(\mathbf{r}') U_{BF} \Psi(\mathbf{r}') \Phi(\mathbf{r}) \tag{5.12}$$

The interaction term between the Fermi gas and the Bose condensate is proportional to by $U_{BF} \propto a_{BF}/m_{BF} n_i$, i.e. proportional to the boson-fermion scattering length and related to the reduced mass of the pair that reads $m_{BF} = 2m_B m_F / (m_B + m_F)$ and to the density of fermions (bosons). By minimizing the total energy of the system, it is first possible to obtain the density profiles of the trapped gases [17], as we have shown in Fig. (5.8), and then to determine the critical value of the number of atoms of both species and also the critical value of the scattering length for which the system is no more stable and it collapses.

In order to consider effect beyond the mean-field, we have to account for an extra term in the Hamiltonian (5.9), including the contribution due to the exchange correlations, related to the density fluctuations that the mean-field theory does not describe [121]. Without entering in the technical details (see [121] and reference

therein), it is possible to derive the expression for this exchange-correlation energy $E_{xc}(n_B, n_F)$ in the case of homogenous system and considering only the second order in the boson-fermion scattering length a_{BF} :

$$E_{xc}(n_B, n_F) = \frac{2\hbar^2 a_{BF}^2}{m_R} f(\delta) k_F n_F n_B \quad (5.13)$$

where $k_F = (6\pi n_F)^{1/3}$ is the Fermi wave vector and $f(\delta)$ is a dimensionless function that depends only on the fermions and bosons masses ($\delta = (m_B - m_F)/(m_B + m_F)$).

If we now consider this additional term:

$$H = H_B + H_F + H_I + H_{ex} = H_B + H_F + A a_{BF} + B a_{BF}^2 \quad (5.14)$$

where A and B contain the dependence from the density of both fermions and bosons. If we look more closely the expression for the exchange energy and if we compare it with the mean-field interaction term, we see that, while this last can be positive or negative (if $a_{BF} > 0$ or $a_{BF} < 0$), leading to a repulsive or attractive interaction between the bosons and the fermions respectively, the second one is always positive, being proportional to a_{BF}^2 . This means that the net result of the exchange energy term is an additional repulsion between fermions and bosons in the trap.

In the case of the ^{40}K - ^{87}Rb mixture, the new term should counteract the attraction between potassium and rubidium induced by the negative mean-field term. The author of [121] affirm that the effect of this "new" repulsive term reads as a correction of 3.5% in the interaction energy respect to the mean-field result and, more important, it leads to a quite notable effect on the density of both species. In particular, they predict a reduction of both bosons and fermions densities of more than 20% with respect to the mean-field result which would prevent the onset of instability of the system for nominal value of the interspecies scattering length a_{BF} . However, it is possible to show that by taking into account only the second order of a_{BF} , with our number of atoms, it is not possible to reach the conditions suitable for the collapse whatever is the magnitude of the scattering length [122]. The explanation of such a behaviour is found by considering that the exchange energy contribution scales quadratically with a_{BF} while the mean-field one goes linear with a_{BF} . As a consequence, the larger is the value of a_{BF} and the larger also becomes the additional repulsion between the two species due to the exchange energy term. For a better description of the system nearby the instability is thus important to consider also other contributions beyond the second order. For example, the third term is proportional to a_{BF}^3 and then it can counteract the effect of the second one. However, the determination of the other contributions beyond the second order is a difficult task and so far it has not been possible due to the complexity of the theory.

5.6 Towards BCS-like transition in the ^{40}K - ^{87}Rb degenerate mixture

In (1.4.3), we have discussed on the possibility of achieving the superfluid regime in a dilute fermionic system [56]. In particular, we have emphasized that the superfluid pairing requires a real attractive interaction between the fermions and that, in the ultracold temperature regime we are dealing with, the most efficient pairing is likely to occur through s -wave scattering of particles. Since in the case of identical fermions such a scattering process is inhibited, we have to consider a system composed by two different fermionic species as, for example, the case of fermions in two different Zeeman levels. Typically, the critical temperature for such Cooper pairing is only a small fraction of the Fermi temperature for the system, and thus the observation of such a transition is expected to be quite hard from the experimental point of view. However, as remarked in (1.4.3) more than one theoretical scheme has been presented in order to get much higher transition temperatures.

In the case of pure fermionic systems, one of the most promising scheme seems to be the one [60] that exploits Feshbach resonances to achieve quite large negative values of the scattering length and to strongly increase the interaction between the fermions. Such a scheme has been directly used by O'Hara et al. [26] in a mixture composed by ^6Li atoms in two different Zeeman levels, trapped in a high confining CO_2 optical trap. They could set the value of the scattering length between these two states to a very large and negative value, $a \simeq -10^4 a_0$ by means of an external magnetic field, inducing, in this way, a strong attractive interaction between the atoms. They have observed a signature of this strong interacting regime of their system by studying the expansion of the Fermi gas. In particular, they have noted an anisotropic expansion of the fermionic clouds after the release from the optical trap. This behaviour is qualitatively different with respect to the theoretical prediction for the expansion of a "normal" Fermi gas, which, as discussed in (1.3.1), is supposed to be completely isotropic, despite of the anisotropy of the trapping potential [124].

Recently, C. Menotti et al. [123] has shown that a superfluid Fermi gas expands in anisotropic way, since it is described by hydrodynamic equations, like the Bose-Einstein condensate. However, the anisotropy in the expansion is not necessarily due to the superfluidity. Indeed, as pointed out in [125], the hydrodynamic equations describe also the situation of a strong collisional regime (hydrodynamic regime), in which the scattering cross-section has reached its maximum value (see (1.1.1)). Subsequently the study of the behaviour of the expanding cloud is not a discriminating way of detecting the superfluid regime, and other observations must be used for determining if the system is superfluid [4], [126].

In the case of boson-fermion mixtures, a large boson-fermion interaction can affect not only the stability of the system [17], as we have presented above, but it can also play a relevant role in the mechanism of Cooper pairing [67], [68], [19].

Indeed, as first suggested in the case of the ^3He - ^4He mixture [127], the interaction between the fermions and the density fluctuations of the bosonic sample, can lead to an effective attraction between fermions. This situation is analogous of what usually occurs in superconductors [128], where the coupling between two electrons is provided by the exchange of lattice phonons.

In the specific case of degenerate dilute boson-fermion mixtures, L. Viverit [19], has evaluated the form of this induced coupling between fermions due to the interaction with a Bose-Einstein condensate. The model presented in [19] is general and it can be applied also to the situation of bare fermion-fermion interaction (as for ^{40}K), showing that the final effective interaction between the fermions can be attractive if the boson-fermion contribution is taken into account. Following [19], we can write the boson-induced interaction between fermions as a product of the fermion-boson interaction $U_{BF} = 4\pi\hbar^2 a_{BF}/m_{BF}$ and the boson density-density response function $\chi(\vec{q}, \omega)$:

$$U_{FBF}(\vec{q}, \omega) = U_{BF}^2 \chi(\vec{q}, \omega) \quad (5.15)$$

where,

$$\chi(\vec{q}, \omega) = \frac{n_B \hbar^2 q^2 / m_B}{(\hbar^2 \omega)^2 - \epsilon_q^0 (\epsilon_q^0 + 2n_B U_{BB})} \quad (5.16)$$

where n_B is the density of the boson, $\epsilon_q^0 = \hbar^2 k^2 / 2m_B$ and $q = |\vec{q}|$ and finally $U_{BB} = 4\pi\hbar^2 a_{BB}/m_B$ is the usual repulsive boson-boson interaction. In the case $\omega = 0$, we see that $U_{FBF} < 0$ whatever is the fermion-boson interaction U_{BF} . It is possible to demonstrate that the condition $\omega = 0$ is always satisfied in the limit $v_F \ll s$, where $v_F = \hbar k_F / m$ is the Fermi velocity and $s = (n_B U_{BB} / m_B)^{1/2}$ the sound velocity in the Bose-Einstein condensate. In this particular case, the induced interaction is attractive in the whole Fermi sphere and it takes the following forms:

$$U_{FBF}(q) = -\frac{U_{BF}^2}{U_{BB}} \frac{1}{1 + (\hbar q / 2m_B s)^2} \quad (5.17)$$

Since $v_F \ll s$, even if $m_B \geq m_F$ the typical momentum exchanged in the interaction $\hbar q \ll 2m_B s$ and we have $U_{FBF}(q) \simeq -U_{BF}^2 / U_{BB}$. This relation suggests that the boson-induced attractive interaction between fermions is always attractive and it does not depend from the exchange momentum. Anyway, despite of (5.17), if $U_{BF} > 0$, phase separation prevents the possible formation of Cooper pairing.

In this approximation, it is possible to derive [19] the relation between the critical temperature for the Cooper pairing and the fermion-boson interaction:

$$T_C = \frac{\gamma}{\pi} \left(\frac{2}{e} \right) T_F e^{1/\lambda} \quad (5.18)$$

where T_F is the Fermi temperature, γ a numerical factor, and the parameter λ is directly related to the scattering length boson-fermion and it reads:

$$\lambda = \frac{(m_F k_F)}{2\pi^2 \hbar^2} U_{FF} \left[1 - \frac{U_{BF}^2}{U_{BB} U_{FF}} \right] \quad (5.19)$$

where $U_{BF} \propto a_{BF}$, $U_{BB} \propto a_{BB}$ and $U_{FF} \propto a_{FF}$. In the case of large fermion-boson interaction, since also U_{FF} is much bigger than U_{BB} , we can see from equation (5.18) that the critical temperature for the pairing can be comparable with the Fermi temperature T_F of the system.

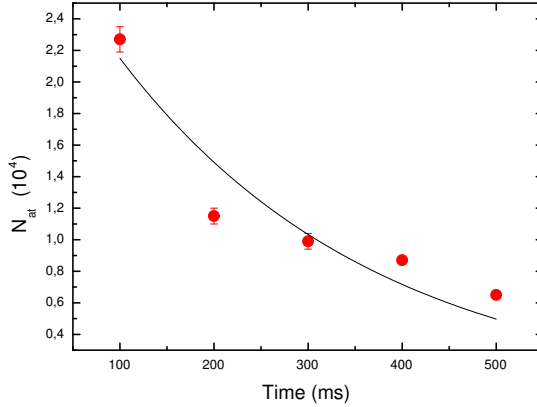


Figure 5.19: Decay of potassium atoms initially trapped in the $|F = 9/2, m_F = 7/2\rangle$ state due to the collisions with the rubidium in the $|F = 2, m_F = 2\rangle$ state. From the measured decay time ($\tau = 290$ ms) we have extracted the inelastic rate $G^{inel} \simeq 2.5 \times 10^{-12} \text{ cm}^3 \text{ s}^{-1}$

The mixture composed by ^{40}K - ^{87}Rb atoms seems particularly interesting from this point of view, due to the large fermion-boson scattering length. Indeed, if we calculate the order of magnitude of the boson-induced attractive interaction between fermionic potassium atoms, by plugging inside the relation for U_{FF} shown above, the nominal value of the ^{40}K - ^{87}Rb scattering length $a_{BF} = -410 a_0$ and of the rubidium-rubidium interaction, $a_{BB} = 100 a_0$, we find that $a_{FF} \simeq -1700 a_0$. This magnitude is very large compared with the "bare" repulsive interaction between potassium atoms $a_{FF} = 174 a_0$, indicating that in case of this mixture this induced attraction can be quite relevant. Furthermore, the optimal condition for the pairing is predicted to occur [129] just at the onset of the collapse with a critical temperature for the pairing as high as $T_C \simeq 0.1 T_F$, a temperature achievable in the experiment.

However, as mentioned above, Cooper pairing is expected to be more efficient through s-wave coupling, thus between non identical fermions.

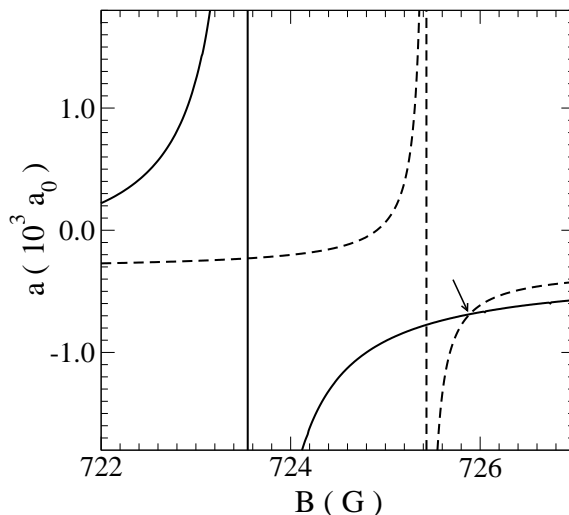


Figure 5.20: Field dependence of the $^{40}\text{K}(9/2, -7/2) + ^{87}\text{Rb}(1,1)$ (full line) and $^{40}\text{K}(9/2, -9/2) + ^{87}\text{Rb}(1,1)$ (dashed line) scattering lengths. The arrow shows the best working point for inducing the Cooper pairing in this spin mixture (see text).

Since our sample is composed by identical fermionic atoms polarized in the $|F = 9/2, m_F = 9/2\rangle$ state, we do not meet this condition for the s-wave pairing. In the direction of the possible observation of Cooper pairing in a gas of ^{40}K , we have then studied the stability of the spin mixture composed by K atoms in two different spin state and rubidium. In detail, we have transferred some potassium atoms in the $|F = 9/2, m_F = 7/2\rangle$ and we have looked at the stability of this new spin mixture composed by rubidium in the $|F = 2, m_F = 2\rangle$ and potassium in $|F = 9/2, m_F = 9/2\rangle$ and $|F = 9/2, m_F = 7/2\rangle$ states. The measurements have been performed on thermal samples of K and Rb in the range of temperature $T = 400 \div 500$ nK. By means of a fast RF-sweep (see section 3.3), typically lasting around 10 ms, we have transferred about 10^4 atoms ($\simeq 20\%$ of the total number) potassium atoms from the $|F = 9/2, m_F = 9/2\rangle$ to the $|F = 9/2, m_F = 7/2\rangle$ state, and we have observed their subsequent decay due to the collisions with the rubidium sample trapped in the $|F = 2, m_F = 2\rangle$ state. In Fig. (5.19) we show the result of a typical measurement performed with $N_{7/2} \simeq 2 \times 10^4$ of potassium in $|F = 9/2, m_F = 7/2\rangle$ and $N_2 \simeq 5 \times 10^5$ rubidium in $|F = 2, m_F = 2\rangle$ at $T = 300$ nK. The evolution of potassium atoms can be described, as in the case presented in (3.3) by the following equation:

$$\dot{n}^K(t) = -G^{inel} n_{|9/2,7/2\rangle}^K(t) n_{|2,2\rangle}^{Rb}(t) \quad (5.20)$$

with the constraint $N_{|9/2,7/2\rangle}^K(t) - N_{|2,2\rangle}^{Rb}(t) = \text{const}$. Here n is the spatial density,

N the atom number and G^{inel} is the inelastic collisional rate. By fitting the experimental results with the exponential decay, solution of (5.20), we have estimated the value for the collisional rate, $G^{inel} = 2.4(1.2) \times 10^{-12} \text{ cm}^3\text{s}^{-1}$, where the uncertainty dominated by the one on atom number. In the case of the degenerate system approaching to the collapse, such an inelastic rate would limit the lifetime of the spin mixture to less than 30 ms, due to the quite large density ($10^{14} - 10^{15} \text{ cm}^{-3}$) that both potassium and rubidium samples have in this phase. In other words, this mixture is not stable enough in the perspective of the pairing by the interaction with bosons, and others must be found.

Among all the available spin mixtures of the ^{40}K - ^{87}Rb system, the more appealing in the context of superfluidity appears the one composed by the rubidium in $|F = 1, m_F = 1\rangle$ and potassium in $|F = 9/2, m_F = -9/2\rangle$ and $|F = 9/2, m_F = -7/2\rangle$, trappable in an optical trap. The main feature of this mixture is that it is stable against inelastic collisional processes, since both the atomic species are trapped in the real ground state. Furthermore [130] we were able to predict the magnitude and the sign of the interactions between potassium and rubidium atoms trapped in such states. Indeed, from the inelastic measurements described above, we could infer the value also of the single scattering length between ^{40}K - ^{87}Rb atoms, $a = -185_{-225}^{+83} a_0$ and then it was possible to calculate the scattering lengths for all the possible spin mixtures for ^{40}K - ^{87}Rb system. In particular, we have found that the scattering length between rubidium in $|F = 1, m_F = 1\rangle$ and potassium in $|F = 9/2, m_F = -9/2\rangle$ is $a = -336_{-102}^{+89} a_0$ and the one for the $|F = 1, m_F = 1\rangle + |F = 9/2, m_F = -7/2\rangle$ is $a = -323_{-105}^{+90} a_0$. As it is possible to see, in both cases, the magnitude is comparable with the one we have measured for the $|F = 2, m_F = 2\rangle + |F = 9/2, m_F = 9/2\rangle$ states, and also the negative sign assures the repulsive character of the interaction, needed for leading the system to the instability.

The knowledge of both the triplet and the singlet scattering length between ^{40}K - ^{87}Rb atoms have also allowed us to predict the location of Feshbach resonances of the different magnetic states of this mixture [130], as shown in Tab. (5.6). In particular, we have determined the magnetic field dependence of the scattering length between the $|F = 1, m_F = 1\rangle + |F = 9/2, m_F = -9/2\rangle$ and of $|F = 1, m_F = 1\rangle + |F = 9/2, m_F = -7/2\rangle$ states, as shown if Fig. (5.20). In this case, we can see a crossing point between the two scattering lengths, corresponding to a coupled Feshbach resonances for these two spin mixtures. In particular, for $B \simeq 726$ Gauss we have that the two scattering lengths assume the same large and negative value $a_{1,(-9/2,-7/2)} \simeq -687 a_0$. This possibility of tuning simultaneously the two interactions can be exploited in the direction of Cooper pairing: indeed, as mentioned above, the highest critical temperature for the transition to the superfluid regime is predicted [129] to occur just before the system collapses. However, the pairing is possible only if the two spin states are populated by the same number of atoms of fermions. The idea is then to prepare Rb in $|F = 1, m_F = 1\rangle$ state and K in the two levels $|F = 9/2, m_F = -9/2\rangle$ and $|F = 9/2, m_F = -7/2\rangle$ equally

$(f_K, m_{fK})+(f_{Rb}, m_{fRb})$	$a(a_0)$	$B_0(\text{G})$	$-\Delta(\text{G})$
$(9/2, \pm 9/2)+(2, \pm 2)$	-410^{+80}_{-80}		
$(9/2, \pm 9/2)+(1, \pm 1)$	-235^{+92}_{-121}		
$(9/2, 7/2)+(1, 1)$	-245^{+92}_{-120}	319.6^{+13}_{-17}	0.8
		920.3^{+93}_{-93}	0.05
$(9/2, -7/2)+(1, 1)$	-323^{+90}_{-105}	522.9^{+40}_{-55}	0.3
		564.8^{+20}_{-24}	0.1
		646.3^{+35}_{-52}	4.6
		658.0^{+50}_{-58}	0.08
		753.1^{+50}_{-59}	0.3
		787.4^{+60}_{-65}	0.9
$(9/2, -9/2)+(1, 1)$	-336^{+89}_{-102}	505.3^{+31}_{-49}	0.03
		547.1^{+28}_{-28}	0.2
		593.9^{+34}_{-44}	4.0
		741.2^{+60}_{-65}	0.9
		921.0^{+92}_{-94}	10^{-4}
$(9/2, -9/2)+(1, 0)$	-279^{+92}_{-114}	477.0^{+35}_{-47}	0.1
		590.3^{+31}_{-26}	3.9

Table 5.1: Compendium of ^{40}K - ^{87}Rb scattering properties. The zero-field s -wave scattering length for the different stable spin mixtures is shown together with the location and the width of the relative Feshbach resonances.

populated. By simultaneously tuning the two interactions $a_{1,-9/2}$ and $a_{1,-7/2}$ we would like to reach the situation nearby the collapse for the two mixtures where the pairing between the fermions should occur.

Conclusions and perspectives

In this thesis we have described the experimental realization of dilute degenerate mixtures. In particular, isotopes of potassium are cooled to quantum degeneracy by means of sympathetic cooling with rubidium atoms.

Sympathetic cooling turned out to be very efficient thanks to the large inter-species scattering cross-sections between K and Rb. In this way it has been possible the achievement of the first Bose-Einstein condensate of ^{41}K and the investigation of the features of a boson-boson mixture of ^{41}K - ^{87}Rb and of a fermion-boson mixture of ^{40}K - ^{87}Rb . We have accurately measured the collisional properties between potassium and rubidium atoms and we have been able to estimate the magnitude and the sign of the interactions of all the K-Rb isotopic pairs.

The boson-boson mixture is characterized by a large and repulsive interaction between the two species. This feature has permitted the production of a stable binary condensate of ^{41}K and ^{87}Rb . We have seen the effects of the strong coupling between the two BECs by studying the dynamics of the two superfluids in the magnetic trap. By forcing a dynamical overlap between the two clouds, we have observed the exchange of angular momentum between the two condensates, evidenced by the onset of scissors mode-like oscillation.

Sympathetic cooling of the fermionic isotope ^{40}K has made possible the realization of a degenerate mixture composed by a Fermi gas of potassium and a Bose-Einstein condensate of rubidium. The large and attractive character of the interactions has assured a very efficient cooling of K even in the degenerate regime allowing the attainment of temperatures as low as $T = 0.2 T_F$. The strong interspecies attraction between fermions and bosons has led to an instability of the mixture above a critical number of atoms of the two components. In particular, such a boson-fermion interaction was able to overwhelm the natural repulsion between the fermionic potassium atoms, inducing the collapse of the Fermi gas.

Several are the perspectives opened by the realization of such K-Rb degenerate

mixtures. First of all, the possibility of having ultracold miscible gases of two different atomic species is particularly important in the direction of producing heteronuclear cold molecules. These kind of system would be characterized by the long-range dipole-dipole interactions, which are expected to largely modify the ground state and the excitation properties of the mixture. Furthermore, the strength of such interactions is likely to be larger than that of the short-range forces, typical of ultracold atomic gases. This feature makes such a system suitable for performing quantum-computing schemes [14]. Among all the proposed sources of cold heteronuclear molecules, the most promising one is represented by mixtures composed by two different alkali atoms, due to the relative facility in achieving very low temperatures in such samples. In particular, in case of dipolar bosons, it has been recently suggested [131] the possibility of creating dipolar molecular BEC by confining a binary condensate of two atomic species in an optical potential. In such a potential it would be possible to arrange pairs of different atoms in each lattice site and by photo-association technique to create heteronuclear molecular BEC. Our binary BECs, composed by ^{41}K - ^{87}Rb atoms, appears very suitable for implementing such a scheme. Indeed, we have recently predicted the existence of several Feshbach resonances in this boson-boson mixture [130], by which we should be able to change the sign of the K-Rb interaction from the initial repulsive value to a large attractive one, which would favour the formation of potassium-rubidium pairs in the lattice.

The strong and attractive character of the interactions between ^{40}K and rubidium atoms is instead very interesting for the quest of superfluidity regime in a dilute gas of fermionic potassium. Indeed, as reported in [19], a strong and attractive boson-fermion coupling is likely to induce a large attraction between fermions, similarly to what usually occurs in the normal superconductors. In the case of a Fermi gas in two different spin states (reproducing the s -wave coupling in the superconductors), such induced fermion-fermion interaction can lead to the BCS pairing at temperatures comparable with respect to the Fermi temperature of the system. In our experiment, we have already observed one effect of the large attractive character of the ^{40}K - ^{87}Rb interaction, i.e. the collapse of the Fermi gas driven by the presence of the rubidium Bose-Einstein condensate. The onset of the collapse is predicted to be the optimal situation for the pairing since the critical transition temperature corresponds to just $T_C \simeq 0.1 T_F$. In the future experiment we will consider a mixture composed by the Rb BEC in $|F = 1, m_F = 1\rangle$ state and a two components Fermi gas in $|F = 9/2, m_F = -9/2, -7/2\rangle$ trapped in an optical trap. The idea is to reproduce the condition of the collapse in this new mixture and to observe the pairing between fermions. Also in this case, we have predicted the possibility of tuning the interactions between these states by Feshbach resonances [130]. In particular, we have found a value of the magnetic field for which we should be able to simultaneously change the character of the interaction between these three states to a very large and attractive one, favouring even more the possible pairing between potassium atoms.

Another interesting and unexplored direction is to consider the Fermi gas

trapped in an optical lattice. In particular, by confining the atoms very tightly in one direction, it is possible to realize a quasi- $2D$ Fermi gas. Such a system is expected to show new characteristics with respect to the traditional $3D$ case, as it has been recently proposed [132]. One of the most intriguing feature is the possibility of controlling the interactions between the fermions by varying the strength of the optical confinement. Indeed, in the weak coupling regime, it should be possible to observe the Cooper pairing in such quasi- $2D$ system at temperatures of the order of $1/10$ of the Fermi temperature T_F . In the opposite strong-coupling regime, it has been predicted the formation of weakly bound quasi- $2D$ dimers of fermions which are expected to form a Bose-Einstein condensate.

Bibliography

- [1] M. H. Anderson, J. R. Ensher, M. R. Matthews, C. E. Weiman, and E. A. Cornell, *Science* **269**, 198, (1995).
- [2] K. B. Davis *et al.* *Phys. Rev. Lett.* **75**, 3969 (1995).
- [3] C. Bradley *et al.* *Phys. Rev. Lett.* **75**, 1687 (1995).
- [4] F. Dalfovo, S. Giorgini, L. P. Pitaevskii, and S. Stringari, *Rev. Mod. Phys.* **71**, 463 (1999).
- [5] M. Inguscio, S. Stringari, C. E. Wieman Eds., *Bose-Einstein Condensation in Atomic Gases*, Proceedings of the International School of Physics "Enrico Fermi" Course CXL (IOS Press Amsterdam 1999).
- [6] See the special issue of *Nature* **416**, 206 (2002).
- [7] S. L. Cornish *et al.* *Phys. Rev. Lett.* **85**, 1795, (2000).
- [8] D. G. Fried *et al.* *Phys. Rev. Lett.* **81**, 3811 (1998).
- [9] A. Robert *et al.* *Science* **292**, 46 (2001).
- [10] Tino Weber, Jens Herbig, Michael Mark, Hanns-Christoph Ngerl, and Rudolf Grimm *Science* **299**, 232 (2002).
- [11] G. Modugno, G. Ferrari, G. Roati, R. J. Brecha, A. Simoni, and M. Inguscio *Science* **294**, 1320 (2001).
- [12] G. Modugno, M. Modugno, F. Riboli, G. Roati, and M. Inguscio *Phys. Rev. Lett* **89**, 170406 (2002).

- [13] K. Goral *et al.* Phys. Rev. Lett **88**, 190404 (2002).
- [14] D. DeMille Phys. Rev. Lett **88**, 067901 (2002).
- [15] G. Roati, F. Riboli, G. Modugno, and M. Inguscio Phys. Rev. Lett **89**, 150403 (2002).
- [16] K. Gibble and B. J. Verhaar Phys. Rev. A **52**, 3370 (1995).
- [17] R. Roth, and H. Feldmeier Phys. Rev. A **65**, R021603 (2002).
- [18] G. Modugno, G. Roati, F. Riboli, F. Ferlaino, R. Brecha, and M. Inguscio, Science **297**, 2240 (2002).
- [19] L. Viverit Phys. Rev. A **66**, 023605 (2002).
- [20] For a review on the Ultracold Interactions see the contributions of J. Dalibard and D. Heinzen in [5]
- [21] B. DeMarco, J. L. Bohn, J. P. Burke Jr., M. Holland, and D. S. Jin Phys. Rev. Lett. **82**, 4208 (1999).
- [22] C. J. Joachain, *Quantum Collision Theory* (North Holland, Amsterdam) (1983).
- [23] M. Arndt, M. Ben Dahan, D. Guery-Odelin, M. W. Reynolds, J. Dalibard, Phys. Rev. Lett. **79**, 625 (1997).
- [24] B. DeMarco, and D. S. Jin Science **285**, 1703 (1999).
- [25] S. R. Granade *et al.*, Phys. Rev. Lett. **88**, 120405 (2002).
- [26] K. M. O'Hara *et al.*, Science **298**, 2179 (2002).
- [27] C. J. Myatt *et al.*, Phys Rev. Lett. **78**, 586 (1997).
- [28] G. Truscott, *et al.*, Science **291**, 2570 (2001).
- [29] F. Schreck, *et al.*, Phys. Rev. Lett. **87**, 080403 (2001).
- [30] Z. Hadzibabic, *et al.*, Phys. Rev. Lett. **88**, 160401 (2002).
- [31] H. F. Hess Phys. Rev. B **34**, 3476 (1986).
- [32] N. Masuhara *et al.* Phys. Rev. Lett. **61**, 935 (1988).
- [33] W. Ketterle, and N. J. Van Druten, Advance in atomic, molecular, and optics physics, **37**, 181 (1996).
- [34] M. Prevedelli, F. S. Cataliotti, E. A. Cornell, J. R. Ensher, C. Fort, L. Ricci, G. M. Tino, and M. Inguscio Phys. Rev. A **59**, 886 (1998).

- [35] D. J. Wineland, R. E. Drullinger, F. L. Walls, Phys. Rev. Lett **40**, 1639 (1978).
- [36] K. Góral, L. Santos, M. Lewenstein, Phys. Rev. Lett. **88**, 170406 (2002).
- [37] K. Mølmer, Phys. Rev. Lett. **80**, 1804 (1998).
- [38] D. A. Butts and D. S. Rokhsar, Phys. Rev. A **55**, 4346 (1997).
- [39] K. Huang "Statistical Mechanics" (John Wiley and Sons, New York).
- [40] L. Vichi, M. Inguscio, S. Stringari, G. M. Tino J. Phys. B: At. Mol. Opt. Phys. **31**, L899 (1998).
- [41] G. Ferrari Phys. Rev. A **59** R4125 (1999).
- [42] B. DeMarco, S.B Papp, and D. S. Jin Phys. Rev. Lett. **86**, 5409 (2001).
- [43] B. DeMarco, and D. S. Jin Phys. Rev. A **76**, R10 (1998).
- [44] T. Busch, J. R. Anglin, J. I. Cirac, and P. Zoller Europhys. Lett. **44**, 1 (1998).
- [45] J. Ruostekoski, and J. Javanainen Phys. Rev. Lett **82**, 4741 (1999).
- [46] S. N. Bose Z. Phys. **26**, 178 (1924).
- [47] A. Einstein Kgl. Preuss. Akad. Wiss. p261 (1924).
- [48] A. Einstein Kgl. Preuss. Akad. Wiss. p3 (1925).
- [49] C. J. Pethick and H. Smith "Bose-Einstein Condensation in Dilute Gases" Cambridge University Press (2002).
- [50] In the case of negative scattering length, it is possible to show that if the number of atoms is large enough, the system is no more stable and it collapses [4; 51].
- [51] J. M. Gerton *et al.* Nature, **408**, 692 (2000).
- [52] S. Stringari Phys. Rev. Lett **77**, 2370 (1996).
- [53] F. A. van Abeelen, B. J. Verhaar, and A. J. Moerdijk, Phys. Rev. A **55**, 4377 (1997).
- [54] E. Timmermans and R. Cotê, Phys. Rev. Lett. **80**, 3419 (1998).
- [55] G. Ferrari, M. Inguscio, W. Jastrzebski, G. Modugno, G. Roati, A. Simoni, Phys. Rev. Lett **89**, 053202 (2002).
- [56] For a review see G. V. Shlyapnikov in Proceedings of XVIII International Conference on Atomic Physics ICAP2002 (Editors: H. R. Sadeghpour (ITAMP), D. E. Pritchard (CUA), and E. J. Heller (CUA)).

- [57] L. P. Gor'kov and T. K. Barkhudarov, *Sov. Phys. JEPT* **13**, 1018 (1961).
- [58] The pairing through p -wave scattering between identical fermions can occur but at temperatures typically much lower than the critical temperature for the s -wave coupling. Anyway, in the presence of more than one fermionic component [59], it has been shown that this temperature for the p -wave coupling can be strongly increased.
- [59] M. A. Baranov *JEPT Lett.* **64**, 301 (1996).
- [60] M. Holland, S. J. J. M. F. Kokkelmans, M. L. Chiofalo, and R. Walser, *Phys. Rev. Lett.* **87**, 120406 (2001).
- [61] E. Timmermans *et al.* *Phys. Lett. A* **285**, 228 (2001).
- [62] M. L. Chiofalo *et al.* *Phys. Rev. Lett.* **88**, 090402 (2002).
- [63] S. J. J. M. F. Kokkelmans *et al.* *Phys. Rev. A* **65**, 053617 (2002).
- [64] J. N. Milstein *et al.* *Phys. Rev. A* **66**, 043604 (2002).
- [65] Y. Ohashi and A. Griffin *Phys. Rev. Lett.* **89**, 130402 (2002).
- [66] W. Hofstetter, J. I. Cirac, P. Zoller, E. Demler, and M. D. Lukin, *Phys. Rev. Lett.* **89**, 220407 (2002).
- [67] H. Heiselberg, C. J. Pethick, H. Smith, L. Viverit, *Phys. Rev. Lett.* **85**, 2418, (2000).
- [68] N. J. Bijlsma, B. A. Heringa, H. T. C. Stoof, *Phys. Rev. A* **61**, 053601, (2000).
- [69] H. Wang, *et al.*, *Phys. Rev. A* **62**, 052704 (2000).
- [70] T. Loftus, C. A. Regal, C. Ticknor, J. L. Bohn, and D. S. Jin *Phys. Rev. Lett.* **88**, 173201 (2002).
- [71] E.G.M. van Kempen, *et al.*, *Phys. Rev. Lett.* **88**, 093201 (2002).
- [72] J. L. Roberts *Phys. Rev. Lett.* **86**, 4211, (2001).
- [73] C. Fort, A. Bambini, L. Cacciapuoti, F. S. Cataliotti, M. Prevedelli, G. M. Tino, and M. Inguscio *EPJD* **3**, 113 (1998).
- [74] F. S. Cataliotti, E. A. Cornell, C. Fort, M. Inguscio, F. Marin, M. Prevedelli, L. Ricci. G. M. Tino, *Phys. Rev. A* **57**, 1136 (1998).
- [75] G. Modugno, C. Benko, P. Hannaford, G. Roati, and M. Inguscio *Phys. Rev. A* **60**, R3373 (1999).
- [76] J. L. Hall, L. Hollberg, Ma Long-Sheng, T. Baer, and H. G. Robinson, *Journal de Physique*, **42**, 1981 (1999).

- [77] W. Wohlleben *et al.* EPJ D, **15**, 237, (2001).
- [78] L. Cacciapuoti, Phd Thesis.
- [79] B. DeMarco, Phd Thesis.
- [80] M. D. Barrett, J. A. Sauer, and M. S. Chapman Phys. Rev. Lett. **87**, 010404, (2001).
- [81] T. Esslinger, I. Bloch, T.W. Hänsch, Phys. Rev. A **58**, R2664 (1998).
- [82] For a exhaustive review see: J. Weiner *et al.* Rev. Mod. Phys. **71**, 1-85 (1999).
- [83] E. Tiesinga *et al.* Phys. Rev. A **46**, R1167, (1992).
- [84] E. Tiesinga *et al.* Phys. Rev. A **47**, 4114, (1993).
- [85] S. Inouye *et al.* Nature, **392**, 151 (1998).
- [86] For a discussion of the classical case of parametric heating see L. D. Landau and E. M. Lifschitz, *Mechanics* (Pergamon, Oxford, 1976), pp 80-84.
- [87] S. Friebe *et al.* Phys. Rev. A **57**, R20, (1998).
- [88] A. Mosk, *et al.*, Appl. Phys. B **73**, 791 (2001).
- [89] A. Yannopoulou, *et al.*, Int. J. Quant. Chem. **57**, 575 (1996).
- [90] A. Dervianko, J. F. Babb, and A. Dalgarno, Phys. Rev. A **63**, 052704 (2001).
- [91] M. Marinescu and H. R. Sadeghpour, Phys. Rev. A **59** 390 (1999).
- [92] B. M. Smirnov and M. I. Chibisov, Sov. Phys. JETP **21**, 624 (1965).
- [93] E. Tiesinga, *et al.*, J. Res. Natl. Inst. Stand. Technol. **101**, 505 (1996).
- [94] We have checked that a $\pm 1\%$ uncertainty in the highly accurate C_6 coefficient adopted in this work does not affect the results of the paper.
- [95] S. D. Gensemer and D. S. Jin Phys. Rev. Lett. **87**, 173201 (2001).
- [96] F. Ferlaino, R. J. Brecha, P. Hannaford, F. Riboli, G. Roati, G. Modugno, and M. Inguscio J. Opt. B **5** (2003).
- [97] Tin-Lun Ho and V. B. Shenoy, Phys. Rev. Lett. **77**, 3276 (1996).
- [98] C. K. Law, H. Pu, N. P. Bigelow and J. H. Eberly, Phys. Rev. Lett. **79**, 3105 (1997); H. Pu and N. P. Bigelow, Phys. Rev. Lett. **80**, 1130 (1998).
- [99] E. Timmermans, Phys. Rev. Lett. **81**, 5718 (1998).
- [100] P. Ao and S. T. Chui, Phys. Rev. A **58**, 4836 (1998).

- [101] M. Trippenbach, K. Góral, K. Rzazewski, B. Malomed and Y. B. Band, J. Phys. B **33**, 4017 (2000).
- [102] R. A. Barankov, preprint cond-mat/0112326.
- [103] B. D. Esry *et al.*, Phys. Rev. Lett **78**, 3594 (1997); C. K. Law, *et al.*, Phys. Rev. Lett **79**, 3105 (1997).
- [104] F. Riboli, and M. Modugno Phys. Rev. A **65**, 063614 (2002).
- [105] H. Wang, *et al.*, Phys. Rev. A **62**, 052704 (2000).
- [106] E.G.M. van Kempen, *et al.*, Phys. Rev. Lett. **88**, 093201 (2002).
- [107] P. Maddaloni, *et al.*, Phys. Rev. Lett. **85**, 2413 (2000).
- [108] M. Modugno, F. Dalfovo, C. Fort, P. Maddaloni, and F. Minardi Phys. Rev. A **62**, 063607 (2000).
- [109] P. Nozieres and D. Pines *The theory of quantum liquids*, (Perseus Books, Cambridge MA, 1966)
- [110] D. Guery-Odelin and S. Stringari, Phys. Rev. Lett. **83**, 4452 (1999).
- [111] O. M. Maragò, *et al.*, Phys. Rev. Lett. **84**, 2056 (2000).
- [112] M. Modugno, G. Modugno, G. Roati, C. Fort, and M. Inguscio cond-mat/0207158 (2002).
- [113] M. Edwards, C. W. Clark, P. Pedri, L. Pitaevskii, and S. Stringari, Phys. Rev. Lett. **88**, 070405 (2002); G. Heshenblaikner, E. Hodby, S. A. Hopkins, O. M. Maragò, and C. J. Foot, Phys. Rev. Lett. **88**, 070406 (2002).
- [114] S. Stringari, Phys. Rev. Lett. **77**, 2360 (1996).
- [115] D. M. Stamper-Kurn *et al.*, Phys. Rev. Lett. **81**, 500 (1998).
- [116] L. P. Pitaevskii and S. Stringari Phys. Rev. A **235**, 398 (1997).
- [117] F. Ferlaino *et al.* Phys. Rev. A **66**, 011604 (2002).
- [118] C. Raman *et al.* Phys. Rev. Lett. **83**, 2502 (1999).
- [119] H. Hu, X. Liu, and M. Modugno, cond-mat/0301182 (2003).
- [120] R. Roth *Priv. Comm.*
- [121] A. P. Albus, F. Illuminati, and M. Wilkens arXiv:cond-mat/0211060 (2002).
- [122] M. Modugno *Priv. Comm.*

- [123] C. Menotti, P. Pedri, S. Stringari Phys. Rev. Lett. **89**, 250402 (2002).
- [124] A similar behaviour of the expansion of two components Fermi gas has been recently observed by C. A. Regal and D. S. Jin in cond-mat0302246
- [125] L. Pitaevskii and S. Stringari Science **298**, 2144 (2002).
- [126] F. Chevy *et al.* Phys. Rev. Lett **85**, 2223, (2000).
- [127] D. Pines, in *Liquid Helium*, Proceedings of the International School of Physics "Enrico Fermi" Course XXI (Academic Press, New York, 1963).
- [128] P. G. Gennes *Superconductivity of Metals and Alloys* (Benjamin, New York 1966).
- [129] L. Viverit and S. Giorgini Phys. Rev. A **66**, 063604, (2002).
- [130] A. Simoni, F. Ferlaino, G. Roati, G. Modugno, and M. Inguscio cond-mat/0301159 (2003).
- [131] B. Damski *et al.* cond-mat 0208375 (2002).
- [132] D. S. Petrov, M. A. Baranov, and G. V. Shlyapnikov cond-mat 0212061 (2002).